

NORTH WIND POWER COMPANY
2 KILOWATT
HIGH RELIABILITY WIND SYSTEM

Phase I - Design and Analysis
Technical Report

July 1981

D.J. Mayer
J.H. Norton, Jr.

Prepared by
North Wind Power Company, Inc.
P.O. Box 315
Warren, Vermont 05674

For
Rockwell International Corporation
Energy Systems Group
Rocky Flats Plant
Wind Systems Program
P.O. Box 464
Golden, Colorado 80401

Subcontract No. PF-71768-F

As part of the
U.S. DEPARTMENT OF ENERGY
WIND ENERGY TECHNOLOGY DIVISION
FEDERAL WIND ENERGY PROGRAM

Contract No. DE-AC04-76DP03533



North Wind 2 Kilowatt High Reliability Prototype
(1980 Photo)

ABSTRACT

This report presents the results of Phase I of a program to design a 2kw high reliability wind turbine for use in remote locations and harsh environments. In Phase I of the program, a predecessor of the proposed design was procured and tested in a wind tunnel and in the freestream to observe operational characteristics. An analytical procedure was developed for designing and modelling the proposed variable axis rotor control system (VARCS). This was then verified by extensive mobile testing of pre-prototype components. A low speed three phase alternator with a Lundel type rotor was designed. Prototypes were fabricated and tested to refine calculation procedures and develop an effective alternator with appropriate characteristics. A solid state field switching regulator was designed and tested successfully. All necessary support elements were designed and engineered. A complete analysis of system reliability was conducted including failure mode and effects analyses and reliability, maintenance and safety analyses. Cost estimates were performed for a mature product in production rates of 1000 per year. Analysis and testing conducted throughout the first phase is included in this report. Final prototype fabrication and testing will be covered in a subsequent Phase II report

FOREWORD

North Wind Power Company (NWPCo) was founded in 1974 with the goal of designing and developing a high performance, cost effective small wind energy conversion system (SWECS) for commercialization in the remote and residential power markets.

This volume describes the details of the Phase I design of a 2kw high reliability wind turbine for use in remote locations and harsh environments. This program was conducted under contract No. PF-71768-F, awarded by Rockwell International Energy Systems Group in January 1978, as a part of the United States Department of Energy's Federal Wind Program. Warren Bollmeier was the Rockwell Technical Monitor and L.D. Cullen was the Rockwell Contract Administrator. Each of these men provided valuable review and guidance throughout the program.

The NWPCo personnel who contributed to this effort were: Donald Mayer, David Sellers, John Norton, Jr., Arnold Johnson, John Kueffner, Douglas Livingston and Glenn Gazley. Numerous consultants also assisted in the program; among them were Professor John Dugundji of M.I.T., Dutch Greimann, Professor Philip Trickey, James McGuigan, Clint Coleman and Hugh Currin.

The final version of this report was edited by Rockwell International personnel at Rocky Flats to increase internal consistency and help clarify the presentation of important information.

PHASE I FINAL REPORT

VOLUME II - TECHNICAL DISCUSSION

TABLE OF CONTENTS

Page

Foreword
Abstract
iii Table of Figures
vi Nomenclature

Page

1 1. INTRODUCTION
1 1.1 Introduction
1 1.2 Previous Wind Machine Experience
2 1.3 Organization
4 2. BASIC TRADE-OFF AND PARAMETRIC ANALYSES
4 2.1 Review of Baseline Design and Critical Development Areas
5 2.2 Early Phase I Tests
9 2.3 1 to 2 kw Generator Trade Studies
12 3. CRITICAL LOADS
12 3.1 Introduction
12 3.2 Wind Regime Definition and Methodology
20 3.3 Important Environmental Conditions
22 4. TECHNICAL DISCUSSION AND DESIGN
22 4.1 Introduction
22 4.2 Rotor Design, Analysis and Testing
43 4.3 Electrical System Design, Analysis and Testing
67 4.4 VARCS Design, Analysis and Testing
87 4.5 Support Structure Design, Analysis and Testing
107 5. RELIABILITY, MAINTAINABILITY AND SAFETY ANALYSIS
107 5.1 Introduction
107 5.2 Reliability Analysis

Page	
108	5.3 Safety Analysis
113	5.4 Failure Modes and Effects Analysis
132	6. PRODUCTION AND COST ANALYSIS
132	6.1 Introduction
132	6.2 Production Facility
133	6.3 Estimated System Costs
134	6.4 Cost of Energy Calculation
137	7. PROGRAM STATUS AND SCHEDULE
137	7.1 Phase I Schedule
140	REFERENCES

APPENDIX - Low Reynolds Number Wind Section Tests in the MIT 12" x 12"
Wind Tunnel

PHASE I FINAL REPORT

VOLUME II - TECHNICAL DISCUSSION

TABLE OF FIGURES

Page	
3	1.1 Phase I Organizational Chart
6	2.1 System Schematic
13	3.1 Gust Chart
14	3.2 Rotor Loads Diagram
16-19	3.3 Critical Loads Tables (a-d)
23	4.1 Parametric Study of Required Rotor Size
25	4.2 Variation of Lift Coefficient with Reynolds Numbers for the N60 Airfoil
26	4.3 Variation of Drag Coefficient with Reynolds Numbers for the N60 Airfoil
27	4.4 Blade Airfoil Sections
28	4.5 Foreshortened 5 m Blade Blank Profile (Bottom View)
29	4.6 Blade Specifications
30	4.7 Blade Stresses (Loaded)
31	4.8 Blade Stresses (Loaded)
33	4.9 Blade Stresses (Unloaded)
34	4.10 Campbell Plot for NWPCo 2kw SWECS
35	4.11 Blade Coating
36	4.12 Leading Edge Protection
38	4.13 Truck Test Diagram
39	4.14 Truck Test VARCS Moment Calibration Device
40	4.15 Blade Element Force Diagram
41	4.16 C_p vs. TSR at Various Pitch Angles
42	4.17 Sample Data - 10°
44	4.18 C_p vs TSR @ 10°
45	4.19 C_p vs TSR @ 31.5°
46	4.20 C_p vs TSR @ 45°
47	4.21 C_p vs TSR @ 60°
48	4.22 C_p vs TSR @ 75°

Page

49	4.23 Alternator vs Generator Trade Analysis
50	4.24 Alternator Rotor Configurations
52	4.25 Lundel Schematic
54	4.26 Dynamometer Test Bed #1
55	4.27 Dynamometer Test Bed #2
57	4.28 Alternator No-Load Saturation
58	4.29 Prototype Alternator Section
60	4.30 Table of Alternator Changes
61	4.31 Alternator #3: Final Design Section
63	4.32 2 kva Alternator Numeration
64	4.33 Electric System Diagram
66	4.34 Field Regulator Diagram
68	4.35 Lightning Protection Diagram
70	4.36 C_t vs TSR
71	4.37 C_t vs Axial Interference Factor
73	4.38 Rotor Performance with Pitch and VARCS Spring Calculations
74	4.39 Assumed Alternator Torque Input Characteristics
75	4.40 Projected Performance Matrix
76	4.41 Graph of M_s vs Pitch Angle
77	4.42 Power Output vs Wind Speed
78	4.43 VARCS Operational Modes
79	4.44 2 kw High Reliability Wind Turbine Monthly Output
80	4.45 No-Load Characteristics
82	4.46 C_t vs TSR @ 10°
83	4.47 C_t vs TSR @ 31.5°
84	4.48 C_t vs TSR @ 45°
85	4.49 C_t vs TSR @ 60°
86	4.50 C_t vs TSR @ 75°
88	4.51 Rotor #7/Alternator #2a Matches
89	4.52 Power vs Wind Speed
90	4.53 Pitch vs Wind Speed
91	4.54 RPM vs Wind Speed
92	4.55 Designer's Sketch

Page

93	4.56 System Cutaway
95	4.57 Master Drawing
96	4.58 System Specifications (a-c)
100	4.59 Rotor Assembly Schedule
101	4.60 Alternator Assembly Schedule
103	4.61 VARCS Assembly Schedule
105	4.62 Saddle and Stub Tower Assembly
111	5.1 Reliability Flow Chart
112	5.2 Reliability Data Sheet
135	6.1 Manufacturing Cost Estimates by Sub-Assembly
136	6.2 Manufacturing Cost Estimates per 1000 units
138	7.1 Major Milestones, Phase I

NOMENCLATURE*

AC - alternating current
AKWH - annual kilowatt hours
amp - ampere
AOM - annual operating and maintenance cost
ASTM - American Society for Testing of Materials
AWG - American wire gauge
@ - at
 α - angle of attack

 β - blade pitch angle

C - centigrade (carbon or chord; where applicable)
cc - cubic centimeter
 C_D - drag coefficient
CDR - Critical Design Review
c.g. - center of gravity
 C_L - lift coefficient
cm - centimeter
COE - cost of energy
 C_p - power coefficient (rotor)
 C_s - system power coefficient
 C_t - thrust coefficient

D - rotor diameter
dbl. - double
DC - direct current
 D_G - generator drag
° or deg. - degrees

Exp. - experimental

F - Fahrenheit
FCR - fixed charge rate
FDR - Final Design Review
FMEA - failure mode and effects analysis
ft or ' - feet
 ft^2 - square feet
ft-lb - foot pound

gm - gram

hp - horsepower
Hz - hertz

I - moment of inertia
IC - installed cost
ID - inside diameter
in or " - inch
in-lb - inch pound
ITDC - intensive testing data collection

* Editor's note: This report contains unconventional nomenclature; however, internal consistency has been maintained.

K - stiffness
 K2 - generator rotor loss factor
 kg - kilogram
 kva - kilovolt amperes
 kw - kilowatt
 kWhrs - kilowatt hours

lb - pound
 L/D - lift to drag (ratio)
 LTDC - long term data collection
 λ - failure rate

M - moment
 m - meter
 m^2 - square meter
 M_3 - out-of-plane blade bending moment
 M_A - aerodynamic moment
 mc/I - bending stress
 MIT - Massachusetts Institute of Technology
 mm - millimeter
 mo. - month
 mov - metal oxide varister
 mph - miles per hour
 M_S - overturning moment
 MTBF - mean time between failure

NA - neutral axis in or out of plane of rotation
 n-m - newton meter
 no. or # - number
 NRC - National Research Center (Canada)
 NWPCo - North Wind Power Company

OAF - output adjustment factors
 O.D. - outside diameter

pA - available wind power
 PD - preliminary design
 PDR - preliminary design review
 ph - phase
 \emptyset - angle of force
 P_R - rated power
 psi - pounds per square inch
 \perp - perpendicular
 ψ - rotor azimuth
 % - percent
 / - per
 + - plus
 \pm - plus or minus

Q - torque
 Q/A - quality assurance
 Q/C - quality control

r - local radius
 Re - Reynolds Number
REA - Rural Electrification Administration
rev - revolution
RFP - request for proposals (when used in text)
RPM - revolutions per minute
 r/R - variation (r) from blade chord line at nondimensional radial station (R) of blade
 R_t - reliability
 ρ - air density

SWECS - small wind energy conversion system

t - one year (or turns)
TSR - tip speed ratio
 θ_t - twist angle

UV - ultraviolet

V - velocity
 \bar{V} - average (mean) wind speed
 v - volt
VARCS - variable axis rotor control system
vs - versus

X - distance

Y - yaw (degrees)
yr - year

1. INTRODUCTION

1.1 Introduction

The philosophy of North Wind Power Company (NWPCo) has been to base the development of new small wind energy conversion systems (SWECS) designs on the utilization of time-proven concepts which are refined and augmented by advances in analytical modelling techniques and materials. Design concepts such as a three bladed upwind rotor, a direct drive or low speed electrical generator, and the Parris-Dunn method of speed control by rotor tiltback--using a variable axis rotor control system (VARCS)--were applied to the 2kw high reliability SWECS. NWPCo's objective for this program was the evolution of a design emphasizing cost effectiveness without compromising performance or reliability. The direct drive generator and the VARCS are critical components essential to this design philosophy.

NWPCo's investigations have shown that no off-the-shelf direct drive generators are available which meet cost and performance goals. High speed generators employing gear boxes were eliminated due to reliability and maintainability considerations. NWPCo's experience with the design and construction of a 4kw direct drive alternator gave NWPCo confidence that personnel, facilities, equipment and suppliers were available to carry out the successful design, construction and evaluation of a 2kw direct drive alternator. During Phase I, NWPCo developed an alternator employing a cast Lundel interdigitated rotor. This design enhances system reliability by eliminating rotating coils while providing significant cost savings over other options.

Simplicity is the foundation of the system reliability. By choosing the rotor tiltback design (VARCS) to control speed, NWPCo has eliminated the need for a variable blade pitch hub assembly with an additional folding tail or shutdown-reorientation device for protection in very high winds. Performance problems such as torsional vibration or mis-pitched blades are significantly reduced by the use of fixed pitch blades and the VARCS.

To carry out the system design, it was necessary to develop new analytical models and to undertake an ambitious program of in-house testing. At the end of Phase I, alternator and VARCS prototypes have been successfully constructed and tested. Final prototype configurations have been designed. Calculations indicate that the system will have a mean time between failures (MTBF) of thirteen (13) years and will equal or better the cost goal of \$1500/kw (in 1977 dollars) at a production rate of 1000 units per year.

1.2 Previous Wind Machine Experiences

NWPCo began with a thorough investigation of existing SWECS designs from pre-REA (Rural Electrification Administration) machines to foreign manufactured units such as the Australian Dunlite and the Swiss Elektro. Our investigation found that certain design features prevalent in the most successful of these wind machines should be maintained in any new SWECS

design. Previous experience has proven the desirability of the following features for the reasons given:

1. Upwind Rotor

The upwind rotor avoids problems of tower shadow, is highly responsive to wind direction variations and is compatible with a variable axis rotor control system (VARCS).

2. Three Bladed Rotor

The three bladed rotor has proven to be a responsive, stable and durable arrangement.

3. Direct Drive, Low Speed Generator

NWPCo's experience has shown that pre-REA machines utilizing direct drive consistently proved more reliable and efficient than geared units.

4. Rotor Tilt or Blade Pitch Control

Various methods of rotor speed control have been examined including braking, yaw position variation and rotor tiltback or blade pitch. Older units of the pre-REA era used blade pitch and (in the case of the Parris-Dunn) rotor tiltback. Each of these methods proved responsive and durable; however, the rotor tiltback method has the added advantages of reducing parts stressed in motion and providing automatic shutdown and reset in high winds and has been chosen as the basis for the NWPCo high reliability design.

In the spring of 1977, NWPCo responded to a wind turbine design competition, sponsored by the DOE and managed by Rockwell International, for the development of a 2kw wind machine for use in remote areas where harsh environmental conditions are probable. Based on our own experiences with pre-REA units, NWPCo proposed a design which emphasized simple yet durable components, a minimum of parts stressed in motion, and complete protection from the environment. In January 1978, NWPCo was awarded a contract to develop a three bladed, horizontal axis, direct drive system with fixed pitch blades. The design phase of this contract has just been completed.

1.3 Organization

Figure 1.1 is the organizational chart for Phase I of Contract #PF71768F. Early in the course of Phase I, John Norton replaced Glenn Gazley as Design Team Leader. Contract work was organized on a team basis related to the relevant engineering disciplines of mechanics, aerodynamics and electronics. Each design team was headed by an employee in the relevant engineering discipline with access to highly qualified outside consultants. Note that consultants are shown in parentheses.

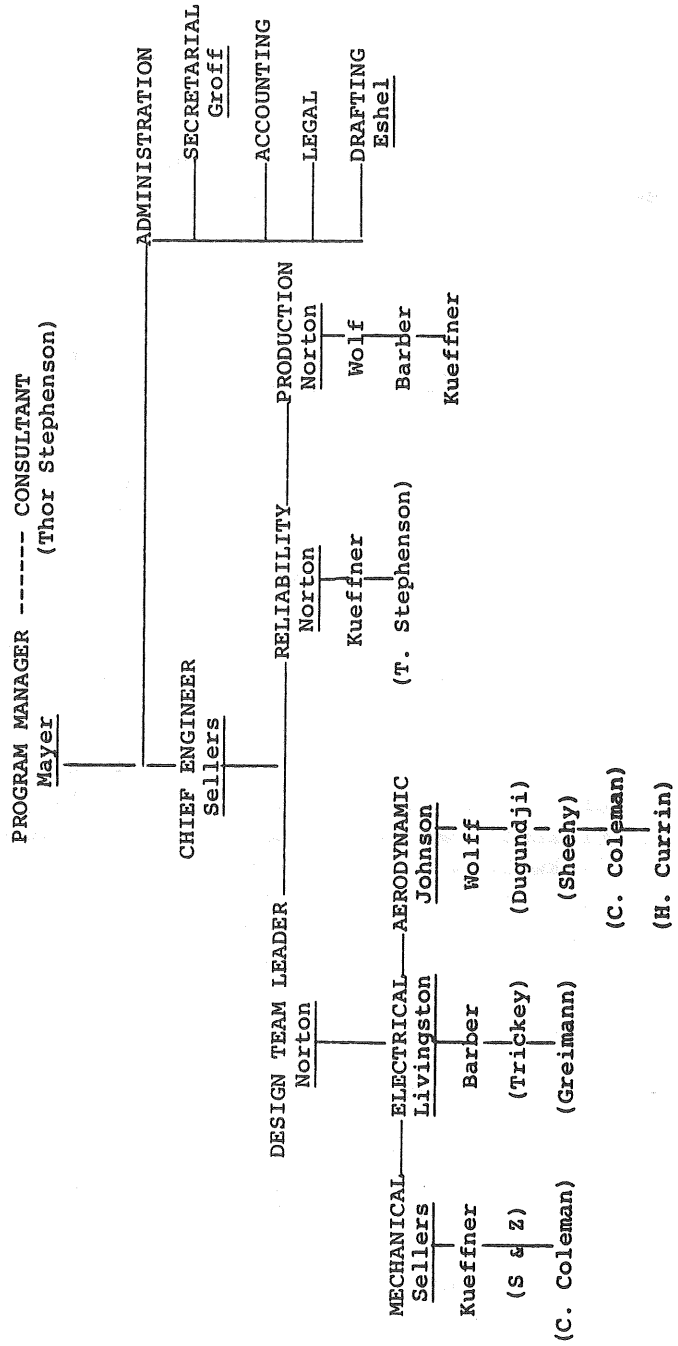
Figure 1.1

Project Organization Chart

NORTH WIND POWER COMPANY, INC.

2kW ORGANIZATIONAL CHART

PHASE I



2. BASIC TRADE-OFF AND PARAMETRIC ANALYSES

2.1 Review of Baseline Design and Critical Development Areas

The originally proposed 1kw design featured a 3.32 meter (m) fixed pitch rotor and a DC shunt wound generator integrated with a variable axis rotor speed control system which initiated rotor tiltback in 18 meter per second (m/s) (40 mile per hour (mph)) winds. The generator was rated to produce 1kw at 9 m/s (20 mph) at a speed of 360 revolutions per minute (rpm.) It would produce constant voltage until a maximum output of 4kw was reached at 15.6 m/s (35 mph) or 800 rpm. At 24.6 m/s (55 mph) the rotor pitched to the horizontal plane and automatic shutdown occurred.

Extensive tradeoff studies were conducted prior to the Preliminary Design Review (PDR.) The design of the generator and the VARCS were identified as critical development areas and detailed analyses were carried out prior to the Critical Design Review (CDR.) The following major design decisions were made prior to contract initiation:

1. The choice of the upwind three bladed rotor was based upon NWPCo's experience with reconditioned older machines. We believe that a three bladed upwind machine is even more stable than the downwind configuration. (In addition, the VARCS requires the upwind orientation.) Blade deflection problems were not anticipated at the proposed rotor diameter of 3.32 meters.
2. Sitka spruce was chosen as the blade material. Experience with wooden blades on the older machines indicated excellent durability and reliability. NWPCo's ability to fabricate blade sets in-house allows iterations of various airfoil options to be quickly tested for durability and performance.
3. The most successful older machines used low speed, direct drive generators which consistently proved more reliable and efficient than geared machines. The base generator proposed was a 1-4kw DC shunt wound unit. The DC generator was chosen because of past experience with rebuilding generators and immediate applicability to battery charging. The sizing, cost-effectiveness and reliability of the DC option, however, were closely scrutinized in extensive pre-PDR trade studies which eventually led to the specification of a 2kw alternator.
4. Simplicity of design and reduction in number of moving parts inherent in the variable axis rotor control system is the foundation of the reliability of the system. NWPCo's design approach emphasizes the need for durability as well. The VARCS method of speed control simplifies the system by eliminating the need for variable pitch blades and a variable position tail by providing automatic shutdown and reorientation. The substantial reduction in the number of moving parts stressed in motion made possible by utilizing the VARCS greatly increases reliability.

Each of these precontract design choices adheres closely to the NWPCo philosophy that reliability is best achieved through design simplicity and durability.

The two critical components which form the basis for system reliability are the VARCS and the low speed, direct drive generator. These components allow the high reliability SWECS to be designed so that only three assemblies move in respect to one another. (See Figure 2.1.)

Each of these assemblies is constructed of sub-components which are rigidly attached limiting movement to flexure only. The first assembly consists of the rotor and fixed pitch blades, the main shaft and the alternator rotor. This assembly rotates on bearings located within the alternator case. The second assembly consists of the alternator case, the stator and the VARCS plate. As wind speed increases, both of these assemblies pitch from the vertical to the horizontal plane on two bearings attached to a hinge pin. The third assembly consists of the VARCS spring and a cast steel saddle to which the tail is rigidly attached. The VARCS motion is restrained by a spiral torsion spring. Spring torsion automatically reorients the machine as wind speed decreases. The third assembly is free to move in yaw in order to orient the machine to wind direction. Some rotor imbalance and tail mechanism failures were recorded by NWPCo's rebuilt Eagle machines due to severe environmental conditions at remote installations. Utilizing the VARCS eliminates these potential failure modes. Since the generator is direct drive, there is no need for a gear box which eliminates high speed parts subject to stress and reduces start-up torque requirements. This simple yet rugged system most effectively achieves contract reliability, cost and performance goals. Prior to PDR, in order to gain experience with the VARCS method of speed control, a Parris-Dunn was tested at the National Research Center (NRC) wind tunnel in Ottawa, Canada.

2.2 Early Phase I Tests

Prior to Preliminary Design Review, NWPCo conducted three major test programs: Wind tunnel tests at MIT of two airfoil sections at low Reynolds number; wind tunnel tests at NRC of a modified Parris-Dunn wind machine; and freestream testing of the Parris-Dunn.

MIT wind tunnel tests were undertaken because very little airfoil section data at low Reynolds numbers is available.

SWECS rotors operate at Reynolds numbers ranging from 100,000 to 300,000, and as low as 20,000 during start-up conditions. Local angles of attack on untwisted blades can exceed 30° and angles of attack during start-up can be as high as 85° . Existing published data was obtained to serve as a tool to the aircraft designer and does not cover the angles of attack or Reynolds number range of interest to the SWECS rotor designer.

MIT's 12"x12" wind tunnel is a low turbulence, open circuit wind tunnel equipped with a three component strain gage balance. Wing sections are cantilever-mounted from the bottom wall of the test section. Velocity is monitored by the difference in static pressure between the test section and settling chamber as based on a pitot static calibration of the test section.

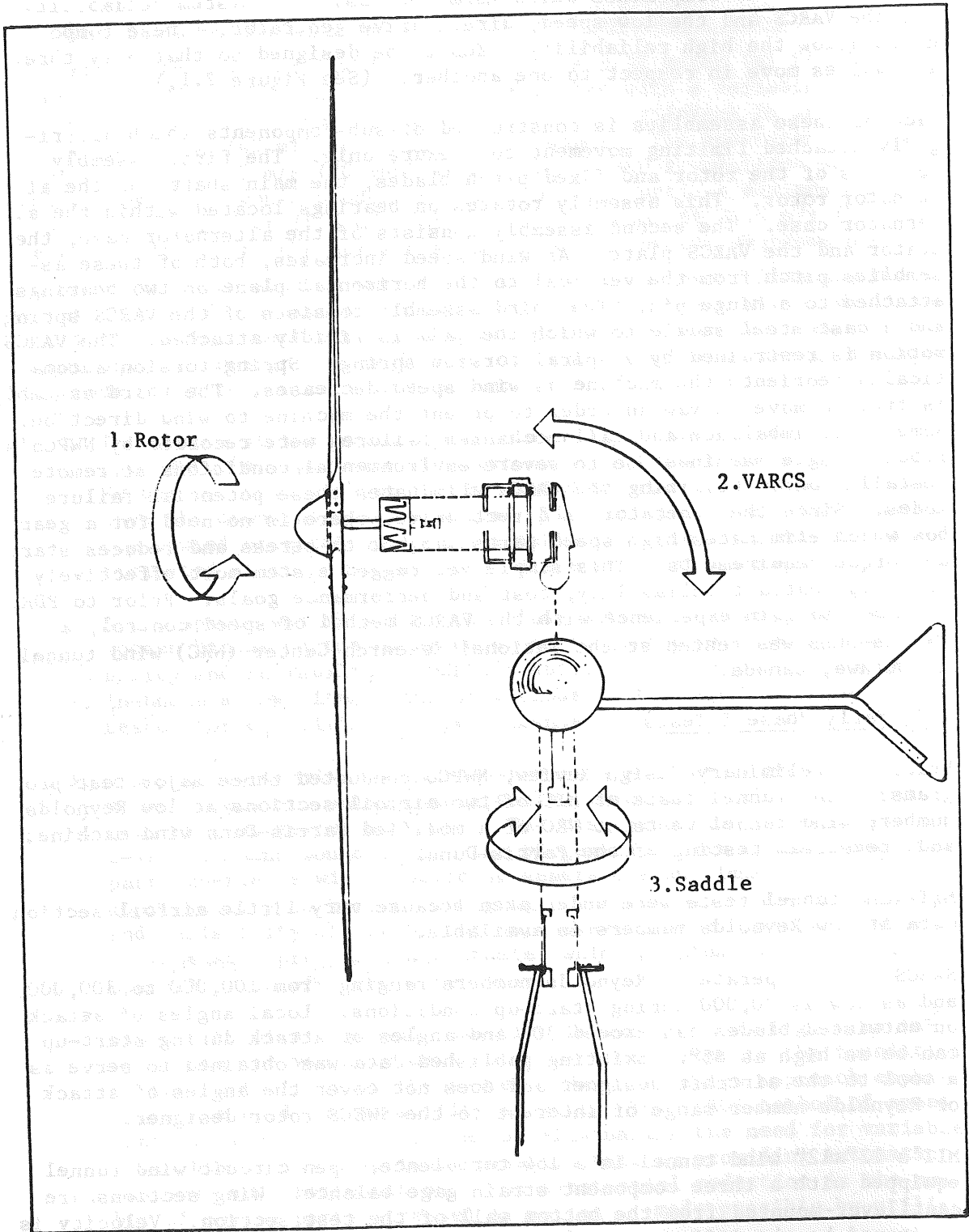


Figure 2.1
System Schematic

Our wing section models had a 3" chord and were trimmed in length to allow a 1/32" clearance from the top wall of the test section. The two sections tested were the FX 76MP120 modified to a thicker section by flattening the bottom of the section as shown in the Appendix and the 20 percent GU 25-5 (11)8 section which had been previously tested at Reynolds numbers ranging from 390,000 to 630,000, Reference 2. The Wortman section had never been tested before.

Wind tunnel tests were run to determine airfoil performance at Reynolds numbers below 390,000. The data obtained indicated transition from subcritical to supercritical flow at a Reynolds number of 250,000. An FX 76MP120 modified section was also tested; its critical Reynolds number turned out to be about 150,000.

Full scale tests of the Parris-Dunn were conducted in March 1978 at the large NRC wind tunnel in Ottawa, Ontario, Canada. These tests had the following objectives:

1. Determine natural damping due to gyroscopic forces.
2. Determine rotor power coefficient (C_p) by measuring velocity upstream and downstream of the rotor.
3. Determine power output versus pitch, C_p versus pitch.
4. Determine rotor start up speed -- to be compared with starting torque of generator.
5. Investigate vibrations induced during tiltback.

A ten-foot diameter rotor based on the MIT data was designed to be tested on the Parris-Dunn unit at NRC. It was designed for a tip speed ratio of 7 and twisted to operate at a 2° design angle of attack. An angle of 2° was chosen to minimize lift, allowing a large enough cross-section to provide a structurally sound blade. In addition, an original Preliminary Design three-bladed Parris-Dunn rotor was refinished. These blades were twisted and tapered, employing a modified Clark Y airfoil section.

The following test plan was used for the NRC wind tunnel tests:

Test 1

Measure tower drag (done without unit at an appropriate time).

Test 2

Test Parris-Dunn with refinished original modified Clark Y blades.

- (1) Upstream/downstream velocity tests with Parris-Dunn in fixed tilt. Determine start-up velocity. Measure velocity upstream/downstream with pitostatic probes at 10, 15, 20, 25, and 30 mph.
- (2) Tests of free tiltback. Begin at 15 mph going up by 5 mph increments until unit reaches 90° tilt position.

Go 2 velocity steps beyond 90° position.

At each velocity step, vary load from 500 to 1000 to 1500 watts (w).
Vary yaw at each velocity to 5°, 10°, 15°, and 355°, 350°, and 345°.

Test 3

Test Parris-Dunn with GU 25-5(11)8 blades matched to Preliminary Design generator output curve.

Repeat test procedures for these blades as in Test 2 (1) and (2).

The NRC tests provided the following results:

1. The GU blade rotor, designed for a tip speed ratio (TSR) of 7, would not break through a TSR of 4 until the rotor-generator pitched back. In the pitched mode, tip speed ratios ranging from 5 to 9 were recorded. Calculations indicated stalled conditions over the entire blade at TSR=4 at low Reynolds numbers. A boundary layer trip was added to each blade (a narrow strip of masking tape on the upper surface at about 15% chord.) Unfortunately, the run without the trip was scrapped by NRC and no data were obtained. The rotor with the boundary layer trip exhibited remarkable performance, attaining overall power coefficients (based on the velocity component normal to the rotor) as high as .45. The boundary layer trip managed to achieve supercritical flow over the blade, resulting in improved rotor output and allowing breakout from the TSR=4 lock at lower tilt angles.
2. As previously mentioned, calculations show a stalled condition at TSR=4 for any wind speed on the NRC rotor. A 5 meter rotor design was later calculated for the 2kw alternator, using the GU section and a working angle of attack of 8° to alleviate stall tendencies at lower tip speed ratios. Calculations indicate that transition to subcritical flow will prevent rotor acceleration past TSR=4 unless a boundary trip is added.
3. At 9m/s and the design RPM of the alternator, the working angles of attack on the GU were found to be of small negative values and performance goals at 9m/s could not be met.

The performance characteristics of the FX airfoil were worked up from the MIT data. The higher Reynolds number data were extrapolated, and the data look similar to that of the GU with peaks C_L , C_D , versus Reynolds number shifted from 400,000 to 200,000. The MIT data in this case covers the entire transition range -- missing in the GU data. A 5-meter rotor designed with the FX section indicates a stall phenomenon at TSR=4, similar to that exhibited at NRC.

In general, it was concluded that high performance airfoils and small rotors do not form promising combinations. Schmidt's data² show that the airfoils of yesteryear had transitions from subcritical to supercritical flow at lower critical Reynolds numbers, i.e. 60,000, as compared with 200,000 to 300,000 for today's high performance airfoils. Schmidt also states that

sharp leading edges promote instant transition into supercritical flow. NWPCo investigations have shown that the evolution of blade sections led to increasingly sharper leading edges. For a SWECS rotor, it appears better to design to a lower C_p and utilize an airfoil section with a low critical Reynolds number.

Following completion of the NRC testing, NWPCo installed the Parris-Dunn on its test tower in Warren, Vermont. At this installation, performance parameters were measured and recorded as at NRC on the strip chart. This testing continued from March 1978 to July 1978, when the unit was taken down and shipped to Rocky Flats. During this period, NWPCo was able to observe the operation of the system under winter and summer conditions, including a 15 minute thunderstorm with winds gusting over 22.4 m/s (50 mph.)

Freestream tests constituted for NWPCo sufficient testing to assure that the control system could operate without the shaft being loaded, and to assure that pitch and yaw damping would probably not be essential in the larger system. The opportunities to observe an operating system under controlled and uncontrolled conditions provided a point of reference for the balance of the first phase of the program.

2.3 1 to 2kw Generator Trade Studies

2.3.1 Introduction

The following base assumptions were made in order to select the optimum rated capacity generator for development under this program:

1. Average monthly load - 320 kilowatt hours per month (kwhr/mo) at the load (not subject to seasonal variations.)
2. The units are designed to charge battery banks and must be capable of providing 320 kwhr/mo to the load. Therefore, the sizing of the unit must take into account efficiency factors due to line losses, batteries, regulators, etc. Output adjustment factors (OAF) are estimated as follows:

a. Regulator efficiency	= .99
b. Diode efficiency	= .98
c. Line losses (100 ft)	= .97
d. Battery efficiency (@50°F)	= .77
e. Regulation efficiency	= .87
f. Load matching	= .95
	= .60
3. Battery bank shall be sized to provide reasonable storage and alarm period, and shall be maintained within manufacturer's recommended temperature range. Discharge depth, in general, shall not exceed 40%.

4. Wind data for Casper, Wyoming adjusted to 7000 ft., as noted by Frost,¹ was selected as the representative wind regime.

5. A detailed component-by-component cost estimate was performed for the 2kw alternator configuration, assuming 1000-unit per year production. Using the 2kw estimate of \$1035.00 as a base-line, estimates of probable cost ratios for the other configurations were determined by D. Livingston and P. Trickey using engineering judgment based on their production data for electric motors and generators of similar types. The derived estimates for other configurations also include adjustments for such variations as increased shaft requirements for larger rotor diameters.

2.3.2 Criteria for Selection

1. Ability to meet load requirements during seasonal wind spectrum variations.
2. Ease of manufacture: component availability, ease of construction, availability of fabrication equipment.
3. Cost per kilowatt hour per year.
4. Reliability of configuration.
5. Applicability of configuration to battery charging.

2.3.3 Ratio Costing of Configurations (assumes 2kw = \$1,035.00)

Configuration	Probable Cost Ratio	Estimated Production Cost (\$)	Estimated Annual Energy Output (kwh)	Energy Cost (¢/kwh/yr)
1kw 10.89-ft rotor	0.48	500	2145	23.3
1-2kw 10.89-ft rotor	0.67	690	2898	23.8
1-3kw 10.89-ft rotor	0.78	807	3220	25.1
1-4kw 10.89-ft rotor	0.88	911	3362	27.1
2kw 16.4-ft rotor	1.00	1035	4545	22.8
2-3kw 16.4-ft rotor	1.22	1263	5506	22.9
2-4kw 16.4-ft rotor	1.39	1435	6209	23.1

2.3.4 Output vs. Load (assumed 320 kwhrs/mo Load)

Configuration	Monthly Summer Output Average (in kwhrs)	% of Load	Monthly Winter Output Average (in kwhrs)	% of Load	Monthly Annual Output Average (in kwhrs)	% of Load
1kw	98	30	406	127	179	56
1-2kw	116	36	590	184	241	75
1-3kw	119	37	689	215	268	84
1-4kw	117	36	746	233	280	88
2kw	212	66	850	270	379	118
2-3kw	233	73	1088	340	459	143
2-4kw	250	78	1263	395	517	162

2.3.5 Trade Study Conclusions

1. Based upon the Output vs Load Table, the 2kw, 2-3kw and 2-4kw machines were the only ones which will meet load demands over the duration of the year. All of the 1 kw units fail to meet the load demands except during the winter season.
2. The 2kw, 2-3kw and 2-4kw units all have good cost-to-output ratios and compare favorably in terms of ability to meet load requirements. The 2-3kw and 2-4kw have better output than the 2kw machine in the summer months (by 11% and 18% respectively), but must be justified in terms of cost per kilowatt hour per year, ease of manufacture, reliability and excess winter production:
 - a. Cost per kilowatt hour per year - The 2kw out-performs all the other units in this area, despite having only a small advantage over the 2-3kw and 2-4kw units.
 - b. Ease of manufacture - The 2kw would be easier to manufacture due to less requirement for current carrying capacity.
 - c. Reliability - Because of the need for carrying higher currents, the 2-3kw and 2-4kw configurations may be less reliable than the 2kw unit.
3. The overall conclusion of this study was that the 2kw is the proper size unit.

3. CRITICAL LOADS

3.1 Introduction

In consideration of the severe service requirements and environmental conditions to which the high reliability unit is subjected, NWPCo has adopted a conservative approach to the calculation of critical loads. The variable axis rotor control system is inherently load-shedding, and safe automatic shutdown is achieved at 90° pitchback. The extreme load cases are due to gusting, and occur throughout the operating range of the VARCS. Values for gust amplitudes were chosen from Boulder area data, as representative of very severe documented conditions. NWPCo made no allowance in its loads calculations for any stress-relieving response by the system, i.e. all gusts were assumed to be "square wave." It is felt that this conservative approach, along with provision of at least 2:1 safety factor, provides enough margin to insure the system against failure caused by the most severe gusting conditions, by sluggish response due to icing, and by extraordinary wind conditions.

3.2 Wind Regime Definition and Methodology

The wind regime is defined in terms of the contract specifications for environmental conditions, i.e. 9 m/s (20 mph) rated wind speed with 54 m/s (120 mph) steady maximum and 75 m/s (165) maximum gust. In the design regime, Boulder area maximum gust data are extrapolated to a gust amplitude of 4.5 times a mean wind speed of 8 m/s (18 mph). A gust chart was developed from this data (see Figure 3.1) and 12 points were selected for examination.² Points 1 through 4 represent gusts, both negative and positive, occurring at a mean wind speed just under 9 m/s before pitchback is initiated. Points 5 through 8 occur at 14 m/s when the machine is pitched back to 54° and is producing power. Points 9 through 12 occur at 70° in a mean wind speed of 20 m/s when the rotor is producing enough torque to sustain alternator output. A thirteenth point was analyzed, i.e. 90° pitchback at 73.8 m/s (165 mph.)

As mentioned previously, gusts are assumed to occur as "square waves", i.e. no ramp times are assigned to the gust events. No calculations for frequency of wind shifts were done in this analysis, and no calculating of gyroscopic loads were done. All rotor loads were calculated at a density of 1.2 kg/m³.

In general, the wind regime is defined as simply and conservatively as possible to insure that design wind conditions are accounted for with an adequate safety margin and without an unnecessarily complex and extensive speculative analysis.

For each point on the gust chart, the blade and rotor loads are calculated for a quasi-steady condition, i.e. no response of the control functions, to the gust. Individual blade loads are calculated for at least 4 azimuth positions unless the loading is critical, in which case 8 positions are examined. Figure 3.2 gives the notation used by NWPCo in this analysis.

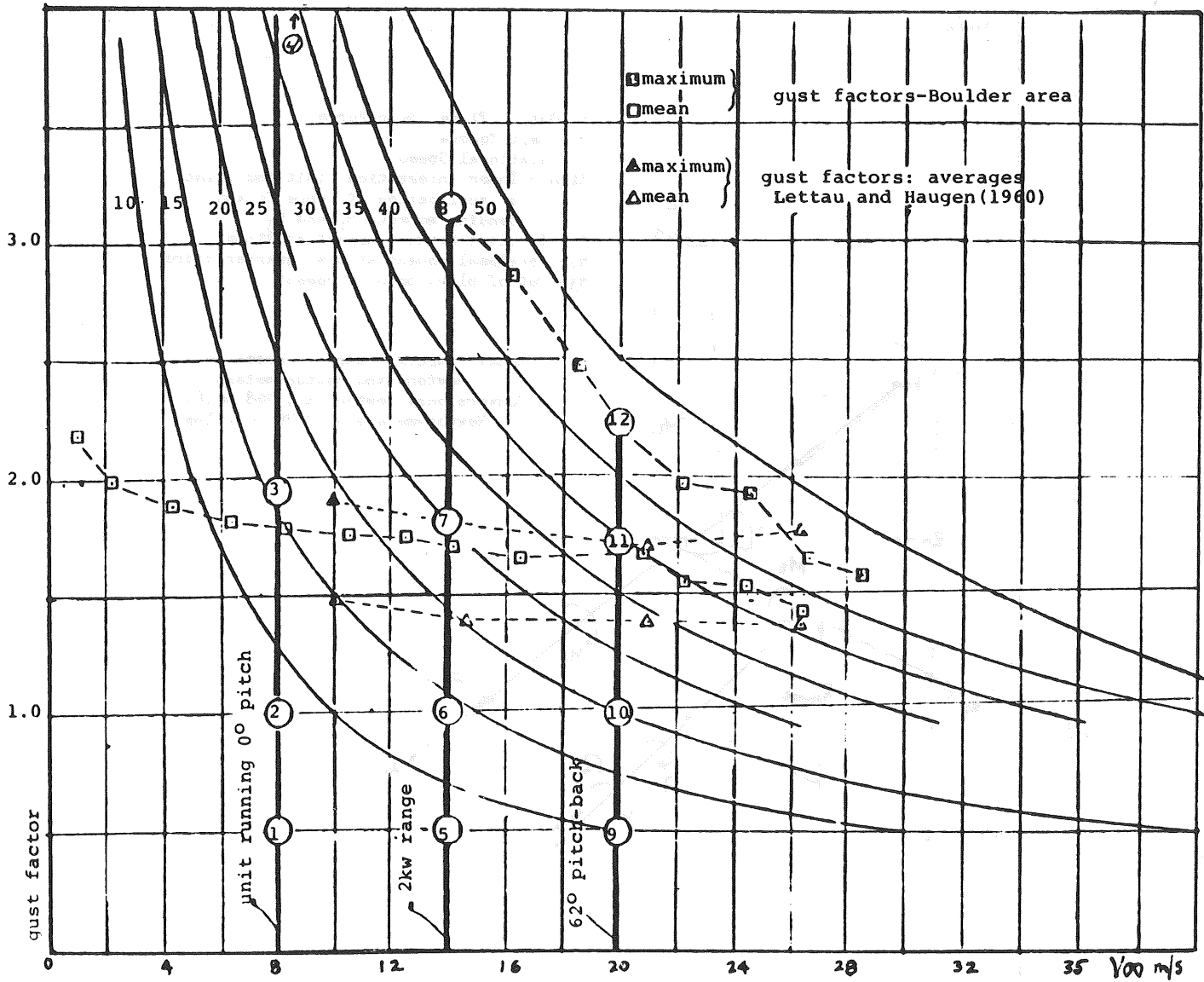


Figure 3.1
Gust Chart

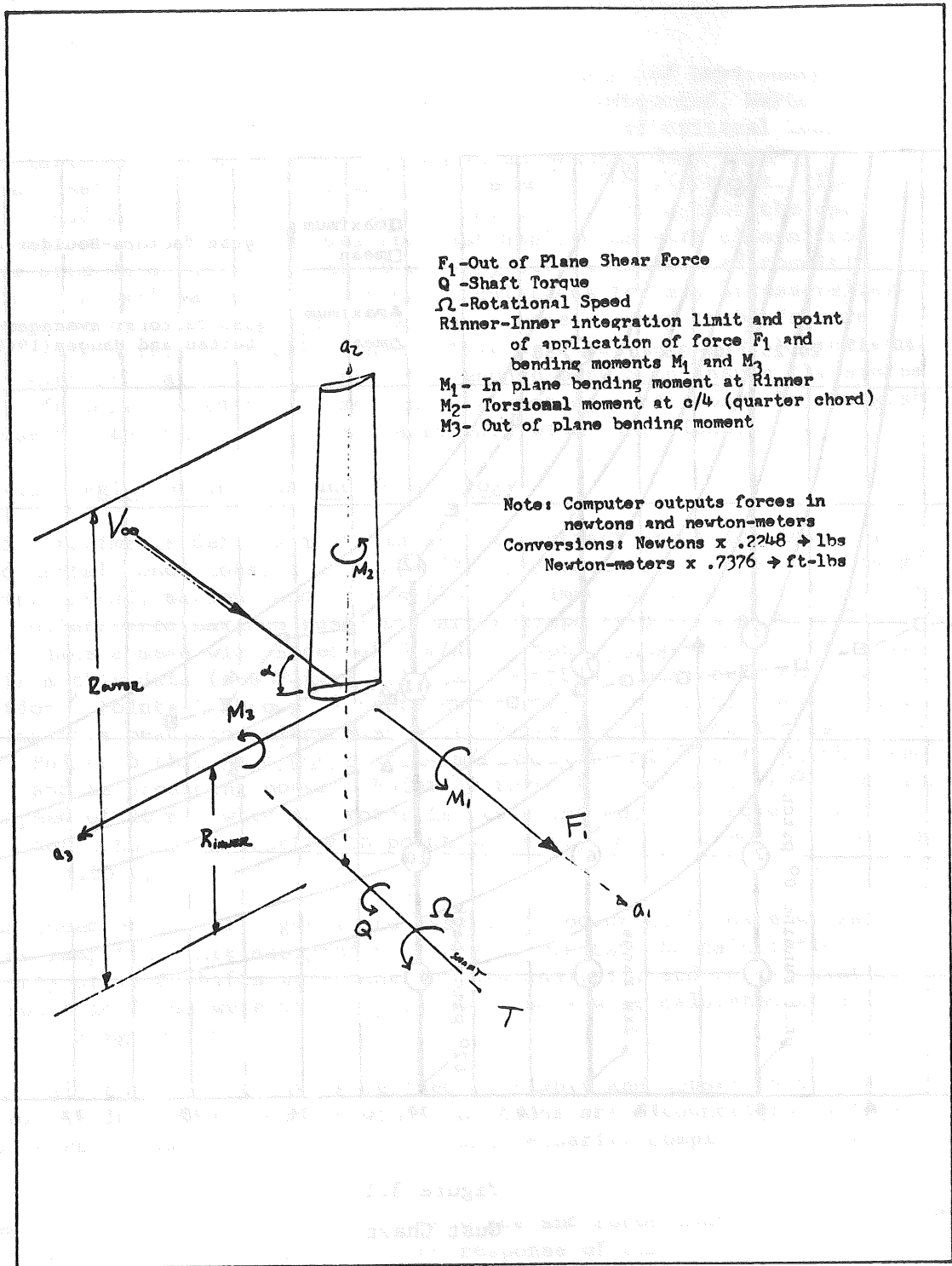


Figure 3.2
Rotor Loads Diagram

A complete chart is then prepared of the rotor and blade loads for all 13 points for the blade root section and for the blade section at a radius of 29.6" ($r/R = .3$) where the transition from the structural G625 to the N60 airfoil occurs. This latter point is expected to be the most highly stressed point on the blade. A stress analysis of each blade section is performed for its respective maximum loads. (See section 4.2.2, Figures 4.7, 4.8, 4.9).

The results of the critical loads calculations are shown in tabular form in Figures 3.3a-d.

Figure 3.3a

Critical Loads Table

Square Wave Gust on Loaded Rotor*

Point	Init. Vel. m/s	β°	RPM	Gust Factor	Final Vel. m/s	X	ψ	M ₁ N - M	M ₂ N - M	M ₃ N - M	F ₁ N	Q N - M	M N - M	Rotor Thrust N	Rotor Torque N - M	Cp
1	8	10°	215	0.5	4	14.08	All	0.6	0.3	-9.0	14.2	0.8	-12.4	42.6	2.5	.076
2	8	10°	215	1.0	8	7.04	All	30.5	0.7	-241.3	168.7	36.2	-281.5	506.1	108.6	.406
3	0	10°	215	1.9	15.2	3.71	All	42.3	3.6	-290.3	213.8	50.6	-341.2	641.5	151.9	.083
4	8	10°	215	4.5	36	1.56	All	51.6	9.8	-495.6	438.2	66.6	-599.9	1314.6	199.7	.008
5	14	50°	241	0.5	7	9.02	0°	0.7	0.4	-11.4	18.0	1.1	-15.7	59.0	3.3	.021
							90°	-0.1	0.7	-11.6	18.3	-0.1	-16.0			
							180°	0.7	0.4	-11.4	18.0	1.1	-25.7			
							270°	1.7	0.2	-17.8	22.8	2.5	-23.3			
6	14	50°	241	1	14	4.51	0°	40.0	0.9	-308.3	214.8	47.5	-359.4	634.3	124.6	.105
							90°	30.7	1.7	-308.3	272.1	37.0	-445.0			
							180°	40.0	0.9	-308.3	214.8	47.5	-359.4			
							270°	38.5	0.8	-219.7	140.7	45.7	-253.2			
7	14	50°	241	1.8	25.2	2.51	0°	54.0	4.3	-362.9	265.0	64.5	-426.0	908.1	288.7	.039
							90°	148.8	2.3	-782.2	598.0	178.6	-924.5			
							180°	54.0	4.3	-362.9	265.0	64.5	-426.0			
							270°	26.6	0.4	-141.6	56.1	40.5	-154.9			
8	14	50°	241	3.1	43.4	1.45	0°	52.7	9.4	-446.3	362.5	65.2	-532.6	1008.6	606.3	.010
							30°	101.8	10.7	-719.6	578.3	123.9	-857.3			
							60°	153.5	14.2	-992.1	805.4	186.7	-1183.8			
							90°	182.0	14.6	-1116.2	915.2	222.3	-1334.0			
							120°	153.5	14.2	-992.1	805.4	186.7	-1183.8			
							150°	101.8	10.7	-719.6	578.3	123.9	-857.3			
							180°	52.7	7.4	-446.3	362.5	65.2	-532.6			
							210°	59.4	0.0	-251.5	106.6	100.4	-276.9			
							240°	252.8	-0.7	-52.5	-159.3	354.4	-14.6			
							270°	244.3	-0.9	-21.4	-210.7	343.1	23.7			
							300°	252.8	-0.7	-52.5	-159.3	354.4	-14.6			
330°	59.4	0.0	-251.5	106.6	100.4	-276.9										

* Inner Integration limit = .238 m (blade root).

Figure 3.3b
Critical Loads Table

Square Wave Gust on Loaded Rotor*

Point	Init. Vel. m/s	β°	RPM	Gust Factor	Final Vel. m/s	X	ψ°	M ₁ N - M	M ₂ N - M	M ₃ N - M	F ₁ N	Q N - M	M N - M	Rotor Thrust N	Rotor Torque N - M	C _p
9	20	61.8°	230	0.5	10	6.03	0°	1.2	0.3	-12.3	19.4	1.7	-16.9	59.3	5.0	0.01
							90°	-0.3	0.8	-12.8	19.7	-0.4	-17.5			
							180°	1.2	0.3	-12.3	19.4	1.7	-16.9			
							270°	3.7	0.2	-41.8	36.2	4.9	-50.4			
10	20	61.8°	230	1.0	20	3.01	0°	47.6	0.7	-309.0	216.7	56.4	-360.6	589.8	131.0	0.03
							90°	30.7	2.3	-426.4	305.3	36.7	-499.1			
							180°	47.6	0.7	-309.0	216.7	56.4	-360.6			
							270°	21.2	0.5	-118.6	56.2	27.4	-132.0			
11	20	61.8°	230	1.7	34	1.77	0°	47.5	4.0	-328.8	242.1	56.8	-386.4	859.1	282.1	0.01
							90°	135.9	3.7	-887.3	673.3	161.9	-1047.5			
							180°	47.5	4.0	-328.8	242.1	56.8	-386.4			
							270°	81.9	-0.3	-11.9	-94.8	114.1	10.7			
12	20	61.8°	230	2.25	45	2.34	0°	47.3	5.2	-361.0	279.2	57.4	-427.5	1005.3	586.8	0.01
							30°	116.5	9.0	-728.8	562.5	141.0	-846.7			
							60°	229.9	6.2	-1165.8	931.0	277.5	-1387.4			
							90°	243.7	5.7	-1290.8	1014.6	291.6	-1532.3			
							120°	229.9	6.2	-1165.8	931.0	277.5	-1387.4			
							150°	116.5	9.0	-728.8	562.5	141.0	-846.7			
							180°	47.3	5.2	-361.0	279.2	57.4	-427.5			
							210°	68.5	0.1	-135.6	15.6	105.5	-139.3			
							240°	186.1	-0.7	-42.8	-205.0	251.9	91.6			
							270°	180.8	-0.8	77.3	-263.5	245.0	140.0			
13	73.8	86.12°	130	1.0	73.8	.462	0°	12.6	0.2	-92.4	64.5	15.0	-107.8	-69.0	66.3	.00
							90°	-15.6	6.2	-11.8	15.4	-24.3	-15.5			
							180°	12.6	0.2	-92.4	64.5	15.0	-107.8			
							270°			Does not compute						

* Inner integration limit = .238 m (blade root).

Figure 3.3d
Critical Loads Table

Square Wave Gust on Loaded Rotor*

Point	Init. Vel. m/s	β°	RPM	Gust Factor	Final Vel. m/s	X	ψ°	M ₁ N - M	M ₂ N - M	M ₃ N - M	F ₁ N	Q N - M	M N - M	Rotor Thrust N	Rotor Torque N - M	Cp		
9	20	61.8°	230	0.5	10	6.03	0°											
							90°											
							180°											
							270°											
10	20	61.8°	230	1.0	20	3.01	0°											
							90°											
							180°											
							270°											
11	20	61.8°	230	1.7	34	1.77	0°											
							90°											
							180°											
							270°											
12	20	61.8°	230	2.25	45	1.34	0°	25.4	4.1	-216.2	242.6	53.2	-415.9	1018.5	458.6	.010		
							30°	60.1	7.0	-415.6	492.0	132.2	-820.6					
							60°	125.9	3.3	-679.8	799.1	260.7	-1337.5					
							90°	137.5	2.2	-758.7	880.1	277.8	-1483.1					
							120°	125.9	2.3	-679.8	799.1	260.7	-1337.5					
							150°	60.1	7.0	-415.6	492.0	132.2	-820.6					
							180°	25.4	4.1	-216.2	242.6	53.2	-415.9					
							210°	8.4	2.3	-102.4	119.6	18.5	-200.8					
							240°	33.0	1.9	-45.1	-23.2	144.7	-25.9					
							270°	66.7	1.9	-7.8	-95.4	222.9	70.8					
							300°	33.0	1.9	-45.1	-23.2	144.7	-25.9					
330°	8.4	2.3	-102.4	119.6	18.5	-200.8												
13	73.8	86.12°	130	1.0	73.8	.462	0°											
							90°											
							180°											
							270°											

NOT CRITICAL

* Inner Integration limit = .823 m (blade root).

3.3 Important Environmental Conditions

The severe environmental conditions have been major factors in the evolution of the design of the NWPCo 2kw high reliability SWECS. The basic machine configuration and rotor speed control system were selected in order to insure machine protection from extreme environmental conditions. Figure 3.4 outlines the specific design choices made in response to each condition.

One of the advantages of the VARCS was its compactness. It can be easily sealed and protected from rain, salt water and ice. All functional components are completely sealed. The VARCS is also a control system which employs large components not critically sensitive to temperature fluctuations. The temperature conditions posed one of the severest design challenges in the program. All materials had to be selected for their continued performance at extremely low temperatures. These included the steels, aluminum, wiring insulation, coatings and grease.

It was determined that little could be done about the occurrence of ice. For this type of equipment, the primary concerns with icing are additional system loads, functional impairment and performance degradation.

All static system wind loading calculations were made with the assumption of increased drag and weight due to a complete covering of 2½" of ice. This assumption was primarily responsible for the selection of the solid leg Rohn tower. The machine geometry provides sufficient clearance between functional parts. The final consideration of performance degradation applies primarily to rotor performance. While some degradation will occur, overall power output calculations indicate that the system will still provide sufficient power and energy for the intended applications.

Finally, care was taken in the selection of materials and fasteners in order to reduce to a minimum the potential for aggravated electrolytic corrosion. Aluminum parts are interfaced only with stainless steel shafts, bolts, bushings, and bearings. In addition, exposed non-stainless steels are galvanized and aluminum components anodized. These precautions will assure the maximum maintainability and life of the complete system.

Figure 3.4

NWPCo's Response - Extreme Environmental Conditions

TEMPERATURE

Low RANGE

HIGH CARBON STEEL; LOW TEMPERATURE GREASE; SPECIAL STEEL SEALS; LOW TEMPERATURE INSULATION; FEW MOVING PARTS (NO GEAR BOX OR BLADE PITCHING MECHANISM)

HIGH RANGE

NO SPECIAL PROVISIONS REQUIRED

RAIN

WEATHERTIGHT FITTINGS AND CONNECTORS; TOTALLY SEALED CONSTRUCTION

SNOW, SLEET, ICING

CLEARANCES PROVIDED; FEW MOVING PARTS

HAIL

RESILIENT BLADE MATERIAL

SALT WATER SPRAY

MATERIAL SELECTION; WEATHERTIGHT FITTINGS AND CONNECTORS; TOTALLY SEALED CONSTRUCTION

DUST

TOTALLY SEALED CONSTRUCTION; WEATHERTIGHT FITTINGS AND CONNECTORS; LEADING EDGE TAPE; POLYURETHANE BLADE COATING

WIND

VARIABLE AXIS ROTOR CONTROL SYSTEM

CORROSIVE ATMOSPHERE

MATERIAL SELECTION; TOTALLY SEALED CONSTRUCTION

LIGHTNING

INSTALLATION PROCEDURES AND TRANSIENT PROTECTION

NOISE

FEW MOVING PARTS; FIELD TESTING

4. TECHNICAL DISCUSSION AND DESIGN

4.1 Introduction

The following section discusses in detail the design analysis and testing of the high reliability 2kw SWECS by sub-system, i.e. rotor, alternator, VARCS and support structure. A brief review of the evolution of the design is presented with a discussion of the relevant criteria. Each section includes a discussion of the analytical techniques as applied to each sub-system, along with a review of component test results and their impact on the design itself and modeling techniques.

This discussion is organized by sub-system for clarity and organization; however, it should be kept in mind that much of this work was conducted simultaneously on the whole machine.

4.2 Rotor Design Analysis and Testing

4.2.1 Preliminary Design Development

The initial proposal specified a three blade 3.32 meter diameter fixed pitch rotor, using twisted blades and a GU-25-5-(11)8 airfoil section. The diameter of 3.32m was based on assumptions of a 1kw generator capacity with 85% efficiency at rated output, to be achieved at 9 m/s. The GU airfoil was proposed initially due to the availability of data at relatively low Reynolds numbers (down to 3.9×10^5), and due to its structural characteristics (20% section). The blade material selected for study and development was Sitka spruce. NWPCo had extensive experience with the performance and fabrication characteristics of this material.

Through the initial stages of the program, preliminary trade-off analyses and component testing indicated some major changes. An analysis of potential load configuration and power requirements in a typical wind regime was conducted in order to determine optimal generator capacity in the 1 to 4 kilowatt range with regard to overall system costs per kilowatt for each option. The complete analysis is included in Section 2.3. This study indicated that a 2kw machine was most suitable for development under this program.

Early generator designs indicated that maximum efficiency would be limited to 75%. As a result, we increased the rotor diameter to 5 meters. (See Figure 4.1.)

Wind tunnel tests of the GU airfoil by NWPCo at the MIT wind tunnel did not confirm preliminary extrapolations of available low Reynolds numbers data at 3.9×10^5 . Later full scale rotor testing at the NRC wind tunnel in Ottawa, Canada confirmed that this airfoil was subcritical in the low range of operating Reynolds numbers and, therefore, unsuitable for further development. (See Section 2.2 for discussion of early testing.)

However, the three blade configuration continued to indicate superior stability and start-up characteristics. The VARCS provided more than

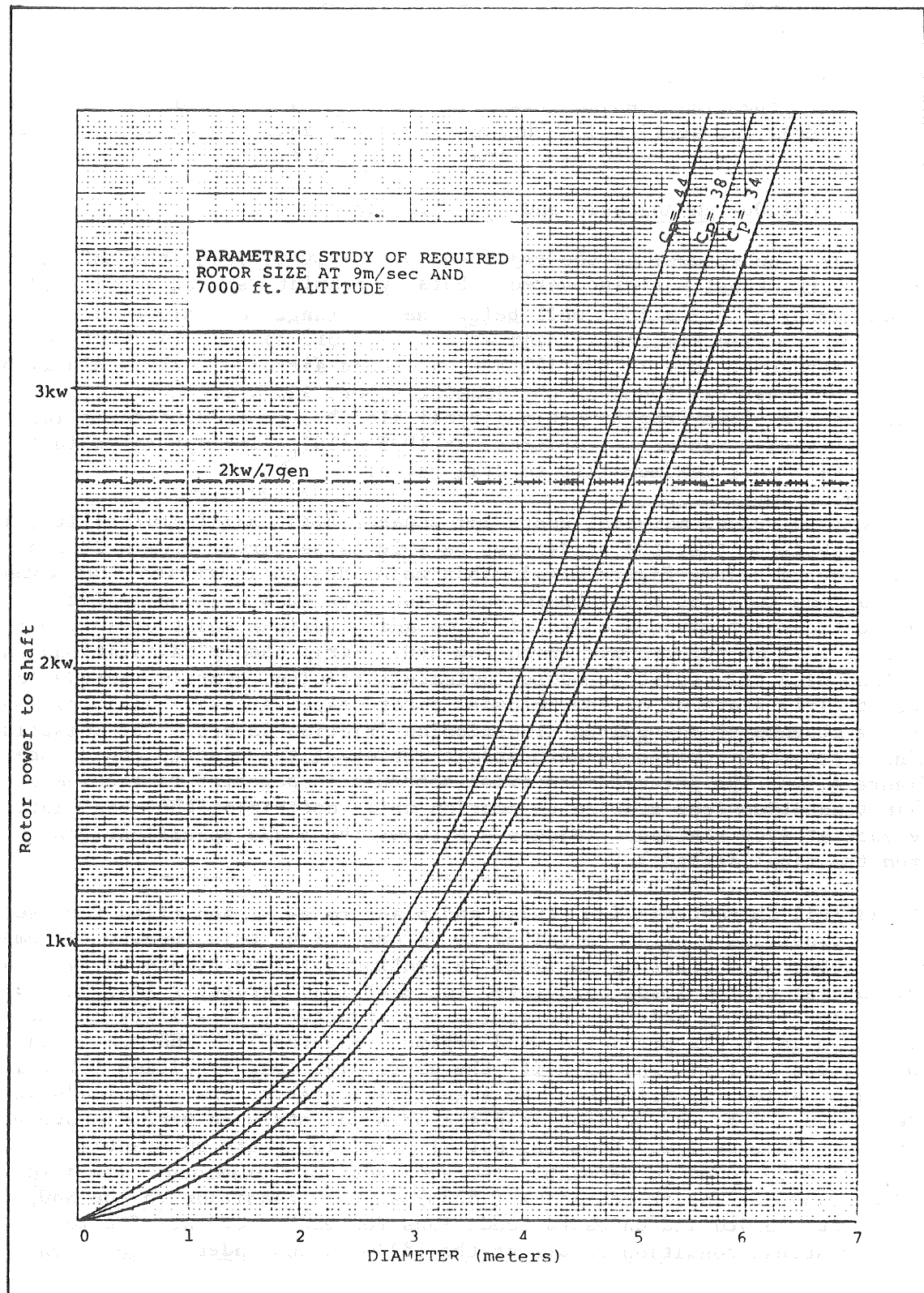


Figure 4.1
Parametric Study of Required Rotor Size

adequate control and safety so that the blades remained fixed in pitch. Further work was done in order to specify the actual blade twist schedule and planform.

As a result of the first four months of rotor design work, the primary elements of the final design were selected for analysis and testing. Design criteria for application throughout the balance of the program were identified and made the focus of the design effort.

4.2.2 Final Design Analysis and Specification

In research subsequent to the rejection of the GU airfoil, the N60 airfoil with 12% thickness was discovered. Data by Schmidt² showed a critical Reynolds number of 6.3×10^4 , well below the low range for this blade of 11.0×10^4 . (See Figures 4.2 and 4.3 for airfoil data.) In order to make up the structure lost in the 12% N60, a second airfoil -- the G 625 with a 20% thickness was found in the Schmidt report and used in the first third of the blade length. This airfoil also has good characteristics at low Reynolds numbers -- critical at 10.5×10^4 , although it exhibits a somewhat lower maximum lift to drag ratio.

In order to reduce material costs and enhance blade manufacturability, it was established that the blade must be able to be carved from a 2" x 8" lumber section (see Figure 4.4.) This major design criterion restricted the maximum twist at the inboard stations. The G625 section is fit in the section with maximum chord of 20 cm and a maximum twist of 13° , permitting 12.5° at the transition to the N60. Strip theory calculations on a blade with this twist schedule indicate sufficient starting torque to permit early start up of the unloaded rotor, especially in consideration of the absence of any geared transmission friction losses. The twist is linear around a continuous aerodynamic center at the quarter chord (see Figure 4.5.) The intermediate twist schedule is selected to achieve a fair transition from station to station while optimizing the axial interference at each station. (Figure 4.6 shows the blade specifications from the final design.)

The airfoil characteristics, twist and planform were then filed for use in the crossflow program described in Volume III of this report. A complete rotor load chart is included in Section 3.3 (see Figures 3.3a-d) and the largest of the loads calculated for each load parameter (m_1 , m_2 , m_3 , f_1) is analyzed in order to determine the structural capability of the blade design in the predicted wind regime. Figures 4.7 and 4.8 detail this stress analysis and identify the particular load condition for which the calculation is performed. No significant static torsional loads were identified. Also, no serious in-plane or shear stresses were discovered for this blade design. However, out of plane loads are substantial and stresses were found to be high. Two sections were examined: the root (.238m) and the one third radius (.823m) at the transition to the N60, under both loaded and unloaded conditions for each section. The most serious stress condition occurs at the .827m radius under no-load condition

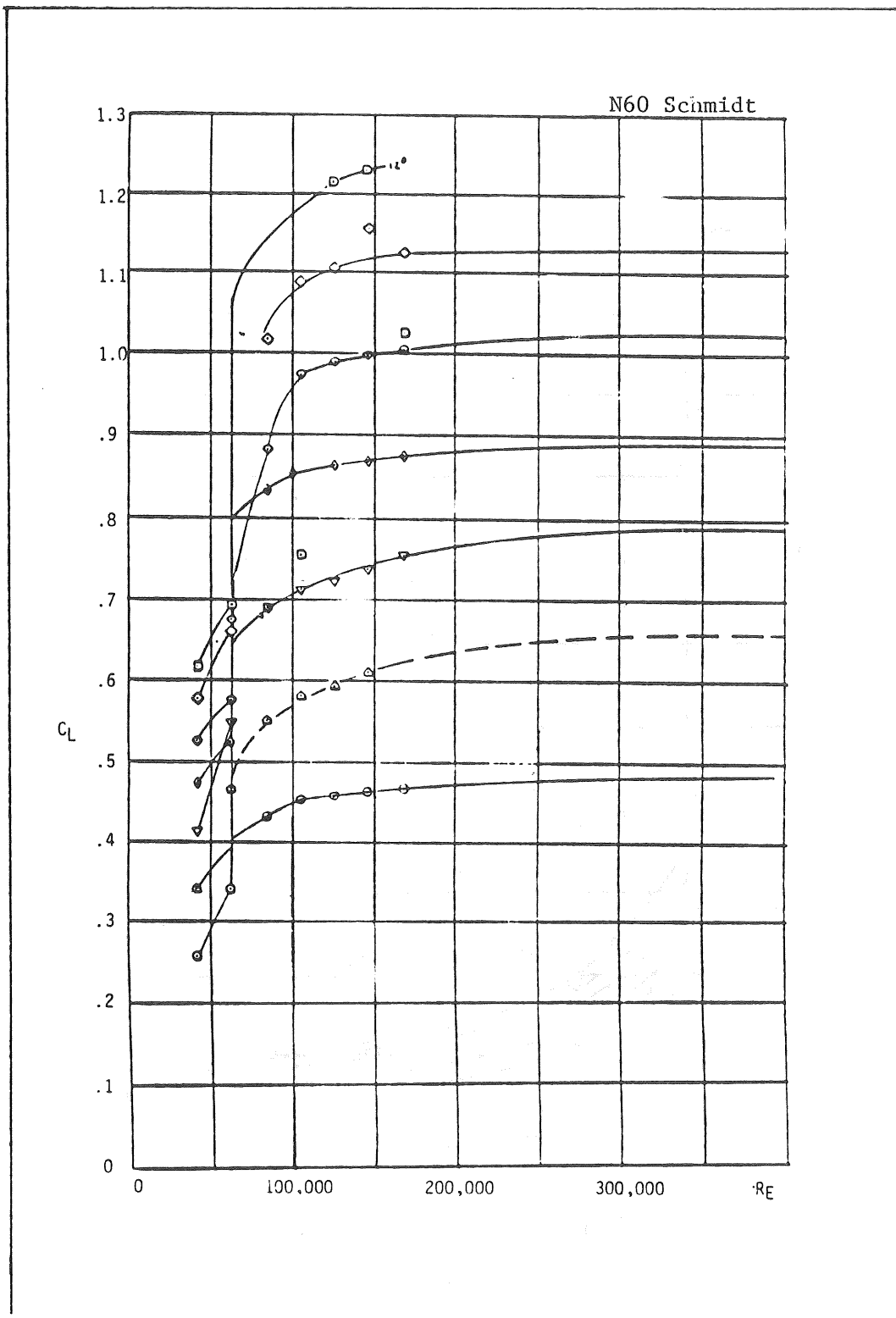


Figure 4.2

Variation of Lift Coefficient with Reynolds Number for the N60 Airfoil

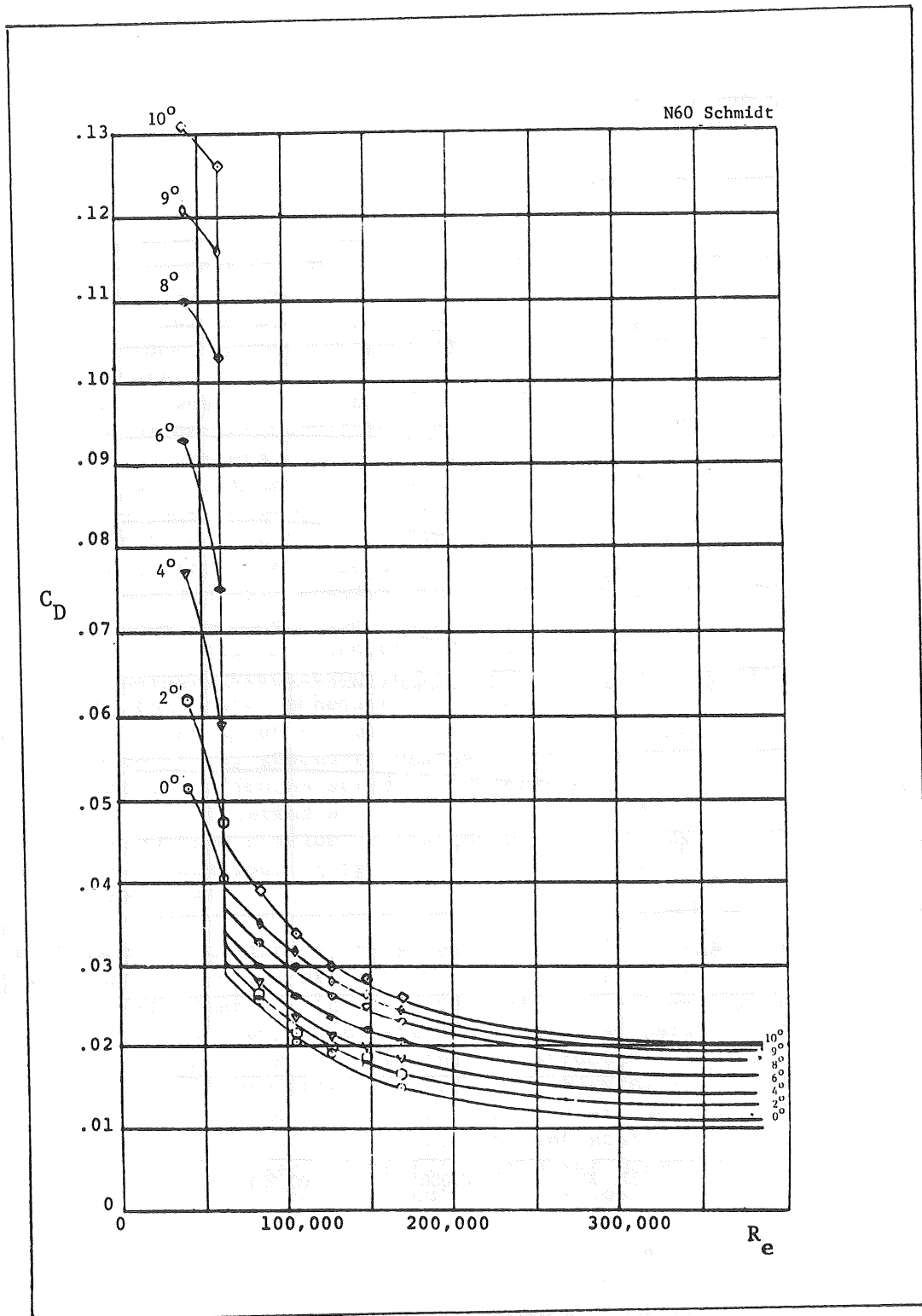


Figure 4.3

Variation of Drag Coefficient with Reynolds Number for the N60 Airfoil

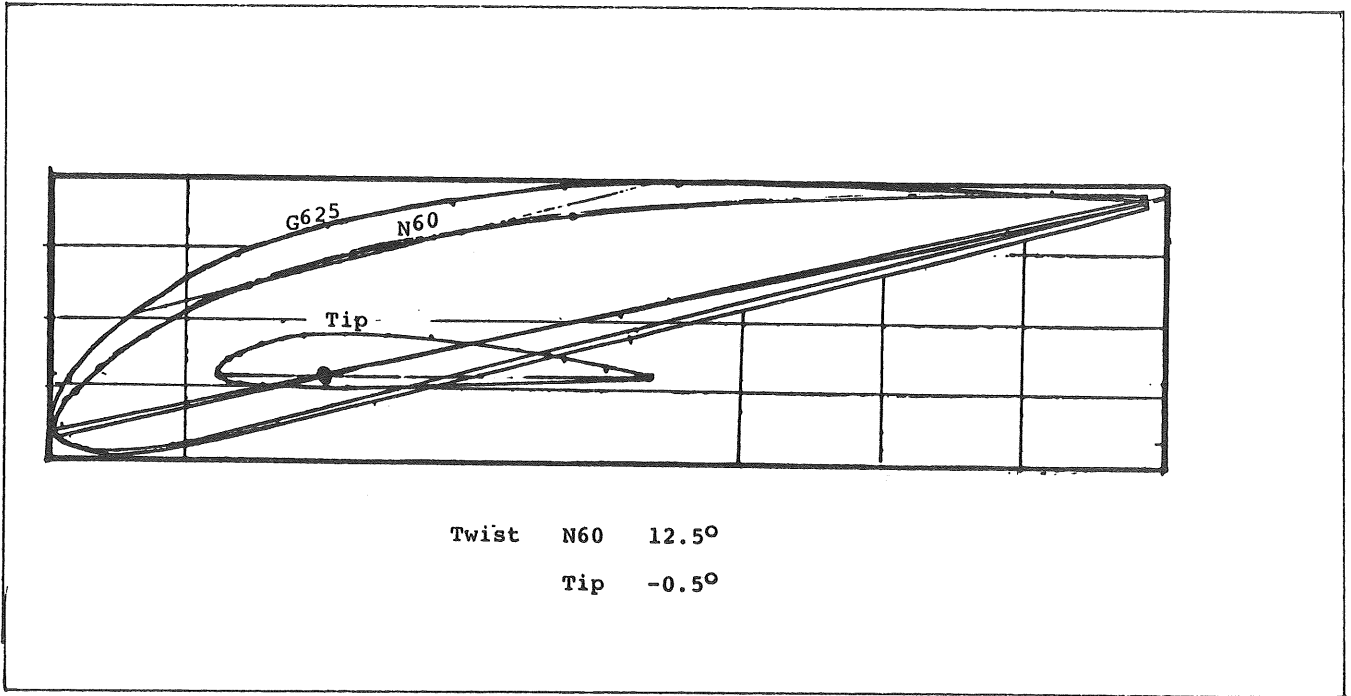


Figure 4.4
Blade Airfoil Sections

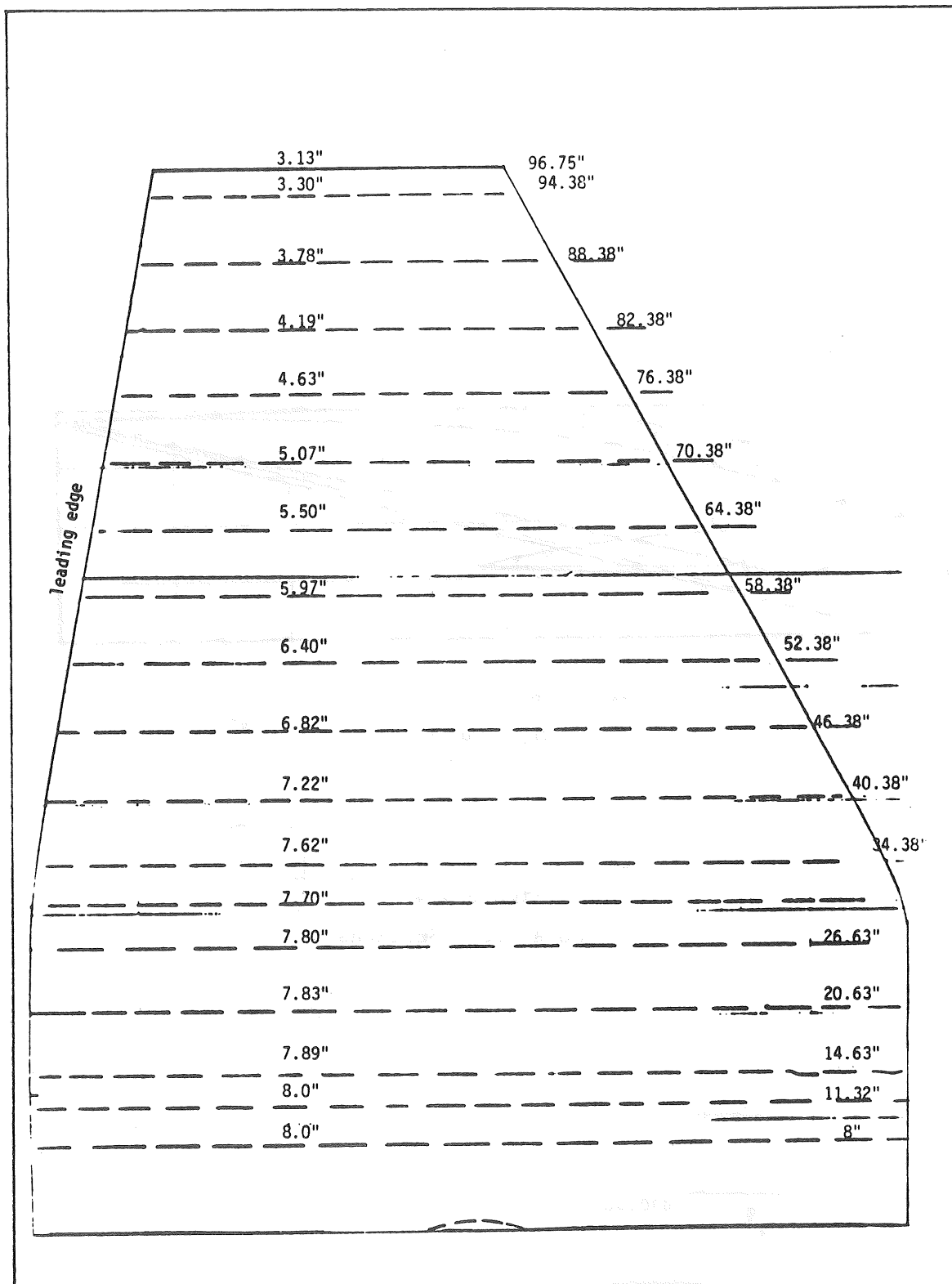


Figure 4.5
Foreshortened 5-M Blade Blank Profile (Bottom View)

Figure 4.6
Blade Specifications

Airfoil #2

r/R -- .238m to .823m (30% radius)
Type -- GU25
Section -- 20% of chord length
Critical Reynolds
Number -- 10.5×10^4

Airfoil #1

r/R -- .823m to 2.5m
Type -- N60
Section -- 12.5% of chord length
Critical Reynolds
Number -- 6.3×10^4
L/D max. -- 56 @ 10° angle of attack
 C_L max. -- 1.25
 C_D max. -- .01

Twist -- Non-linear to approach $\alpha = .33$

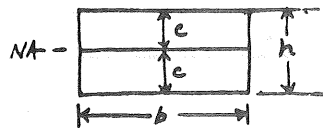
Plan Form

Taper -- Linear 20cm (8") to 8cm (3.1")
Span -- 2.3m
Aspect ratio -- 19.7
Solidity -- 4%
Tip -- Hoerner #2

Figure 4.7
Blade Stresses (Loaded)

Blade stresses will be examined at the blade root ($r = .238m$)
at the termination of the structural section ($r = .823m$).

Blade Root: The section here is rectangular.



$$I = \frac{bh^3}{12} = \frac{8bc^3}{12} = \frac{2bc^3}{3}$$

$$C/I = \frac{3}{2bc^2}$$

Bending Stress¹ = MC/I .

At the root, $b = 6.00"$, $h = 2"$, $c = 1"$.

Type of Bending	Maximum Moment ²	C/I	Bending Stress	Safety ³ Factor
In Plane	229.9 N-m = 2023 in. lb.	.083	168 psi	6.0
Out of Plane	-1290 N-m = 11417 in. lb.	.250	2854 psi	3.6

Shear

Maximum Shear = 701 Newtons = 157.5 lbs.

Cross-sectional Area = 1-.5 in.²

Thus, shear stress = 15 psi \perp to the grain.

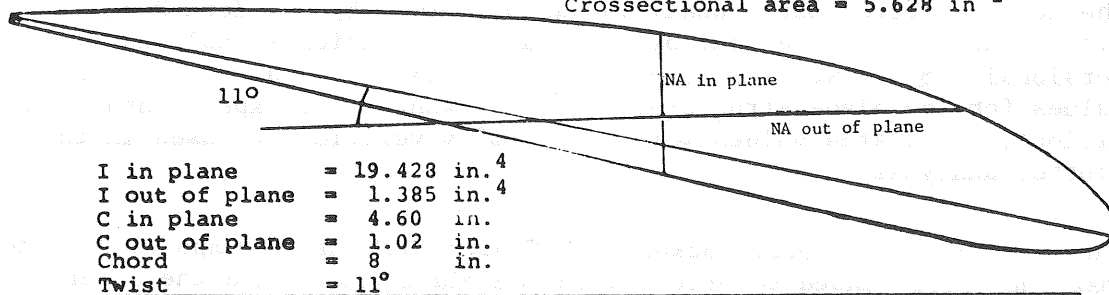
1. Centrifugal loads not included in stress calculations.
2. Maximum Moments: Based on a gust factor of 2.25 at a mean windspeed of 20 m/s and pitch angle of 60° with rotor loaded operation at 200 RPM.
3. Safety Factors: Based on modulus of rupture of 10,200 psi (Sitka spruce at .4 ± .01 specific gravity).

Figure 4.8
Blade Stresses (Loaded)

Stress¹ at $r = 0.823m$:

The neutral axes of the N60 section have been determined and are sketched below.

Crosssectional area = 5.628 in²



I in plane = 19.428 in.⁴
 I out of plane = 1.385 in.⁴
 C in plane = 4.60 in.
 C out of plane = 1.02 in.
 Chord = 8 in.
 Twist = 11°

Type of Bending	Maximum Moment	C/I	Bending Stress	Safety Factor ⁴
In Plane ²	137.5 N-m = 1210 in-lb	.237	287 psi	35
Out of Plane ³	-275 N-m = -2435 in-lb	.737	1728 psi	5.9

Shear

Maximum Shear Force = 335 Newtons 75.0 lb.

Shear = 35.2 psi ⊥ to the grain.

1. Centrifugal loads not included in stress calculation.
2. Maximum Moments: Based on a gust factor of 2.25 at a mean wind speed of 20 m/s and pitch and of 60° with rotor loaded operation at 200 RPM.
3. Maximum Moments: Based on a gust factor of 4.5 at a mean wind speed of 8 m/s and a pitch angle of 10° with rotor loaded operating at 250 RPM.
4. Safety Factors: Based on modulus of rupture 10,200 psi (Sitka spruce .4 ± .01 specific gravity).

when the rotor is subject to gust factors of 4.5 at a mean wind speed of 8m/s (see Figure 4.9). In light of this condition, we have moved the transition point further out the blade radius to reduce the cantilever and provide more material for structure at the inner radius.

An analysis of the blade was performed in order to determine the point at which centrifugal failure of the Sitka spruce blade would occur. This analysis indicated that the RPM at failure proved to be very high (2170 RPM), well above the speed of which the rotor is capable under the most extreme conditions.

The detailed aeroelastic analysis was performed by Dr. John Dugundji of MIT. Blade frequencies out of the plane of rotation (8 Hz) and torsional (28 Hz) were measured. Dr. Dugundji also calculated these values for the blade structure. With allowances for experimental conditions, calculated values were empirically verified and used in the flutter analysis.

Truck tests of the rotor locked at 90° pitchback in a 50 mph wind indicated that the rotor tended to orient with one blade upwind and the other two swept back. Correcting the blade semi-chord for this swept back position (60° off perpendicular to the wind) and using the torsional frequency 28Hz the calculated flutter wind speed for the blade was 287.5 mph, well above the maximum design condition for this rotor. Dr. Dugundji also performed an analysis of the bending frequencies for a Unarco-Rohn 45 GSR guyed tower specified for this system. The first and second tower bending frequencies were graphed with the first and second out-of-plane blade bending frequencies, correcting for the effect of rotational speed on blade stiffness (see Figure 4.10.) The analysis indicated no potential interaction of rotor forcing functions and/or system frequencies.

Figures 4.11 and 4.12 describe blade coating properties and leading edge protection selected by NWPCo. The one-part moisture-permeable polyurethane coating has been used successfully for blade surface protection by NWPCo in its Eagle manufacturing program. It meets all its specifications and offers extreme ease in application. The leading edge tape is used commonly for helicopter rotors. NWPCo's experience in its truck testing program has confirmed its excellent adhesion and extraordinary abrasion resistance.

4.2.3 Final Design Testing and Verification

Due to the rotor pitch method of speed control, available analytical models of rotor performance were not adequate. A dynamics review was held at NWPCo to develop a theoretical model for predicting rotor loads and performance throughout the pitch range. In addition, an ambitious test program was proposed to verify the adequacy of the applied theory, to confirm the values used to design the pitch control spring and to develop test data on the system dynamics. This test program was carried out in two

Figure 4.9
Blade Stresses (Unloaded)

Stress at r - .823m (airfoil transition)

Maximum loads have been calculated for a mean windspeed of 8 m/s and a pitch angle of 10° with the rotor unloaded operating at 455 RPM.

<u>Type of Bending</u>	<u>Maximum Moment*</u>	<u>C/I</u>	<u>Bending Stress</u>	<u>Safety Factor*</u>
In Plane	213 N-m = 1,884 in-lb	.237	446.5 psi	22.87
Out of Plane	1146.4 N-m = 10,139 in-lb	.737	7472 psi	1.36

Shear

Maximum shear force = 1299 Newtons = 292 lb

Crosssectional area = 10.5 in²

Thus, shear stress = 27.8 psi \perp to the grain.

Maximum Moments: Based on a gust factor of 4 at a mean windspeed of 8 m/s and a pitch angle of 10°.

Safety Factors: Based on modulus of rupture 10,200 psi (Sitka spruce .4 ± .01 specific gravity). Centrifugal loading not calculated.

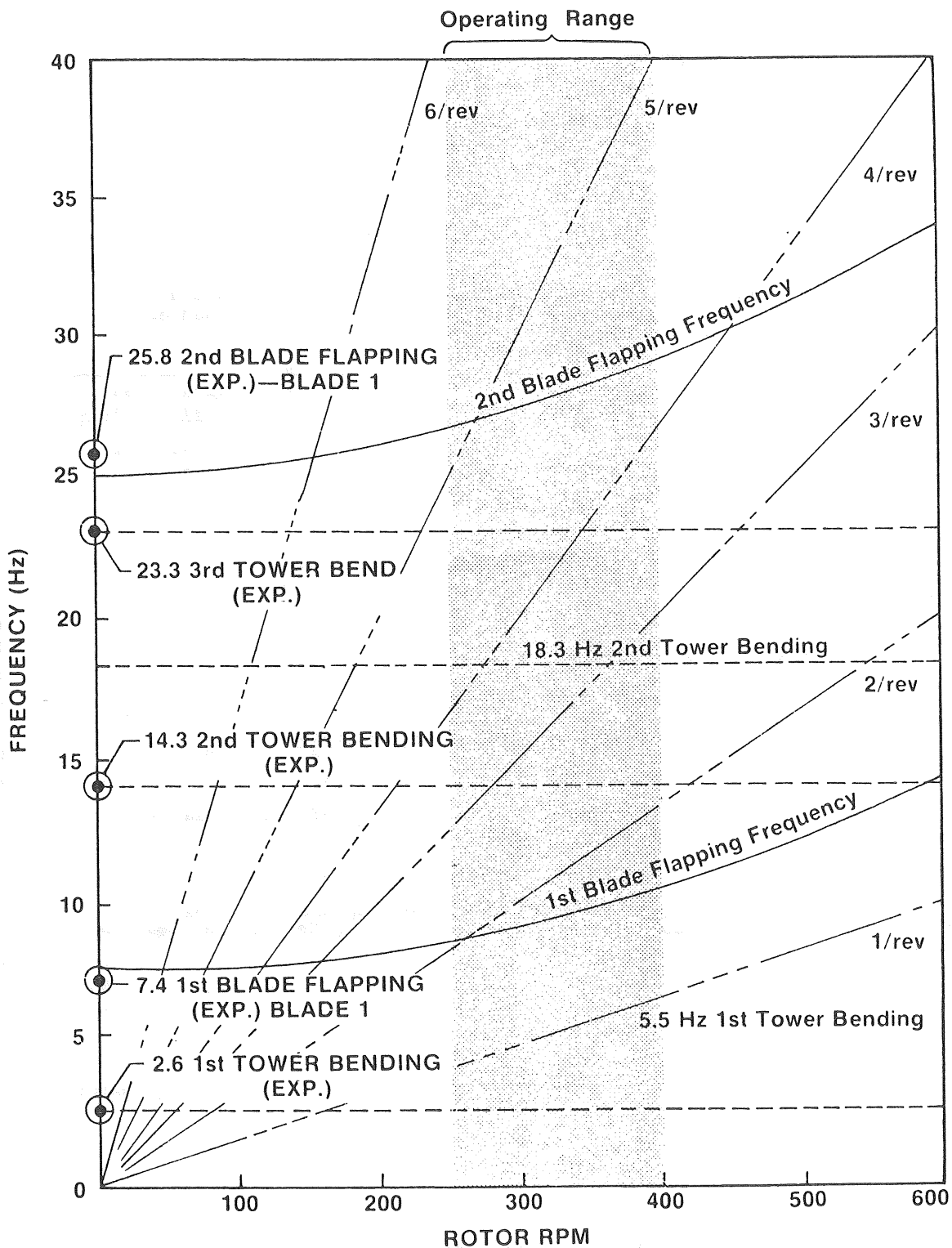


Figure 4.10
Campbell Plot for NWPCo 2kw SWECS

Figure 4.11
Blade Coating

<u>Type</u>	One part polyurethane
<u>Application</u>	3 coat spray
<u>Characteristics</u>	Excellent salt spray resistance Excellent abrasion characteristics Good impact resistance Excellent bond to wood
<u>Experience</u>	Used in North Wind Eagle remanufacture In-house abrasion tests with sandblast Experience in truck tests confirms manufacturer's claims

Figure 4.12
Leading Edge Protection

<u>Type</u>	Scotch 3M Abrasion-resistant Film .012" thick
<u>Application</u>	Self-adhering
<u>Characteristics</u>	Excellent abrasion resistance (aircraft leading edge protection) Excellent solvent resistance UV resistant
<u>Experience</u>	In-house sandblast test showed no wear. Truck test experience indicates outstanding durability and ad- hesion.

series on a moving test bed (a truck). The first of these was designed to measure rotor power throughout the pitch range and at varying tip speed ratios. Simultaneously it was intended that this test would measure the force at the hinge pin to be opposed by the spring in order to maintain desired rotor output.

For the test bed a 1½-ton Dodge 4x4 surplus military weapons carrier was selected. This vehicle provided a substantial support for the test structure, with four wheel drive, a winch and an enclosed bed. A tiltable Rohn 25G tower was mounted on the front bumper to support the SWECS sixteen (16) feet above the ground. An anemometer boom extended eight feet ahead of and four feet to the side of the truck. All instrumentation, inverters, field controls and loads were operated by test personnel in the rear cab. (See Figure 4.13.) Rotor pitch was fixed using a BLH load beam at which bending strain was measured. (See Figure 4.14.) With this facility the rotor pitch could be fixed for a test run during which loads and/or current could be varied to vary tip speed ratios. Wind speed and direction relative to the truck were measured, alternator field and line voltage and amperage were measured, and rotational speed and bending strain at the load beam were measured. All these parameters were recorded on an eight channel strip chart.

The second series used this same test bed to assess operational speed control system performance and observe system pitch dynamics. In this series the measurement and recording of pitch angle was substituted for load beam strain. Results from this load beam data and this second series will be reviewed in a later section.

At the dynamics review it was determined that maps had to be developed of the rotor coefficients of power and coefficient of thrust as a function of tip speed ratio. It was decided to use the work of Lissaman and Wilson as a starting point and modify the analysis to account for extreme cross flow angles. This is accomplished by applying the crossflow angle to recompute the resultant angle of force (θ) for each of the blade stations and azimuthal positions requested. (See Figure 4.15.) Figure 4.16 shows the resulting C_p map for our final rotor design across the full operating range of tip speeds and for each representative pitch angle. (Rotor thrust calculations and the C_t map will be discussed in Section 4.4.)

The desired pitch angle was fixed and the test was run at a selected wind speed within the operating range for that pitch angle. For each angle during a run, the alternator field circuit excitation was varied. This technique permitted variations of tip speed ratio and duplication of data points from dynamometer tests of the alternator. This test was necessary to determine rotor power output for calculation of C_p . Figure 4.17 is a sample test run at 10° pitch. Each track is identified at the left. Note the effect of varying field resistance on line voltage and current and on rotational speed (RPM). This run was taken at approximately 15 mph. Vertical lines outline data points. The data record shown took slightly over three minutes.

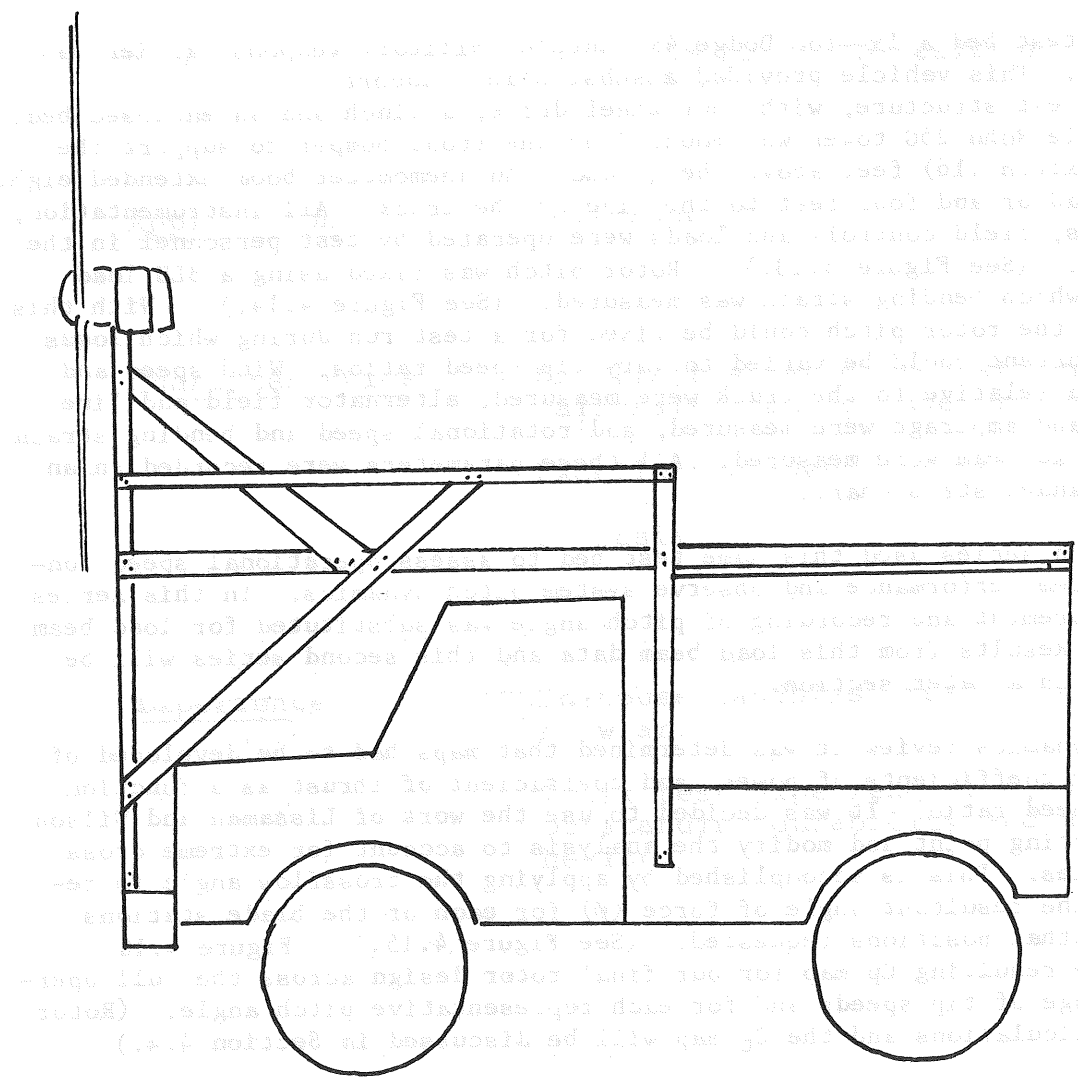


Figure 4.13

Truck Test - Preliminary Support Structure

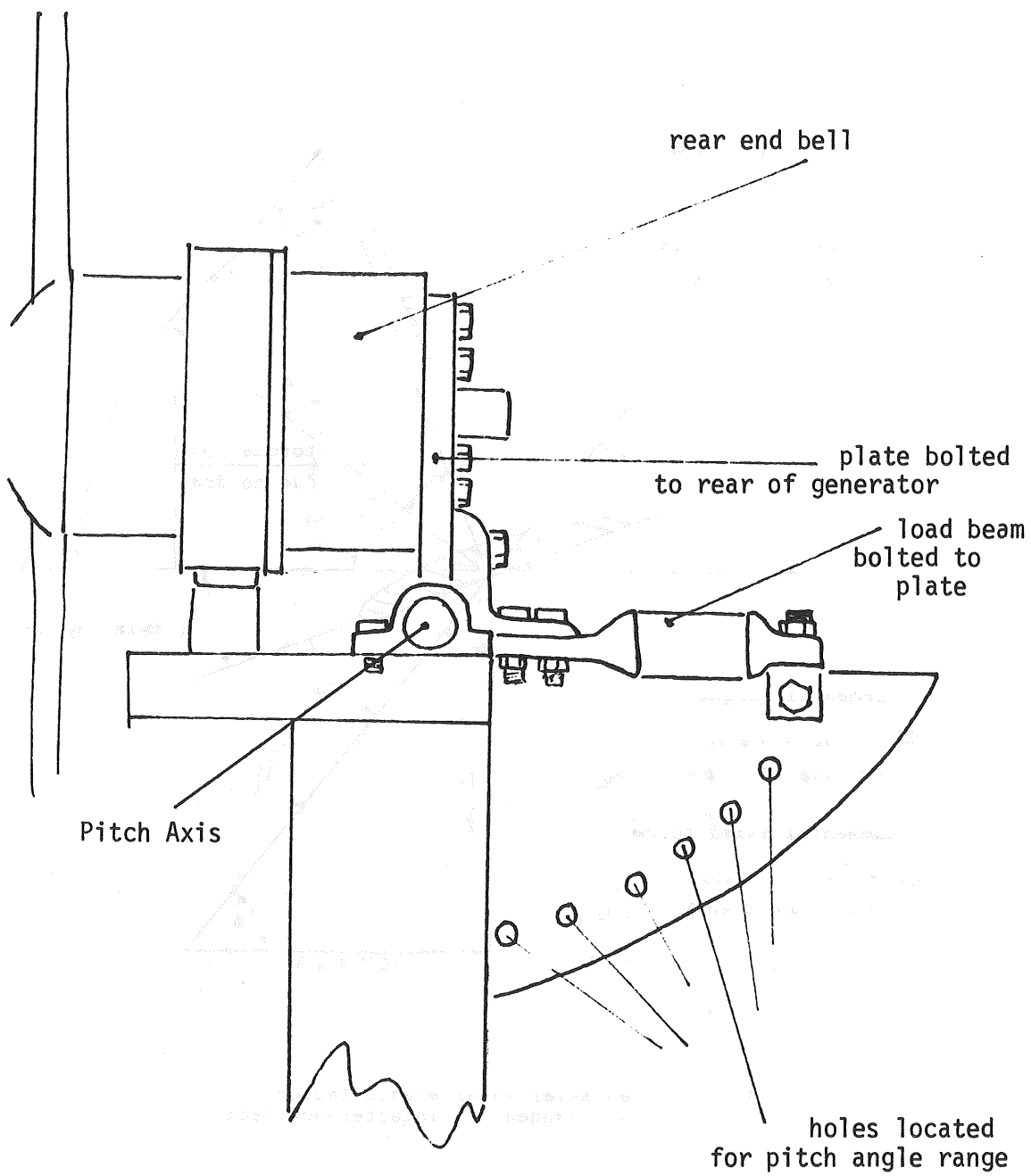


Figure 4.14
 Truck Test - 2kw VARCS Moment Calibration Device

- 1) $\beta = \psi - \alpha$
- 2) $\beta + \theta_\tau + \alpha = 90^\circ$
- 3) $\theta_\tau + \alpha + \gamma = 90^\circ$
- 4) $\therefore \theta_\tau + \alpha = 90^\circ - \gamma$

Substitute 4) into 2)

$$\beta + 90^\circ - \gamma = 90^\circ$$

$$\therefore \beta = \gamma$$

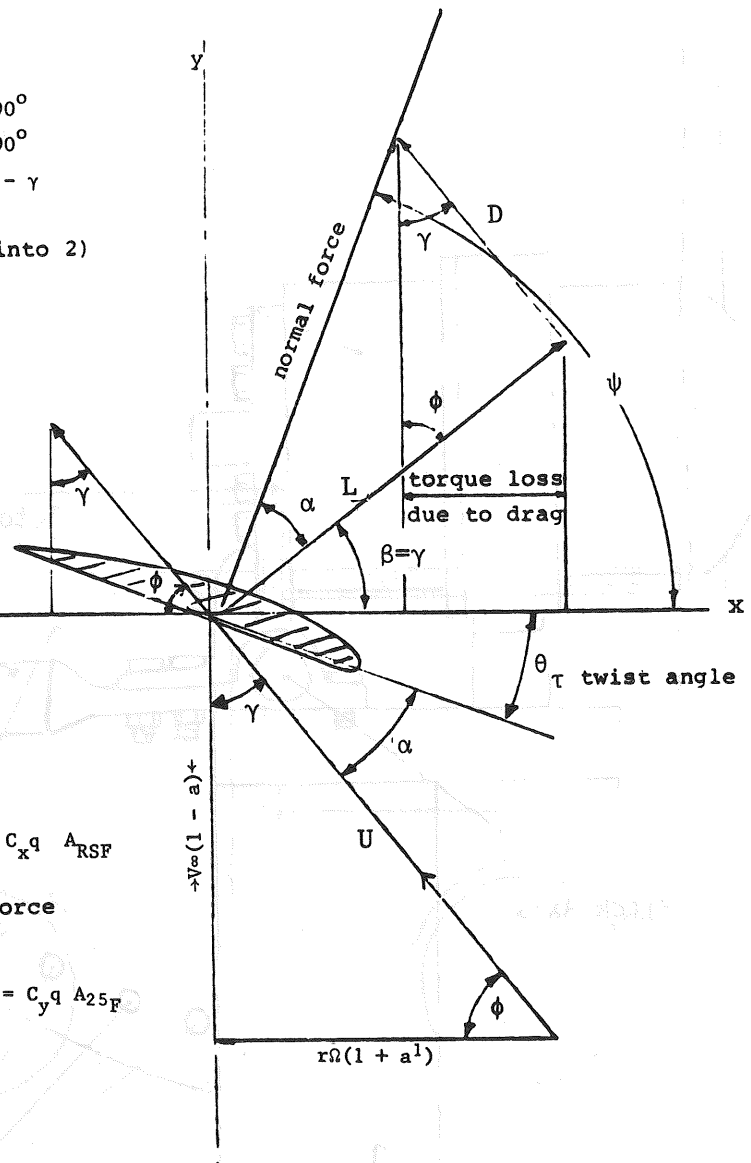
$$\gamma + \phi = 90^\circ$$

Elemental torque

$$\begin{aligned} \frac{\Delta Q}{\tau} &= L \cos \gamma - D \sin \gamma \\ &= L \sin \phi - D \cos \phi = C_x q A_{RSF} \end{aligned}$$

Elemental axial force

$$\begin{aligned} \Delta AF &= L \sin \gamma + D \cos \gamma \\ &= L \cos \phi + D \sin \phi = C_y q A_{25F} \end{aligned}$$



a = axial interference factor
 a' = tangential interference factor

Figure 4.15

Blade Element Force Diagram

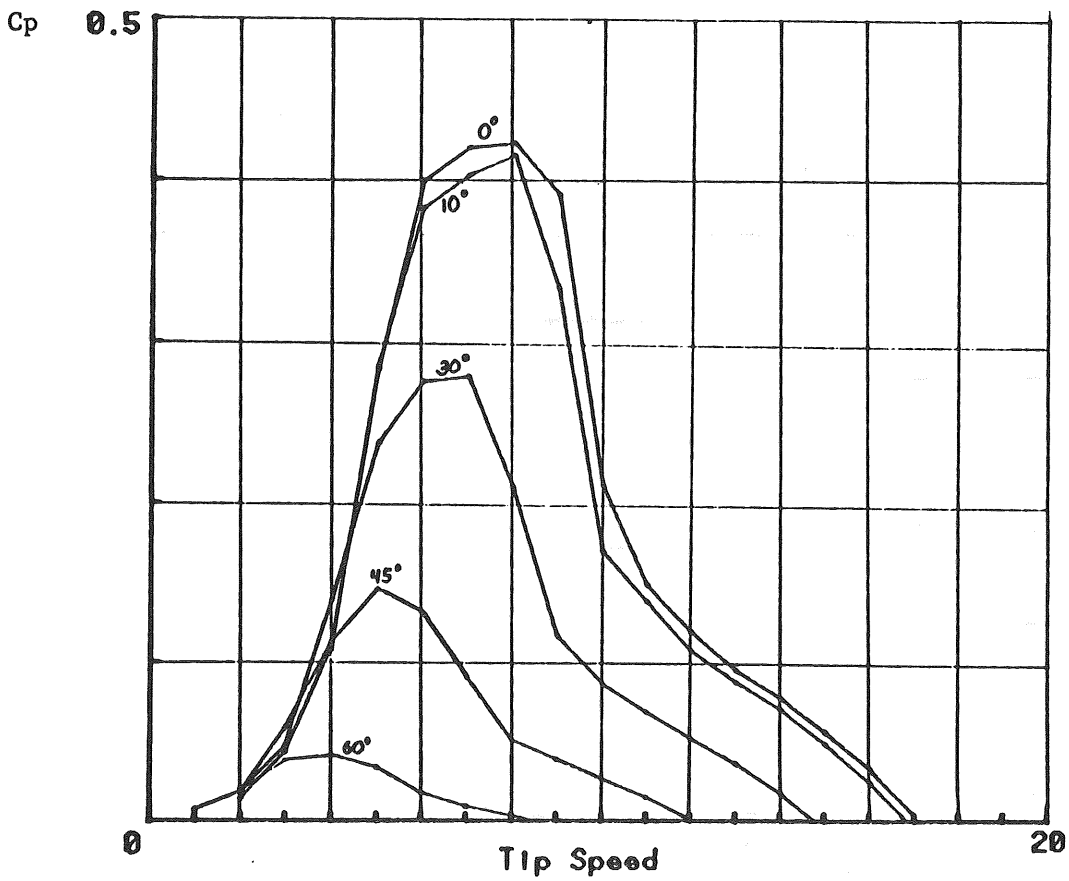


Figure 4.16
 Power Coefficient Vs Tip Speed Ratio at Various Pitch Angles for Rotor #7

Overtuning Force
205 in-lb/ division

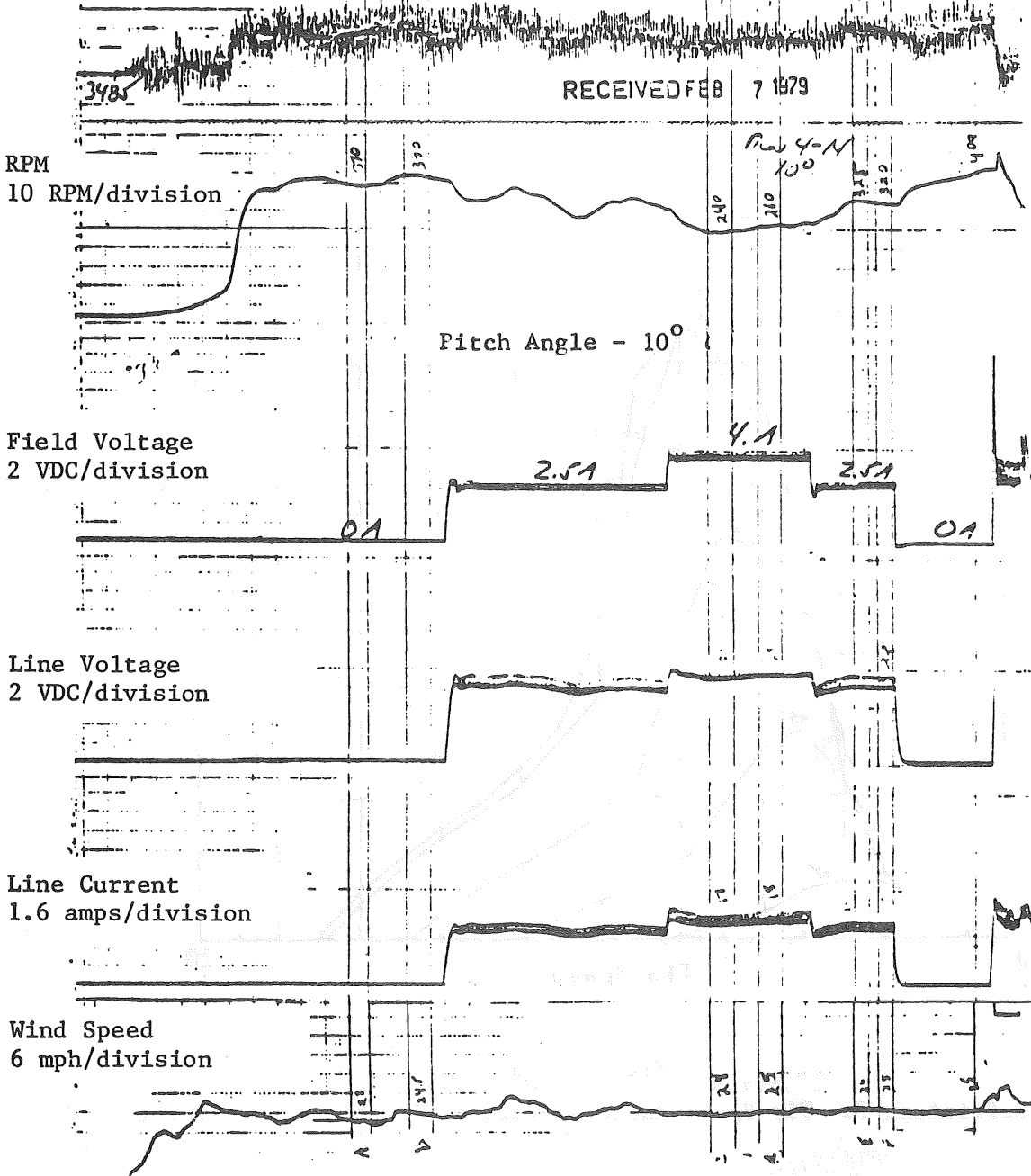


Figure 4.17
Sample Data

Figures 4.18 through 4.22 present rotor performance data points overlaid on the theoretical performance curve of the rotor for that rotor pitch angle. These five angles were chosen as representative. The minimum angle that insured safe tower clearance was 10° . The maximum angle at which power could be generated was 70° . In fact NWPCo was unable to sustain field current at this angle without losing rotational speed.

Although severe test conditions (temperatures below 0°F) limited the total samples taken, the rotor data that was procured exhibits excellent repeatability, not just from run to run, but from day to day, and it exhibits sufficient consistency to draw some important general conclusions about the effectiveness of this model in predicting the performance of wind turbines in extreme crossflow.

In general, the rotor appears capable of extracting somewhat more power than Lissaman and Wilson predict. This conclusion must be tempered by the observation that a wind speed correction factor applied to the 10° data will bring the data points into the curve. However, this same factor does not correct the data at higher pitch angles. The truck itself may have caused a disturbance of the flow field so that the anemometer read a lower wind speed than the rotor saw. The larger discrepancies at high pitch angles definitely indicate an aerodynamic effect not accounted for by the Lissaman and Wilson model.

The conclusion has been supported by truck testing of an active VARCS. In original spring calculations, theoretical rotor performance values were used to determine the necessary control spring rate. In truck tests, rotor output continued to increase beyond the pitchback angle at which predictions had indicated that it would drop off.

4.3 Electrical System Design Analysis and Testing

4.3.1 Preliminary Alternator Design Development

In its initial proposal NWPCo specified a 1-4kw low speed DC generator. Subsequent trade-off analyses indicated that a 2kw generator better suited the load requirements and offered significant cost advantages. (See Section 2.3.) Further study revealed the advantages of an AC alternator over the DC generator (see Figure 4.23.)

Once the alternator was chosen, three possible rotor configuration options existed: (1) conventional wound with laminations; (2) permanent; or (3) interdigitated. Each of these rotor options was investigated for performance, applicability to battery charging, ease of manufacture, reliability and cost. The conventional wound-type rotor was eliminated early in the analysis because of high field power requirements, difficulties in manufacture, and centrifugal forces acting upon the windings. The permanent magnet and interdigitated options both showed favorable performance, reliability and cost characteristics. Figure 4.24 is a representation of the three rotor configuration options.

Cp vs. Tip Speed @ 10° β

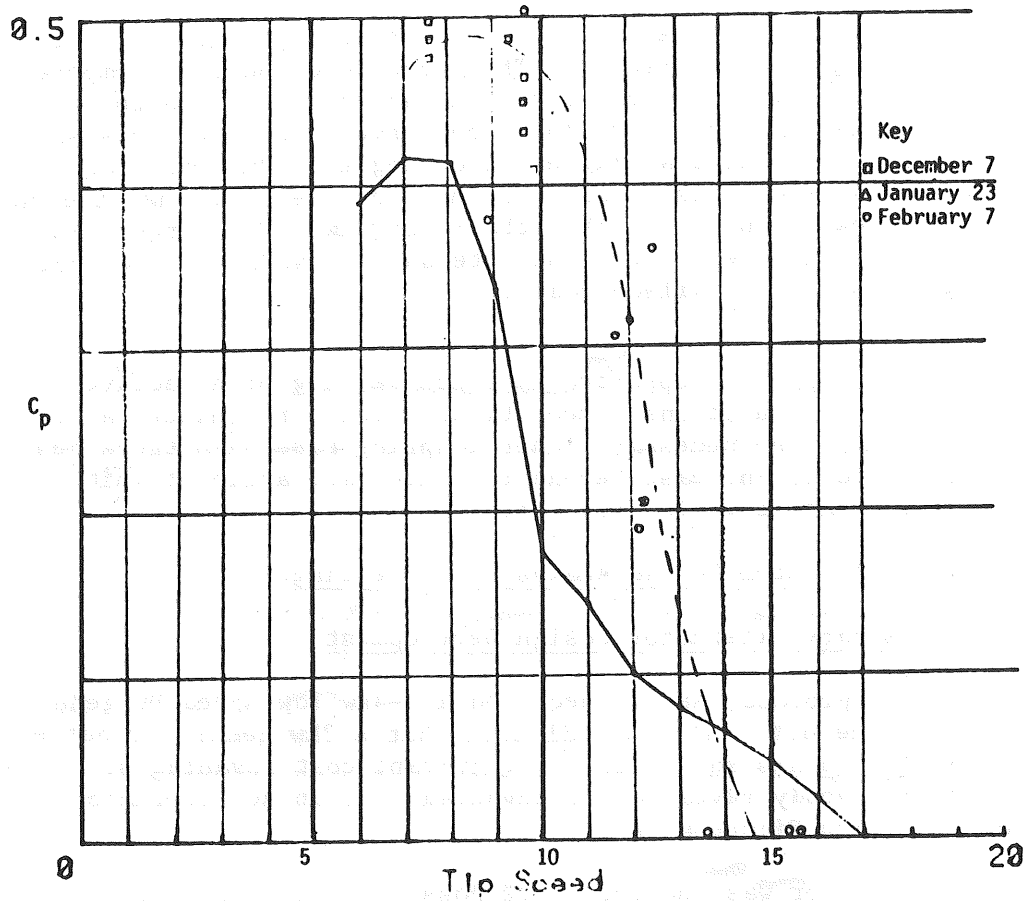


Figure 4.18

C_p Vs Tip Speed at 10° β

Cp vs. Tip Speed @ 45°β

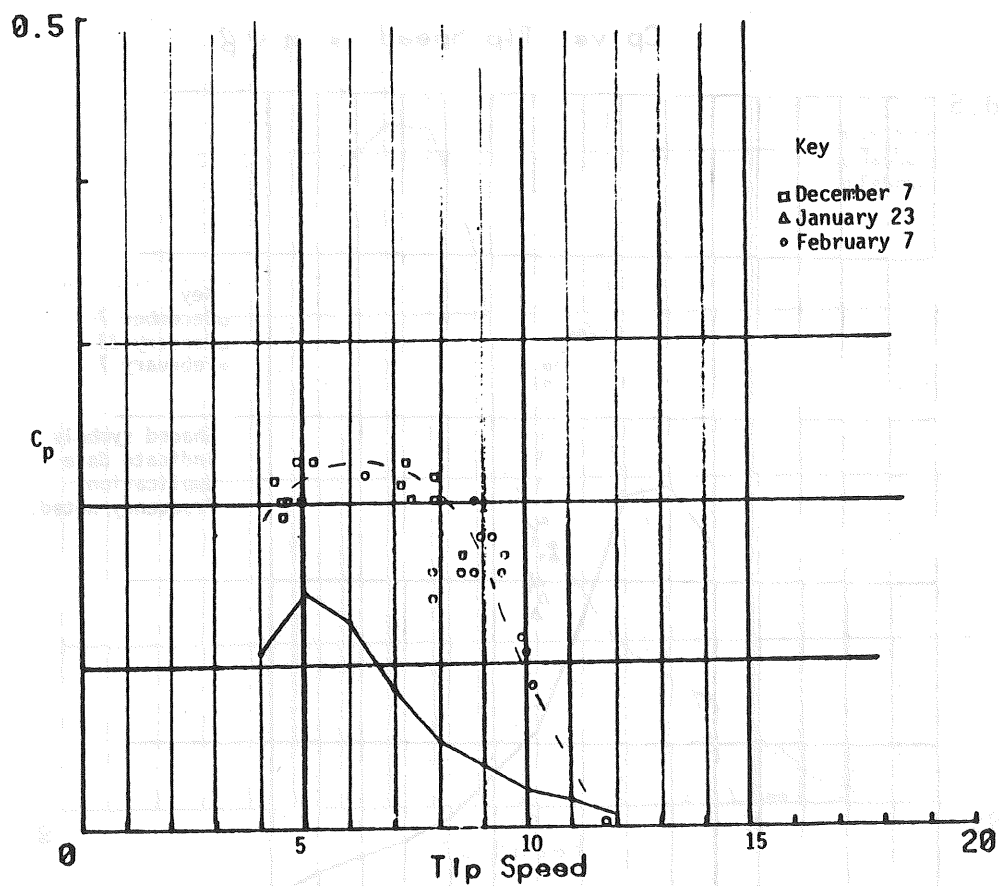


Figure 4.20

C_p Vs Tip Speed at 45°β

Cp vs. Tip Speed @ 60° β

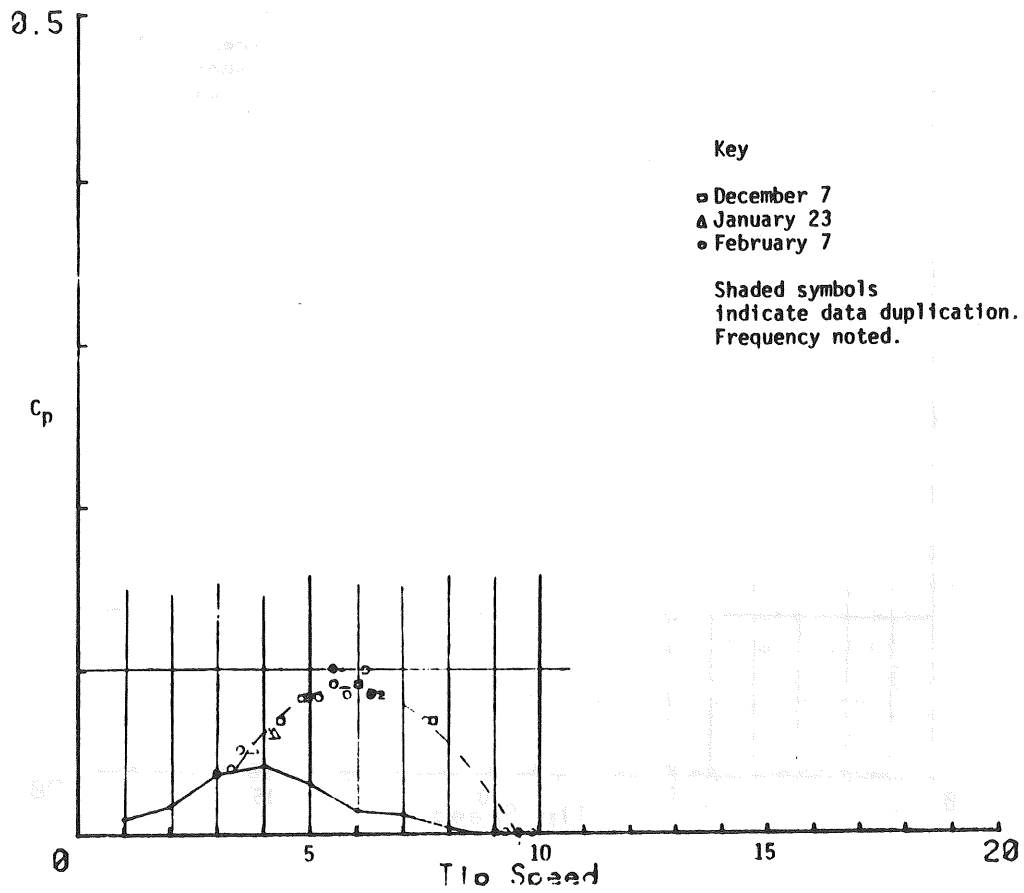


Figure 4.21

C_p Vs Tip Speed at 60° β

Cp vs. Tip Speed @ 75° β

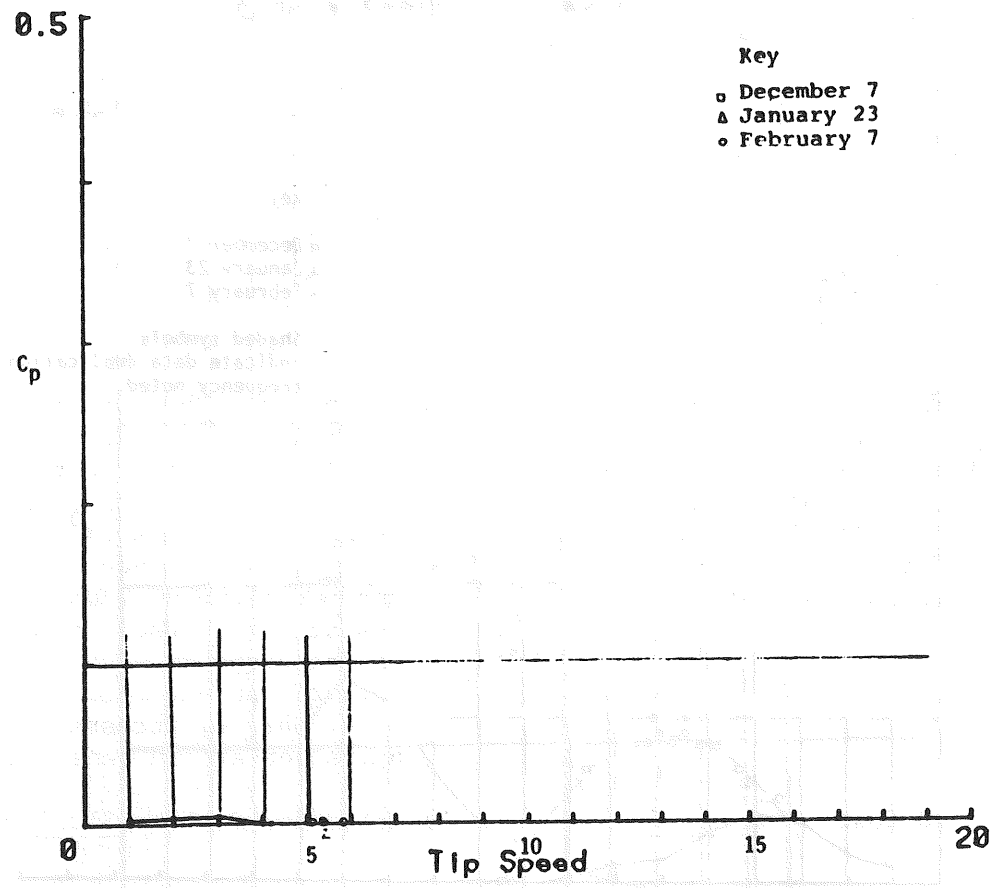


Figure 4.22

C_p Vs Tip Speed at 75° β

Figure 4.23

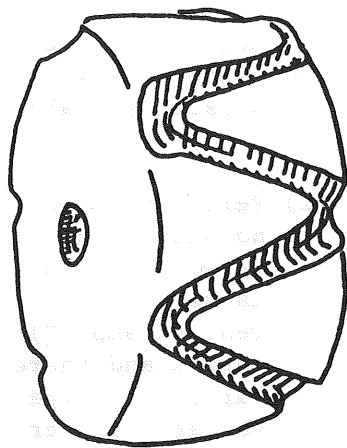
Trade-off Analysis of 2Kw DC Generator Vs 2Kw AC Alternator
with Wound, Permanent Magnet or Lundel Rotating Field

GENERATOR

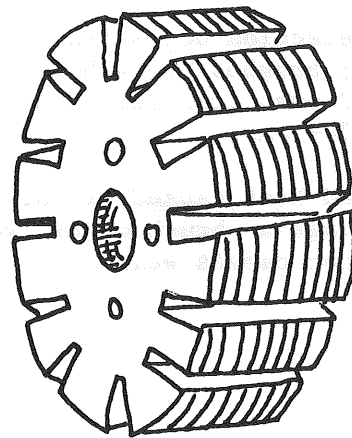
- (1) Brush selection not scientific process; brushes are subject to wear and must transfer high currents (70+ amps).
- (2) Localized heat caused by bar-to-bar voltage as brush moves over commutator causes wear.
- (3) High current in rotating armature in a low voltage machine leads to manufacturing difficulties, since heavy wire must be inserted in slots. This wire is then subject to centrifugal forces which may lead to friction.
- (4) Estimated Costs = \$1565.00

ALTERNATOR

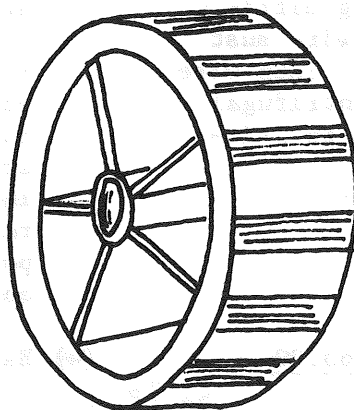
- (1) Rectifier diodes easily calculable with demonstrated reliability.
- (2) Permanent magnet requires no slip rings or brushes. If wound or Lundel rotor is used, only field current (5 amps \pm) is transferred and there are no bar-to-bar type voltage variations over the smooth slip ring surface.
- (3) Wound rotors have smaller wires in slots, but are still subject to centrifugal forces and friction. Permanent magnets eliminate wire. In the Lundel, the rotor has one coil wound around the central shaft in the shape of a solenoid, rather than one coil per pole. Hence, stresses in operation are in tension.
- (4) Estimated Costs = \$1035.00



Lundel



Laminated Rotor



Permanent Magnet

Figure 4.24
Generic Rotor Types

A trade analysis between the permanent magnet and interdigitated rotor options was conducted with the following results:

1. Permanent magnet with magnets in casting or in Lundel type casting:
 - a. Advantages:
 - No sliprings
 - Best theoretical efficiency at rated RPM
 - Variable stack length
 - No losses to field.
 - b. Disadvantages:
 - Assembly difficult
 - Difficult to magnetize
 - Cogging losses
 - Voltage - RPM curve not appropriate to battery charging without control
 - Overspeed-voltage control difficult
 - Flux density permanently reduced by temperature extremes
2. Lundel/Wound Rotor (Interdigitated):
 - a. Advantages:
 - Theoretical efficiency close to permanent magnet
 - Best voltage - RPM curves for battery charging
 - Easier regulation in overspeed conditions
 - Casting material availability
 - Ease of assembly and manufacture
 - b. Disadvantages:
 - Efficiency at rated RPM lower than permanent magnet
 - Stack diameter to length ratio limited

A wound rotor was recommended by NWPCo, as opposed to a permanent magnet rotor, due in part to the greater control of the electro-magnetic field. A mechanical speed control was designed so that a loss of load enhanced the response characteristics of the mechanism. Therefore, it is felt that control of the field was acceptable from the point of machine survival. Field control was desirable due to the low power switching demands of the field as opposed to those of the line output.

4.3.2 Final Alternator Design Analysis and Testing

NWPCo's 2kw low speed alternator is rated to produce 2.5kva AC at 32 volts rotating at 250 RPM with an alternator efficiency of 70%. The stator is a three-phase, lap-wound silicon steel laminated configuration (see Figure 4.25.) The Lundel rotor consists of two six-fingered opposing castings connected by the steel core. The interlocking fingers constitute the 12 poles of the rotor. The rotor winding is coiled around the core, therefore, not subject to shifting caused by centrifugal force. The solenoid type winding is simple and inexpensive to manufacture and in this configuration requires approximately 1/6 of the field power of a conventional wound 12 pole rotor. The system self-excites using the residual magnetism of the Lundel iron to induce a voltage in the stator. As shown in Figure 4.25, the flux path is from the positive rotor core to the positive Lundel teeth, where it jumps the clearance of 0.060 in. to the stator. The path from this point is through the stator to the negative teeth, down through the negative core

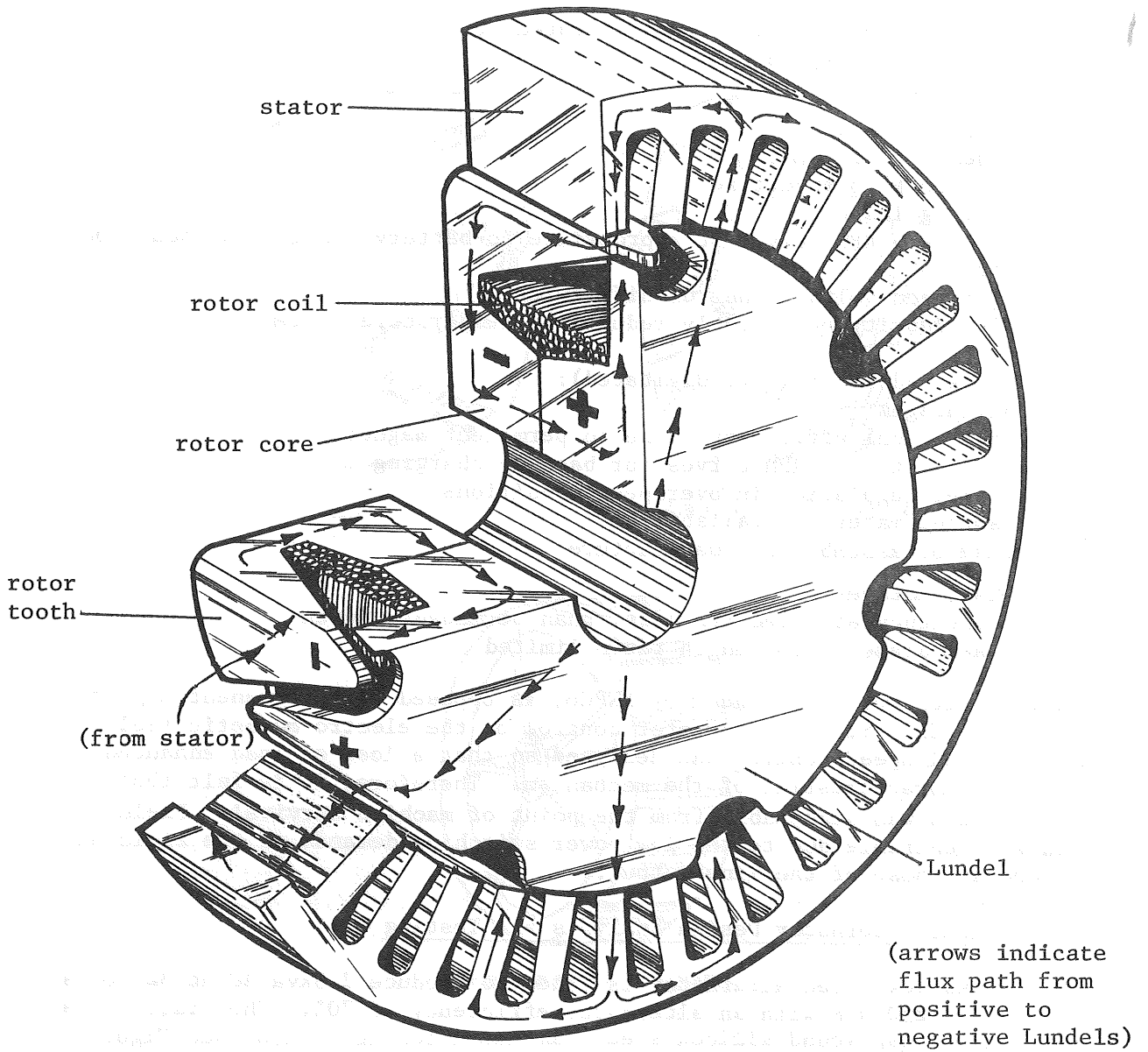


Figure 4.25
Lundel Alternator

and across to the positive core, from which it again flows to the positive teeth and the stator, etc. The machine must rotate at 200 RPM before the induced voltage can overcome the stator resistance and the forward drop of the rectifiers. The electromagnetic field will then build to 32 volts and the machine will pick up the battery load.

Most of our work has focused on the development of the alternator rotor. There is virtually no documentation of Lundel rotors in this size and speed range, so our testing program has been directed at confirming the theoretical calculations used to predict alternator performance.

NWPCo's dynamometer is a precision motoring dynamometer. The following description specifies the dynamometer as it was set up in the NWPCo shop in August 1978. The overall design of the dynamometer allows for a variety of other specifications and applications at a small expense. Figures 4.26-27 show the generalized plan and functions of the facility in two degrees of detail.

The drive section consists of a 10hp DC 0-3000 RPM motor, a 10 hp precision motor controller unit designed and built by Schulz Controls, Inc., New Haven, Connecticut, and custom instrumentation filters, amplifiers and read-outs designed, built and installed by NWPCo.

The motor controller features 0.5% maximum error speed regulation, using a tachometer feedback network. The motor drive is a nominal 10 hp drive with current (torque) limits from 30% to 150% with 3% holding accuracy. Up to 150% of torque is supplied for limited durations, with programmable time constants for error correction, load change and acceleration torque demands. The motor can be fully stalled at the 30% to 50% torque limit setting indefinitely with complete safety. Other motor controller features include motor thermal sensing and readout of all error junction signals, as well as all motor voltage and current levels through the NWPCo instrumentation system. In short, the drive section of the dynamometer is versatile in its programmability and precise in its performance and instrumentation.

An 8:1 RPM reduction is achieved using Wood's timing pulleys and belts, in two reductions. Wood's timing belt drives provide a positive, non-slip, uniform-speed transmission, wide speed range and high efficiency. This transmission was designed with a minimum 1.5 safety factor, for a rated 10 hp. The two transmission shafts--1½ in. and 1 5/8 in.--are supported by Dodge self-aligning pillow blocks. A Wood's sure-flex coupling provides a non-slip, flexible connection between the test unit and transmission shaft.

A Wertronix tachometer generator (100 vDC, 1000 RPM) is used for RPM output. Transmission from the test unit shaft is achieved using a Wood's timing belt drive with a 1:2 speed ratio.

The torque which is applied to the alternator shaft is instrumented to less than one foot-pound resolution using a hybrid system of stock BLH and custom NWPCo instrumentation modules.

The generator (alternator) under test can be monitored in synchronous, battery, or straight resistive load configurations under a wide variety of

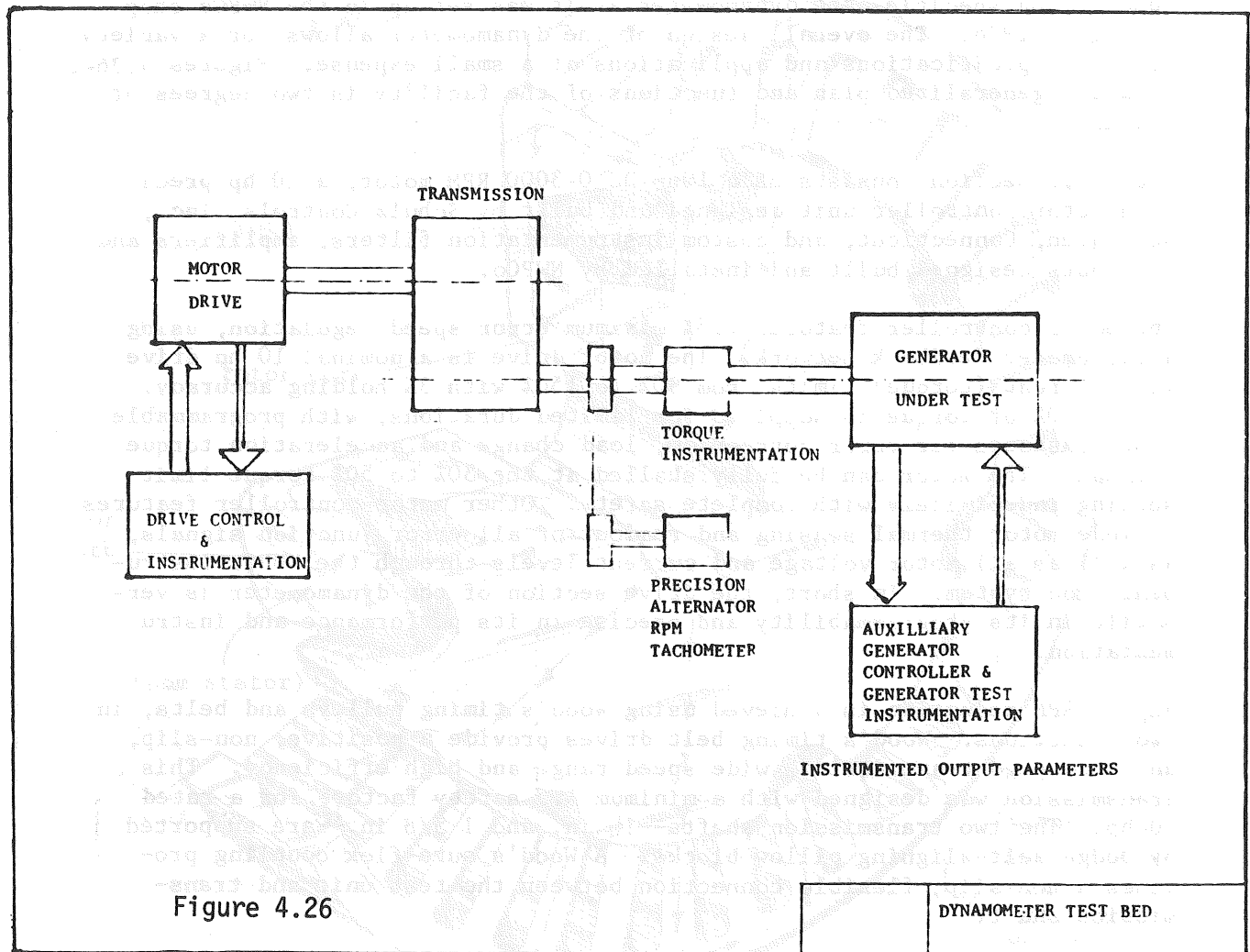


Figure 4.26

Figure 4.26

Dynamometer Test Bed

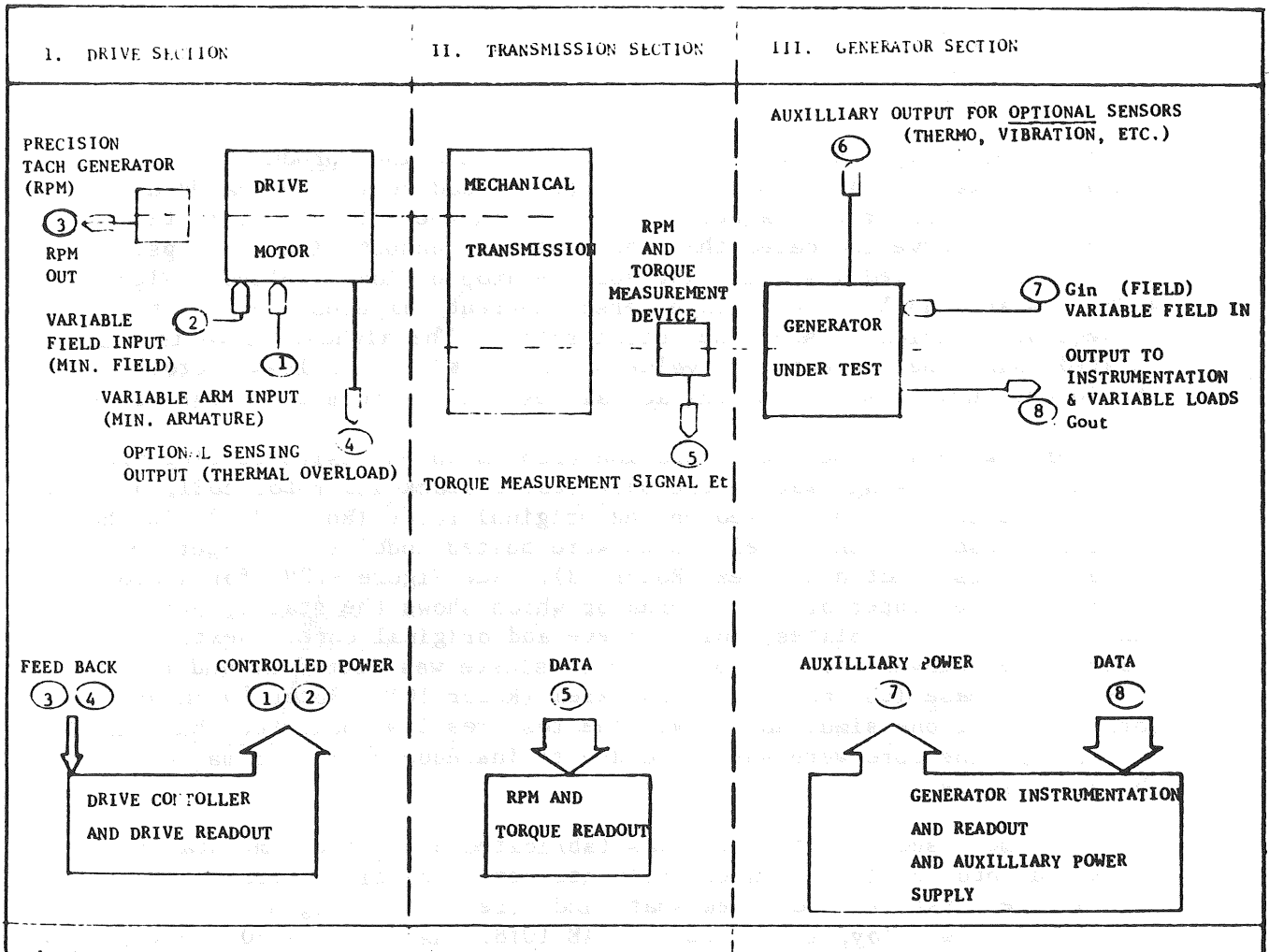


Figure 4.27
Dynamometer Test Bed

electrical loads in a self-excited or programmable external excitation configuration.

NWPCo custom instrumentation consists of analog, digital meter, oscilloscope and strip chart recorder precision monitoring of:

- 1) Output voltage
- 2) Output current
- 3) Internal temperature
- 4) Vibration
- 5) RPM
- 6) Torque input
- 7) Field output
- 8) Field current

Our first prototype failed to meet design calculations producing a maximum of 1227 watts. An examination of the no load curves indicated a premature saturation of the magnetic flux path in the rotor. The initial slope of the curve indicated that there were no unspecified air gaps. Tests also indicated a significant voltage drop of load applied. Figure 4.28 compares no load DC voltage versus current (amperes) for all the subsequent modifications of the initial rotor. The highest curve is calculated using the conventional value of 1.8 for K2 (rotor loss factor). The lowest curve represents the actual test values from the first rotor.

In an effort to analyze the saturation problem an extensive testing program was initiated. Using exactly the same stator stack and rotor coil, a series of modifications was performed on the original rotor (Rotor 1A.) In the first of these, 1/8-in. steel plates were bolted under each finger to enlarge its cross-sectional area (Rotor 1B). See Figure 4.29 for a cross-section at the center of the alternator which shows the stator, original Lundel fingers, the plates, coil, sleeve and original core. Next, the plates were removed and a 5/16-in. thick sleeve was fitted around the rotor core to increase its cross-sectional area (Rotor 1C). Rotor 1D incorporated both modifications simultaneously. The test results indicated that the fingers and the core were saturated due to inadequate or poor magnetic characteristics.

At this time a second alternator was fabricated using the same stator stack and rotor coil with an entirely new set of castings from the same heat as the first set and a new shaft and core of the original dimensions made from a low alloy, mild steel -- SAE 1018. As Figure 4.30 shows, this single variable resulted in performance almost matching that of Rotor 1D.

On the basis of this test program, it was concluded that the rotor geometry-- particularly tooth and core sections and clearances--is crucial. In addition, the rotor material specification must be strictly defined and controlled to assure its magnetic characteristics. Significant improvement would be possible with a core-iron containing .1% carbon or less.

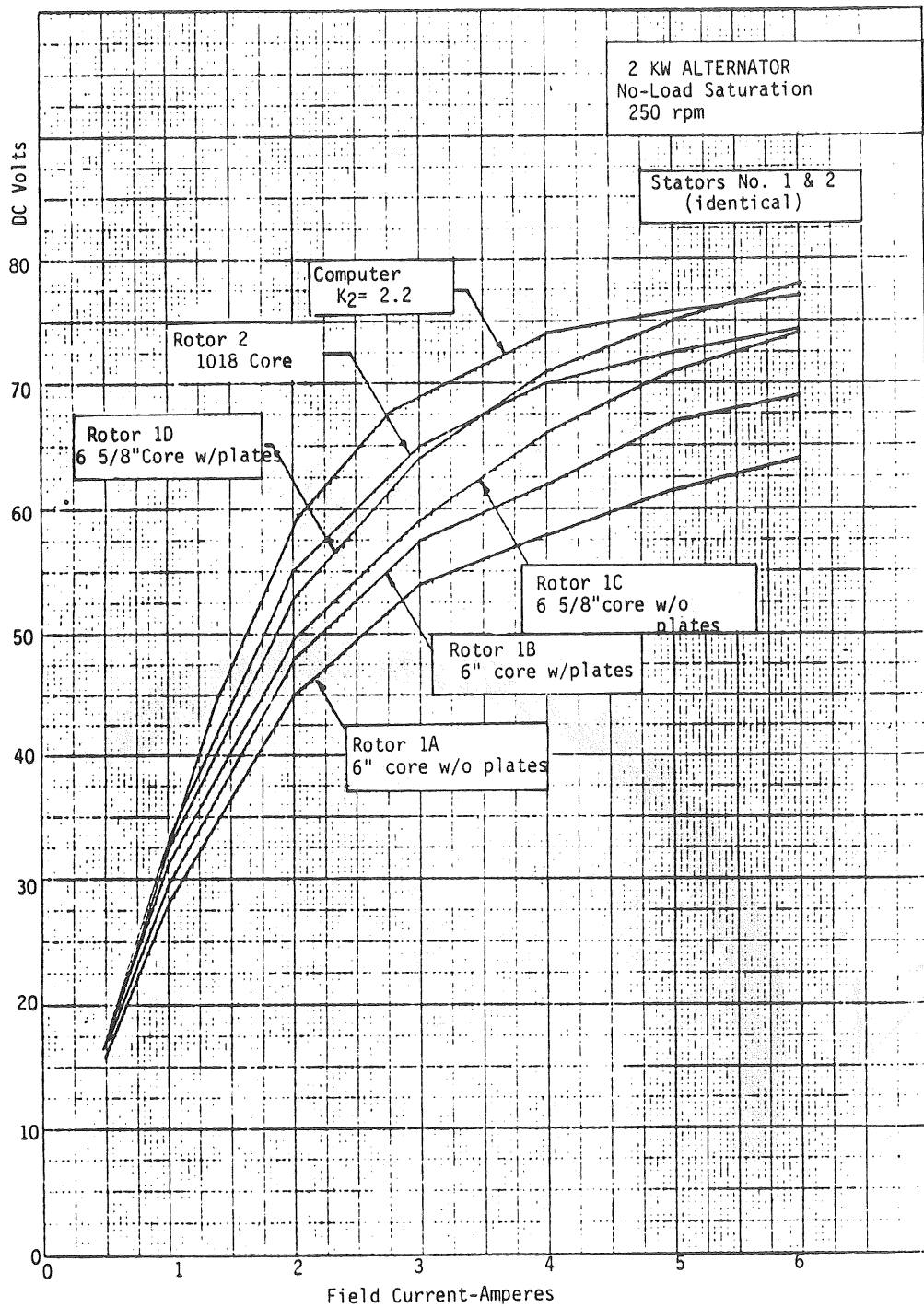


Figure 4.28
2Kw Alternator No-Load Saturation

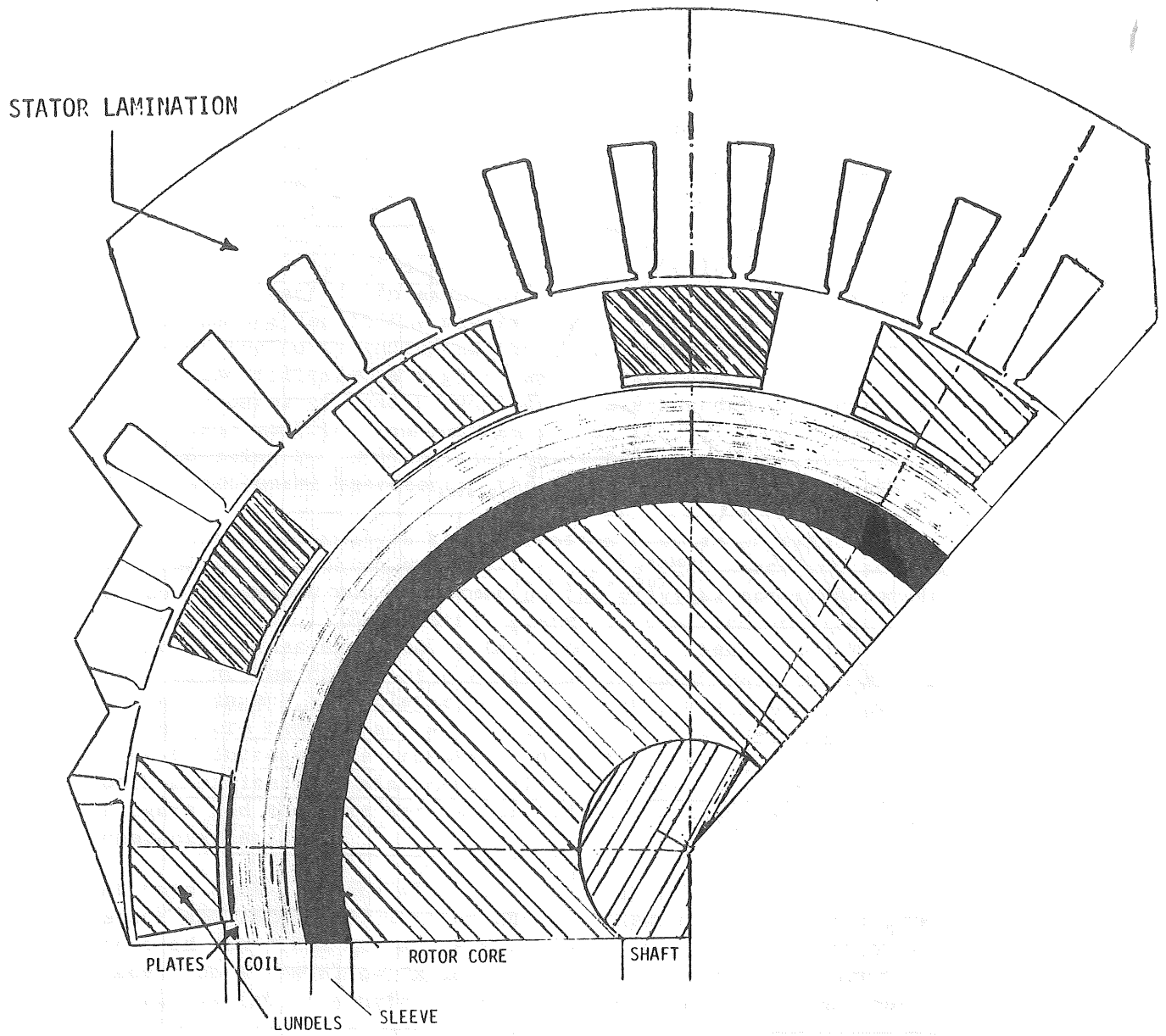


Figure 4.29
Prototype Alternator Section

4.3.3 Final Alternator Design Specifications and Tests

On the basis of the test results from alternator #1 (a-d) and #2, a third alternator prototype was specified and analyzed with a computer model using appropriate values derived from the test program. Table 4.30 indicates the changes made between alternators #1, #2 and #3. (See Figure 4.31 for cross-section of #3.) In the stator, the diameter was increased to increase overall output and allow larger rotor outer diameter. The stator yoke was decreased to make better use of yoke area and further enlarge the stator inner diameter. The enlargement of the slot area and opening permit the use of a heavier wire in the winding.

The increased rotor diameter permits a more favorable length-to-diameter ratio, and hence, a greater core sectional area. Larger finger cross-section and more space for the field winding also becomes possible. The casting was changed to eliminate the need for an extra core piece and, therefore, eliminate one potential air gap. An extremely low-carbon (C=.08%) magnetic iron was found for the Lundel casting which greatly improves the magnetic permeability of the section in the flux path. As a result of these changes, the rotor leakage factor (K₂) is reduced from 2.2 to 1.8 (calculation based on dynamometer tests).

At this time, the stator and rotor windings were re-specified to reduce stator losses and decrease field power requirements, thus increasing overall efficiency.

Laminations and Lundels for Alternator #3 were received in late February and early March 1979. The stator stack was laid up and wound according to the specification presented at FDR. Testing began shortly thereafter.

No-load tests indicated that the rotor saturated at lower voltage than expected (75 vDC vs. 77 vDC). Externally excited load tests, however, indicated that power output was more than satisfactory. At 250 RPM with 4 amperes in the field, the output was 2508 watts (DC) with a .59 ohm load. With maximum input, field output was 4042 watts with a 2-ohm load. Self-excited tests showed that the alternator produced a maximum output of 2100 watts at 250 RPM with a 1 ohm load. At this condition, the output voltage was 42 vDC with 3.6 ampere field current. The overall efficiency was 75%. It was concluded from this test that rotor saturation was limiting voltage, and hence current to the field. Previous tests had indicated that between 4 and 5 amperes in the field were required to achieve the desired output. A new field coil was then wound, using one gauge heavier wire and the same number of turns (858 turns, #16 AWG.)

In subsequent tests with the new field coil, the alternator produced 2950 watts DC output at 250 RPM with 5.6 amps in the field at 50v. The overall efficiency was 73% with a 1 ohm load. Increasing the load to 1.7 ohms decreased output to 2691 watts at 30 vDC at an efficiency of 68%. The field would not support heavier loading.

Once self-excited, the field would not build until 200 RPM. Cold, the rotor had no measurable residual magnetism and the alternator would not

Figure 4,30

Table of Alternator Changes

ITEM	NOS. 1 & 2	NO. 3
Stator O.D.	14.375	15.375
Rotor	9.843	11.199
Yoke	1.085	.710
Slot Area in ²	.335	.581
Slot Opening	.098	.252
Rotor Core Diameter	6.000	6.875
Rotor Core Length	3.000	3.500
Rotor End Thickness	1.370	1.500
Finger Area in ²	1.165	1.277
L/D Ratio	.305	.268
Stator Winding	11t,10AWG	9t,13AWG
Rotor Coil	858t,19AWG	858t,17AWG
Rotor Leakage	2.2 (meas.)	1.85 (calc.)

A. Stator Changes

1. Increased diameter allows for increased output, requires no major mechanical changes.
2. Moving slots outward better utilizes yoke area; gives larger stator I.D.
3. Larger slot area allows for heavier winding.
4. Effect of these changes is easily and accurately calculated.

B. Rotor Changes

1. Increased diameter provides lower L/D ratio.
2. Greater core area.
3. More space for field coil winding.
4. Use of two-piece core/finger construction eliminates air-gap.
5. Specification of Genecast G47 alloy will greatly improve magnetic quality of rotor.
6. Rotor leakage factor (K₂) should decrease to 1.85 or less.

C. Winding Changes

1. Changing stator from 11-9 turns reduces reactive losses by 3.
2. Stator losses decrease by 43%.
3. Field power decreases by 43%.
4. Overall efficiency up from 63% to 73%.
5. Rated output voltage still reached at less than 150 RPM.
6. Changing rotor from 19AWG to 17AWG decreases voltage requirement for rated field current by 26%.

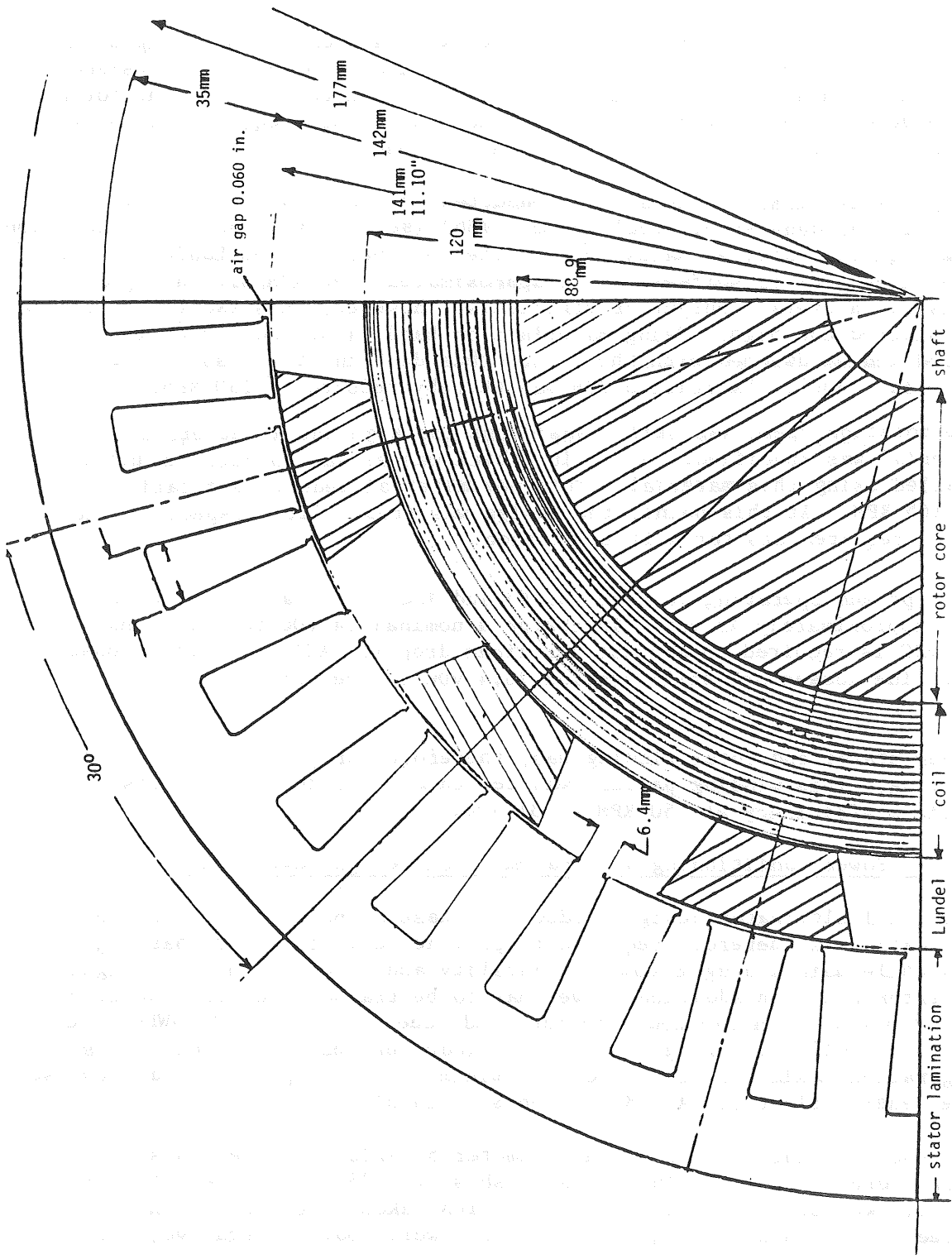


Figure 4.31
 Alternator #3 - Final Design Section

self-excite. This was due to the high permeability of the Lundel material. Permeability and retentivity are inversely proportional. Some degree of permanent magnetism had to be introduced in the rotor.

Therefore, a hardened tool steel washer was fabricated and clamped in the core between the two Lundels. It was designed to provide the residual magnetism necessary to induce enough stator voltage to overcome the forward drop across the diode bridge. This induced voltage requirement is very small, on the order of 2 v at 250 RPM, no load.

Complete dynamometer tests were conducted on the #3 alternator with a 1/16-in. hardened-tool steel washer (#3b) (see Figure 4.32.) The addition of the magnetic material sandwiched in the core between the Lundels allowed the alternator to self-excite at approximately 190 RPM with no apparent penalty in overall output or efficiency. However, this excitation RPM was considered too high. Using materials on hand, a second washer was prepared and sandwiched with the first, thus doubling the mass of magnetic material (#3c). Excitation RPM was thereby reduced to 180 RPM.

The rotation speed was still considered too high and a better magnetic material was specified. A 1/8-in thick washer was fabricated and installed using this material. This new material reduced excitation speed to 165 RPM. At this point, the design was frozen with respect to the magnetic requirements for self-excitation.

The optimum operating voltage for #3 and #3d stator and rotor windings was approximately 45 vAC. To charge a nominal 24 vDC battery bank 32 vDC is required to account for diode drop (2 vAC), slip-ring losses, and line losses and still provide 26.4 vDC to the batteries.

A new stator and rotor winding was, therefore, proposed and prepared for testing. This winding pattern was designed to produce 2300 watts with optimum efficiency at 250 RPM at 31 vDC.

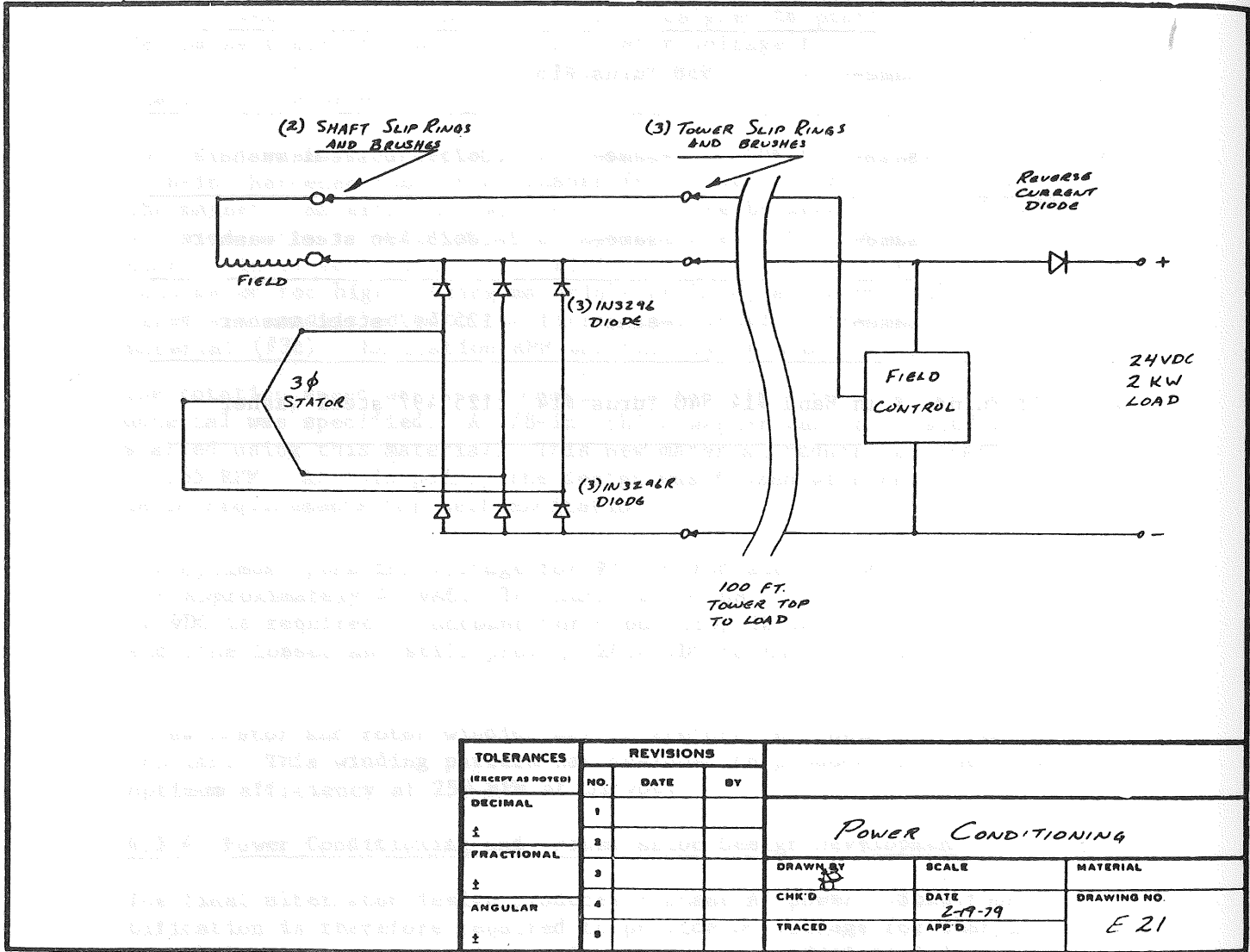
4.3.4 Power Conditioning and Transmission Design Development

The final alternator design produces 3 phase AC power. Some form of rectification is therefore required to provide DC voltage for charging batteries while maintaining maximum reliability and producing minimum signal interference. In addition, power has to be transmitted from the generator in free yaw, down the tower to the load (see Figure 4.33.) NWPCo specified a full wave bridge, using one diode per phase per side. This configuration maximizes efficiency and minimizes DC ripple. The diodes used are General Electric #A70PB (IN3296 & IN3296R).

For the alternator field, 2-in diameter by 9/16-in wide brass slip-rings were specified. The field brushes are .25-in square metal graphite, two per ring. Since rectification takes place on the unit, only three power leads are required off the tower: output negative, common

Figure 4.32
2 KVA Alternator Numeration

NUMBER	STATOR	ROTOR	OTHER
3	9 Turns, 4 in Hand #13	858 Turns #17	—
3A	-same-	858 Turns #16	—
3B	-same-	-same-	.0625 496 steel washer
3C	-same-	-same-	2-.0625 496 steel washer
3D	-same-	-same-	.125 497 steel washer
4	11 Turns, 4 in Hand #14	540 Turns #14	.125 497 steel washer



TOLERANCES (EXCEPT AS NOTED)	REVISIONS			POWER CONDITIONING		
	NO.	DATE	BY	DRAWN BY	SCALE	MATERIAL
DECIMAL	1			DRAWN BY <i>[Signature]</i> CHK'D TRACED DATE 2-9-79 APP'D		DRAWING NO. E 21
±	2					
FRACTIONAL	3					
±	4					
ANGULAR	5					

NO. 1082-0/211

Figure 4.33
Electric System Diagram

positive and field negative. Three brass slip-rings, 6.03-in diameter by 11/16-in wide, were specified for transmission off the tower. The two sets of power brushes are 1/2-in square metal graphite, two per ring. The field brushes are .25-in square (the same as the alternator), two per ring.

The power cable specified is #2 AWG copper for 100 feet of transmission from tower top to load. For a load at 24 volts, 2kw, the voltage drop is calculated to be 2.7 volts.

The alternator voltage at peak output has been established at 32 volts AC to account for charging a 12 cell battery bank at 2.2 per cell, 2 volts forward drop at the rectifier and up to 3.6 voltage drop in transmission. The field regulation has been set to limit output voltage at the battery to 28 vDC to protect the batteries from over charging. The setting can be varied for different battery banks.

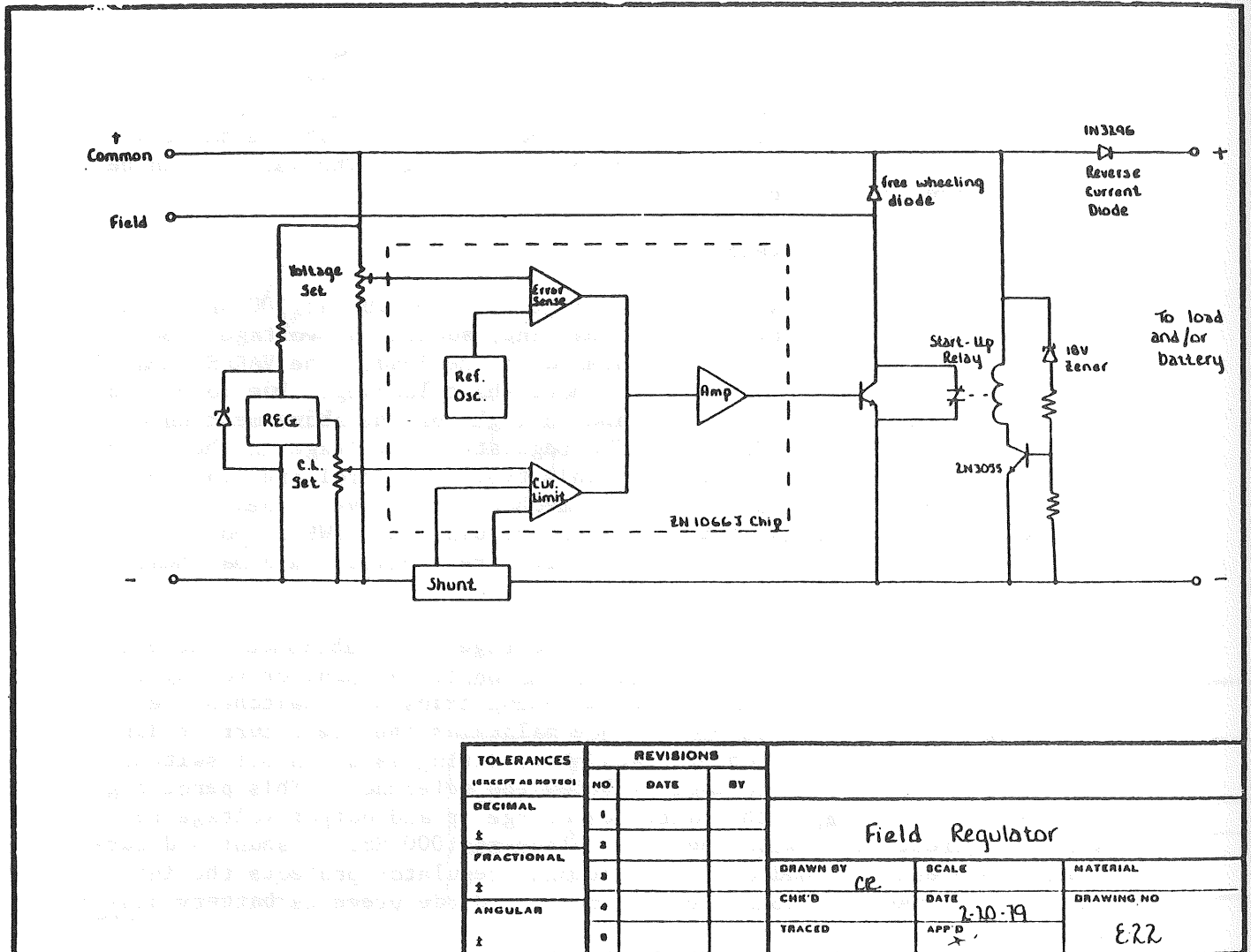
4.3.5 Regulator Design Development

The 2kw alternator produces variable voltage up to 57 vDC at 300 RPM. In order to protect the battery from overcharging, additional voltage regulation is required when output exceeds demand at the load. The VARCS remains an effective speed governor with and without shaft loading. Due to considerations of reliability and expense, and in light of the above mentioned characteristics of VARCS, NWPCo chose to regulate the voltage in the field circuit. A number of alternatives for this type of control are available including variable resistors with electromechanical relays, linear solid state transistors and solid state switching regulators. NWPCo chose the last of these alternatives due to its inherent reliability, minimal heat dissipation and low cost.

Using a reference oscillator, a reference voltage is established (see Figure 4.34.) The voltage set and error sense monitor alternator voltage. As voltage exceeds the reference, the switching transistor switches the field current while a free-wheeling diode maintains the field current during the off cycle. The switching transistor, acting as an on/off switch, is on 100% when alternator voltage is below the reference. This percentage is reduced to a minimum as the batteries charge up and output voltage resets to the reference. Switching takes place at 1000 Hz. A shunt and current limit prevent overload and an additional regulator protects the integrated circuit. An additional reverse current diode prevents battery discharge.

In order to maintain maximum field power at start-up and assure an initial zero voltage drop at the regulator, a start-up circuit was added consisting of a zener diode, transistor and electromechanical relay which is closed to bypass the regulator at start-up and opens when field voltage begins to rise.

A Ferranti IC was chosen for the regulator because it required a minimum of peripherals and offered additional control functions such as current



TOLERANCES		REVISIONS			Field Regulator		
(EXCEPT AS NOTED)		NO.	DATE	BY	DRAWN BY	SCALE	MATERIAL
DECIMAL		1			CE	DATE 2-10-79	DRAWING NO
±		2					
FRACTIONAL		3					
±		4					
ANGULAR		5					
±		6			TRACED	APP'D X	E22

Figure 4.34
Field Regulator Diagram

limiting and load dumping. NWPCo's regulator uses the current limit capability to protect against overload and short circuit, acting as a self-replacing fuse.

4.3.6 Lightning Protection Provision

The objective of this effort was to provide protection of the entire electrical system in case of lightning strikes and lightning-induced transients and surges. The system consists of the alternator rectifier diodes, the power wiring, the tower transmission, the field regulator and the load. NWPCo's past experience has indicated that very little can be done to protect against direct hits, however, provision can be made against mild and indirect strikes and induced transients.

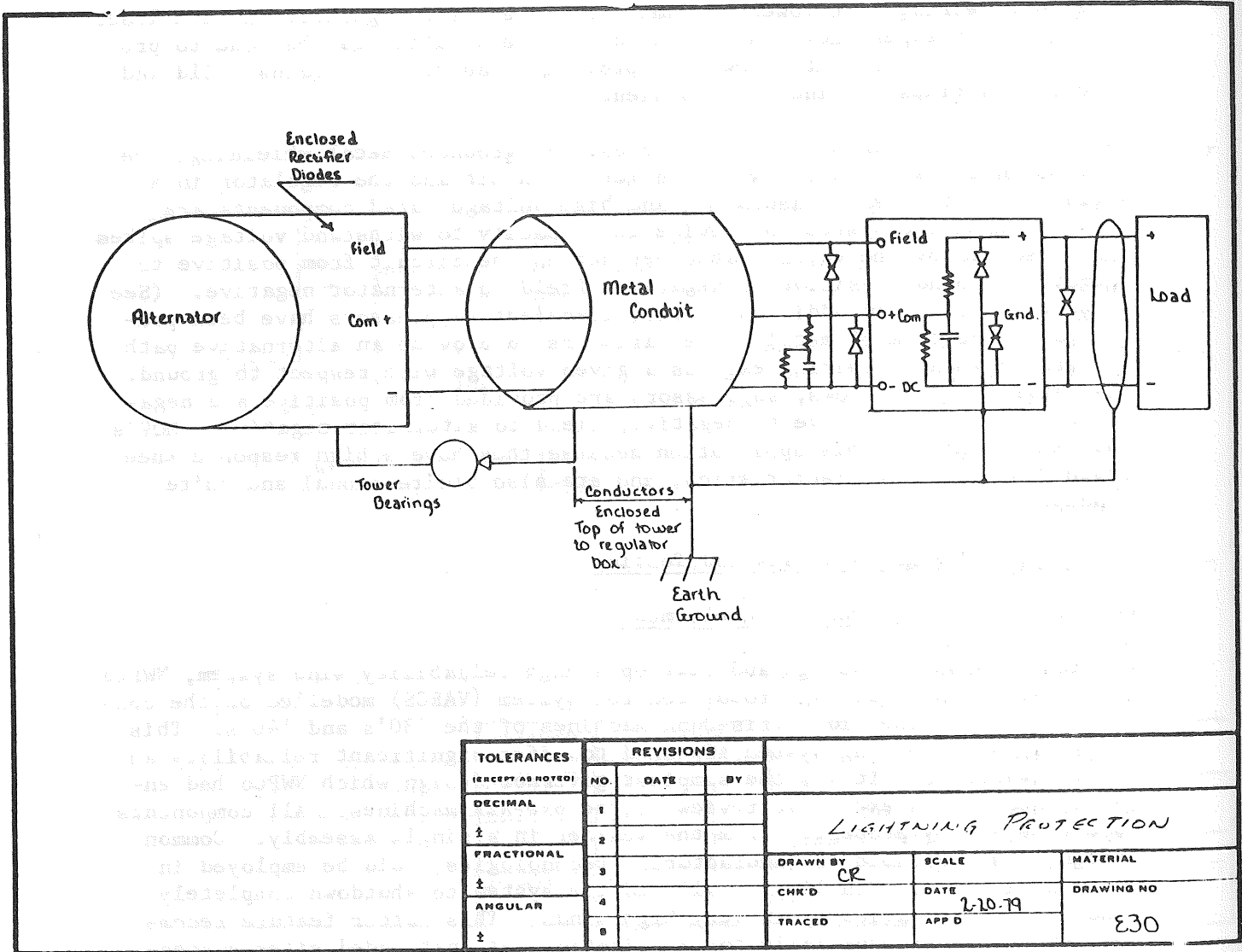
All system components have been enclosed in grounded metal shielding; the diodes in the alternator, wires in metal conduit and the regulator in a metal cabinet. Heavy insulation and high voltage rated components are specified in the system to provide the capacity to withstand voltage spikes not absorbed by the voltage absorber set in the circuit from positive to negative ground, positive to negative, field to alternator negative. (See Figure 4.35.) In addition, active transient suppressors have been provided in the form of metal-oxide varistors to provide an alternative path to ground whenever wiring exceeds a given voltage with respect to ground. As Figure 4.35 shows, suppressors are provided from positive and negative to ground, positive to negative, field to alternator negative. MOV's are excellent for this application because they have a high response knee, high dissipation characteristics, and are also bidirectional and quite inexpensive.

4.4 VARCS Design, Analysis and Testing

4.4.1 Preliminary Design Development

In its proposal to design and develop a high reliability wind system, NWPCo specified a variable axis rotor control system (VARCS) modelled on the control system of the old Parris-Dunn machines of the '30's and '40's. This rotor speed governing system appeared to offer significant reliability and cost advantages. It was the simplest governor design which NWPCo had encountered in its extensive review of the pre-REA machines. All components could be easily protected from the weather in a single assembly. Common techniques available to manufacturing technologies could be employed in its fabrication. Finally, it allowed the system to shutdown completely and re-set automatically in very high winds. This latter feature recommended the VARCS especially for applications at unattended sites susceptible to extreme weather.

Early in the program, it became apparent that there was no precedent for the analytical development of a total system design employing this type of control system. In fact, there were no readily available theoretical techniques for modelling the performance and loading of a wind turbine in extreme crossflow (+20°.) First, NWPCo had to determine the performance of the rotor at extreme crossflow angles in order to establish a pitch schedule



TOLERANCES (EXCEPT AS NOTED)	REVISIONS			DRAWN BY CR	SCALE	MATERIAL
	NO.	DATE	BY			
DECIMAL	1			CHR'D	DATE 2-10-79	DRAWING NO E30
FRACTIONAL	2					
ANGULAR	3			TRACED	APP'D	
	4					
	5					

LIGHTNING PROTECTION

Figure 4.35
Lightning Protection Diagram

which would assure maximum alternator output. Then, the rotor thrust at each specific wind speed and pitch angle associated with the desired performance was determined to calculate the load at the hinge to be resisted by the control spring.

An analytical model was needed to calculate rotor coefficients of power and coefficients of thrust for a range of tip speed ratios at each rotor pitch angle. In order to establish a consensus on the nature and degree of accuracy of such a model, NWPCo held a "dynamics" review at its offices in Warren, Vermont. Present at this review were Dr. John Dugundji of MIT, Tom Sheehy of Sikorsky Helicopter, Dr. Forrest Stoddard of U.S. Windpower Associates, Clint Coleman and Hugh Currin of Windworks, Dr. Craig Hanson and Sandy Butterfield from Rocky Flats, and the NWPCo staff. Dr. Dugundji presented a paper which proposed an analysis of airfoil section parameters at discrete radial stations for a number of azimuthal positions to determine overall rotor performance and loads at a given tip speed ratio and pitch angle. Clint Coleman presented a similar model developed by Robert Wilson of Oregon State based on Lissaman and Wilson strip theory.³ This model calculates the angle of attack (α) for the airfoil at a discrete number of radial stations at a particular azimuth. As crossflow angle is increased (by pitchback), a new resultant wind velocity (u) and angle (θ) are calculated for each station and azimuth (see Figure 4.15.) Summing all the points calculated gives overall torque and thrust for the rotor at each tip speed ratio and pitch angle.

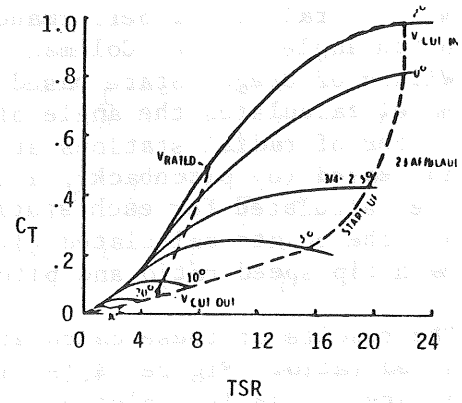
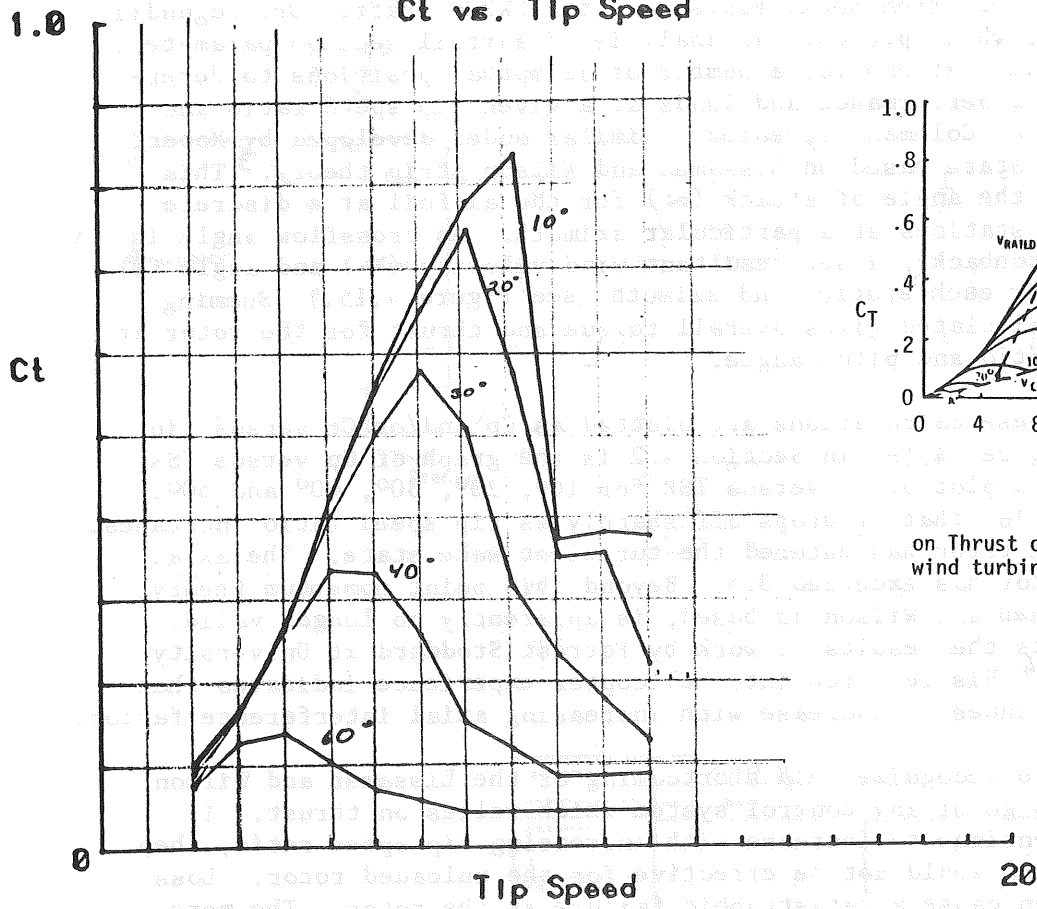
The results of these calculations are plotted as C_p and/or C_t versus tip speed ratio. Figure 4.16 in Section 4.2 is the graph of C_p versus TSR. Figure 4.36 is a plot of C_t versus TSR for 10° , 20° , 30° , 40° and 60° . Note in Figure 4.36 that C_t drops off sharply as tip speed ratio increases. At this point the rotor has entered the turbulent wake state. The axial interference factor has exceeded 0.5. Beyond this point momentum theory, upon which Lissaman and Wilson is based, is apparently no longer valid. Figure 4.37 plots the results of work by Forrest Stoddard at University of Massachusetts.⁴ His research into helicopter experience indicates that axial thrust continues to increase with increasing axial interference factor.

It is important to recognize this shortcoming of the Lissaman and Wilson theory in the design of any control system which relies on thrust. If thrust did not continue to increase with increasing tip speed ratio, then this control system would not be effective for the unloaded rotor. Loss of load could then cause a catastrophic failure at the rotor. The more sophisticated "vortex filament theory" does predict increasing thrust. Graphs developed by Hamilton Standard were used to fill in the back side of the Lissaman and Wilson graphs⁵ (see Figure 4.36, insert.)

4.4.2 Final Design Analysis and Specification

The Lissaman and Wilson model became the primary analytical tool in the VARCS design and development. Hugh Currin, then of Windworks, Inc., translated this analysis into a versatile and workable program in Tektronix 4051 Basic which allowed extensive rotor performance modelling.

Ct vs. Tip Speed



Effect of Variable Pitch on Thrust of an Optimum, 2-bladed wind turbine

Figure 4.36

C_t Vs Tip Speed

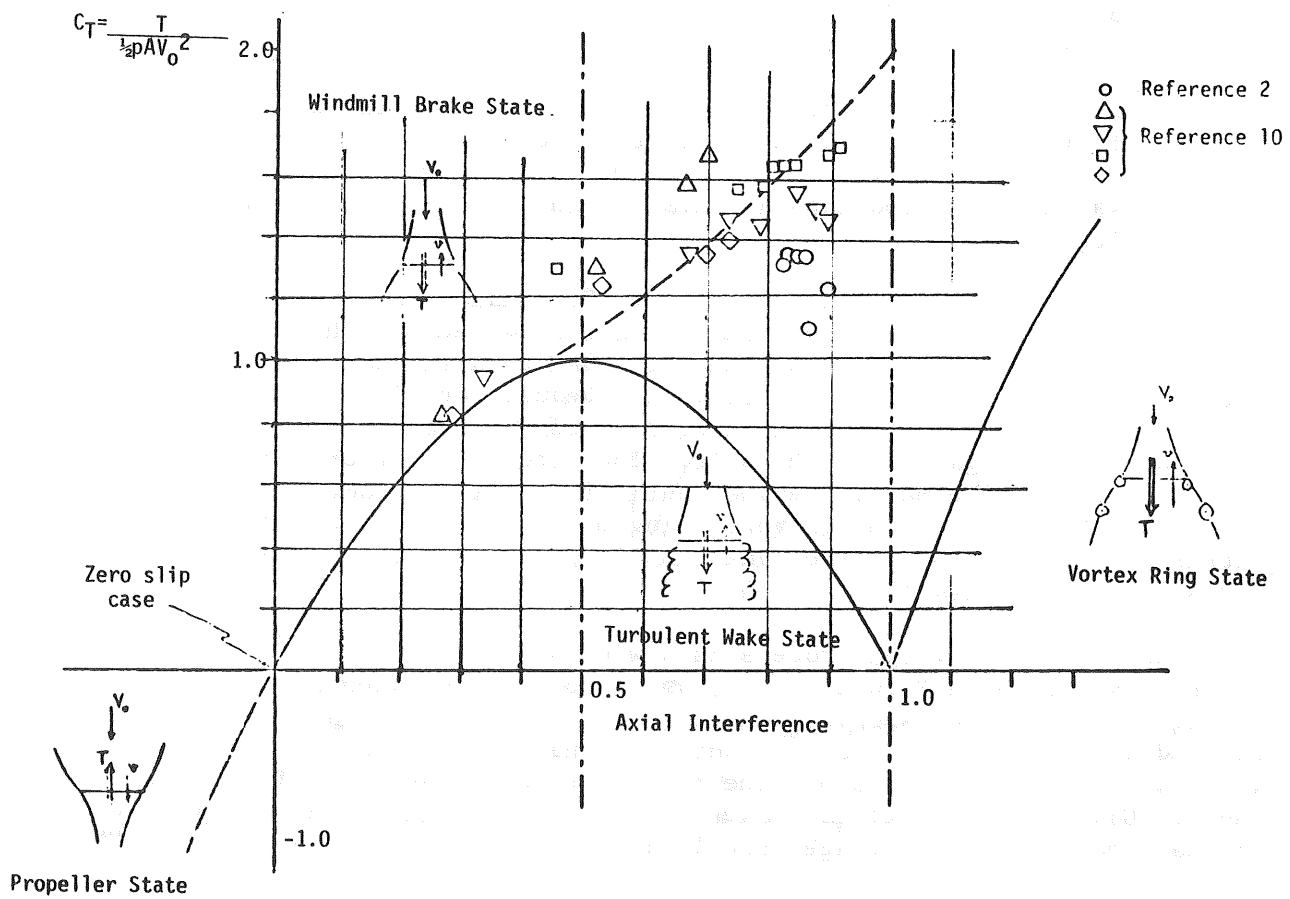


Figure 4.37
 C_t Vs Axial Interference Factor

As mentioned earlier, rotor thrust is then added to aerodynamic drag of the system to calculate the overturning moment at the hinge point. Figure 4.38 explains this calculation and the equation used. Note that the element M_A , aerodynamic moment, generated by the component of wind parallel to the rotor, is considered negligible and was not included in the calculation of overturning moment, M_S . This was the consensus of those present at the dynamics review although considerable interest was expressed in measuring this moment.

With these tools in hand, it is possible to calculate a spring rate which opposes the overturning moment, generated largely by thrust below 60° pitch, so as to extract maximum power up to the point at which the crossflow angle becomes so great that the rotor cannot develop enough torque to sustain any load.

The mechanical design team determined that a linear spring would be the most easily manufactured and the most reliable configuration. The aerodynamic problem, therefore, was to find an optimum performance and pitch schedule which translated into a linear graph of overturning moment versus pitch angle.

Using calculated torque requirements for the final alternator design (Figure 4.39), and the rotor performance maps developed by the Currin program (Figures 4.15 and 4.36,) a system performance matrix was developed to match a projected pitch and performance schedule for all relevant parameters. (See Figure 4.40) C_t and generator drag were reduced to overturning moment and plotted against pitch angle. The pitch and performance schedule were altered and the matrix revised until this graph became linear. Figure 4.41 is the final graph of overturning moment versus pitch angle for the matrix in Figure 4.45. The final VARCS spring constant is determined by the slope of this graph.

The result of this design process is a wind system with the theoretical power curve shown in Figure 4.42, and a control function as diagrammed in Figure 4.43. It should be noted that this curve is based on statically derived values. It does not account for dynamic stall and wake effects which will tend to flatten out the top of the curve and extend the power range. Given the theoretical power curve, the average monthly output in kilowatt hours versus average annual wind speed is plotted in Figure 4.44.

Finally, the pitch schedule and rotational speed for the final design have been calculated for the unloaded rotor by extrapolating the C_t curves on the basis of the Hamilton Standard Curves. Figure 4.45 shows the results of this calculation. As indicated, rotational speed is quite a bit higher although pitchback initiates at a much lower wind speed (7.3 m/s). Maximum thrust on the tower, of course, remains the same and 90° pitch is attained at the same wind speed as for the loaded case. Although the control function continues to be effective, perhaps even safer, out of plane rotor loads are substantially increased. This problem is addressed in the section on rotor design and analysis (Section 4.2) and has been resolved by a minor re-design of the blade.

Figure 4.38

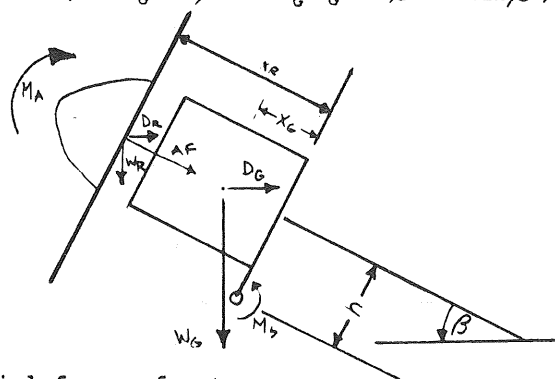
Rotor Performance with Pitch and VARCS Spring Calculations

We initially projected our VARCS mechanism to control RPM for a constant 2.5 kva output in windspeeds up to 40 mph (19 m/s) and shutdown (i. e. pitch to 90°) at 60 mph (28.6 m/s). Using alternator torque characteristics and the rotor performance maps developed by the Lissaman and Wilson program, a system performance matrix was developed for these parameters:

$$\beta^{\circ} \quad C_t \quad D_G \quad \bar{V} \quad \text{RPM} \quad X \quad C_p \quad Q$$

The following analysis was used to find the required spring moment:

$$M_s = AF(h) + M_A + D_G(h \cos \beta + X_G \sin \beta) - W_G(X_G \cos \beta - h \sin \beta) - W_R(X_R \cos \beta - h \sin \beta)$$



- Where:
- AF = Axial force of rotor
 - D_G = Generator drag = f (β)
 - h = Distance from pivot pin to shaft axis
 - X_R = Distance from pivot pin to rotor
 - X_G = Distance from pivot pin to generator c. g.
 - W_G = Generator weight
 - W_R = Rotor weight
 - β = Pitch angle of unit
 - D = Rotor diameter
 - M_A = An aero moment due to force parallel to the rotor

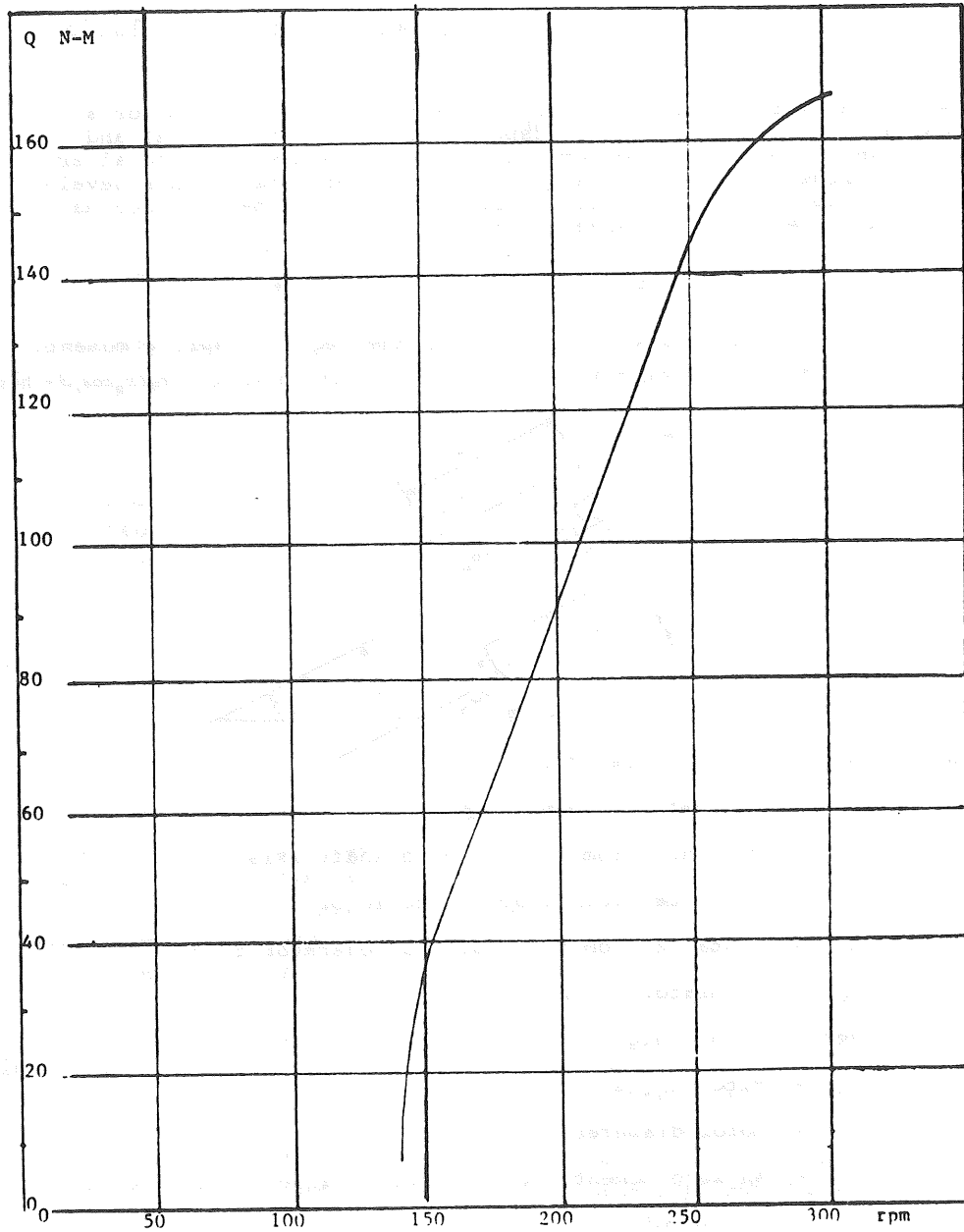


Figure 4.39
 Assumed Alternator Torque Input Characteristics as of 1/22/79

Figure 4.40

PPM #4: Projected Performance with 62.3 In-Lb /Deg. Spring
(Q-Matched with Anticipated Alternator Requirements)

β	C_t	DG	V_m/s	RPM	X	C_p	Q (n-m)	P_R (Watts)	P_{Output} (Watts)
Initial Setting			4.88	150	8.05	.435	37.9	595	345
			6.2	175	7.4	.428	65.6	1202	697
			7.25	200	7.23	.426	91.2	1910	1168
0	.72	.021 lb	9.12	250	7.18	.425	145.1	3798	2203
10	.675	.405 lb	9.37	250	6.99	.392	145.1	3798	2203
20	.63	.62	9.60	246	6.71	.348	140.9	3629	2105
30	.53	.94	10.18	240	6.18	.272	134.1	3370	1955
40	.40	1.51	11.2	232	5.43	.186	126.7	3078	1785
50	.26	2.72	12.9	220	4.47	.104	114	2626	1523
60	.15	4.88	16.2	200	3.23	.038	91.8	1922	1115
70	.085	11.54	20.8	168	2.12	.010	57.1	1004	582
80	.036	23.0	25.6	102	1.04	.001	22.9	245	None*
90	0	108.0	47.0	0	0	0	0	0	None

*RPM too Low to Self-Excite

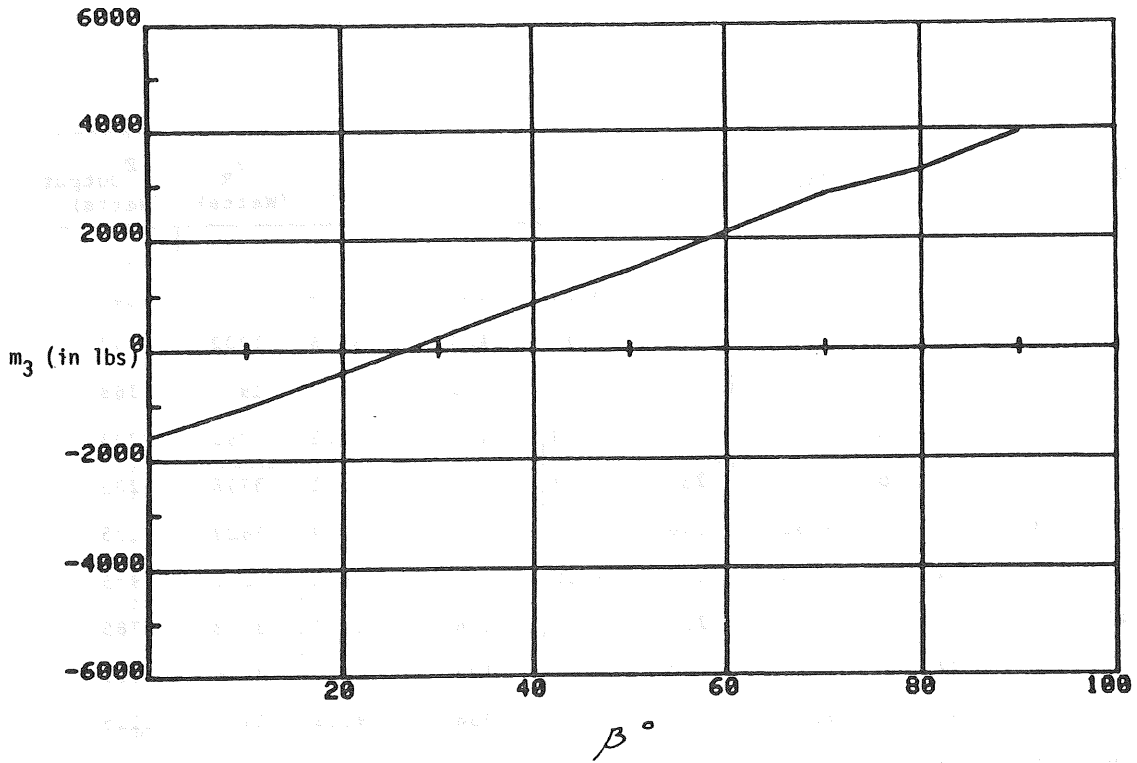


Figure 4.41
 Spring Moment Vs Beta
 (Q-Matched VARCS Spring 1/24/79)

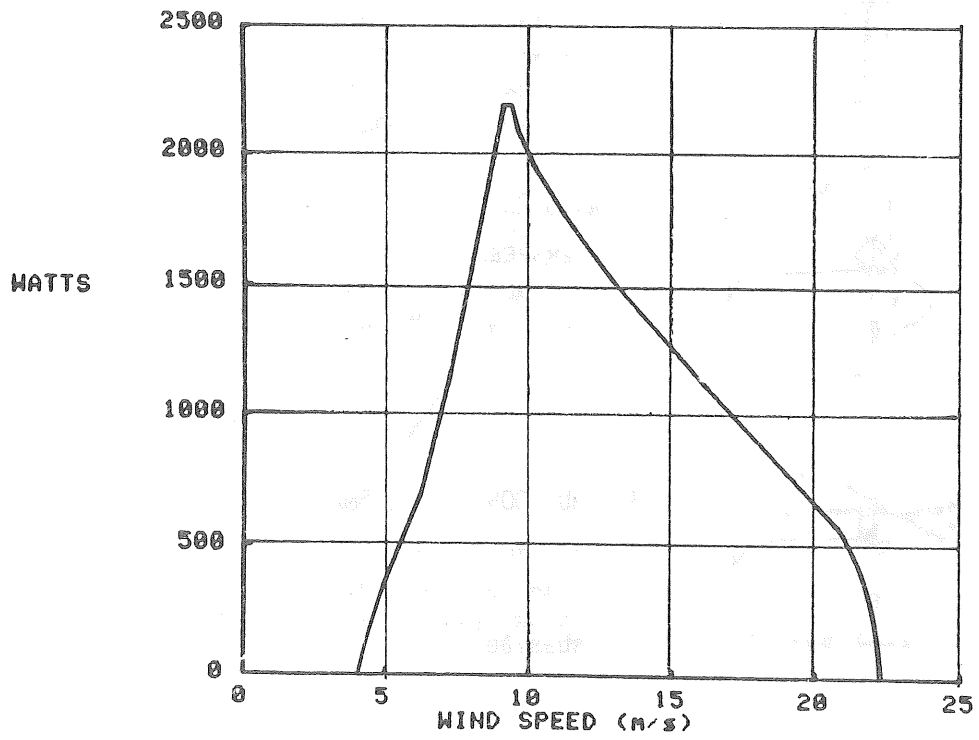
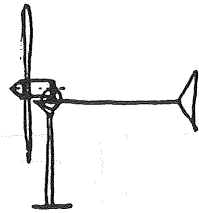


Figure 4.42
Power Output Vs Wind Speed (M/S)



1. STANDARD OPERATIONAL MODE

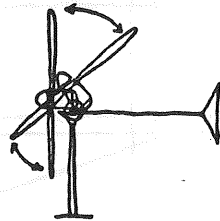
5° PITCH AT START-UP TO ACCOUNT FOR
BLADE DEFLECTION

CUT-IN WIND SPEED: 10MPH

MAX WIND SPEED THIS MODE: 21MPH

MAX POWER OUTPUT THIS MODE: 2203WATTS

MAX RPM THIS MODE: 250RPM

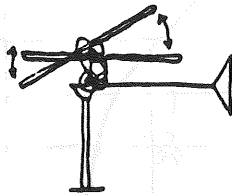


2. AXIS ROTATION VERTICALLY

OVERSPEED CONTROL

CONTROL INITIATION: 21MPH

SHUTDOWN: 105MPH

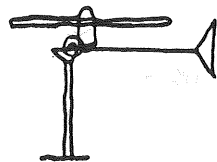


3. SHUT DOWN --- 105MPH

AXIS ROTATION TO 90°

POWER AND RPM'S APPROACH 0

SPRING TENSION REALIGNS ROTOR AS GUSTS
SUBSIDE



4. MANUAL SHUT DOWN

SERVICE AND MAINTENANCE

Figure 4.43

Variable Axis Rotor Control System (VARCS)
Operational Modes

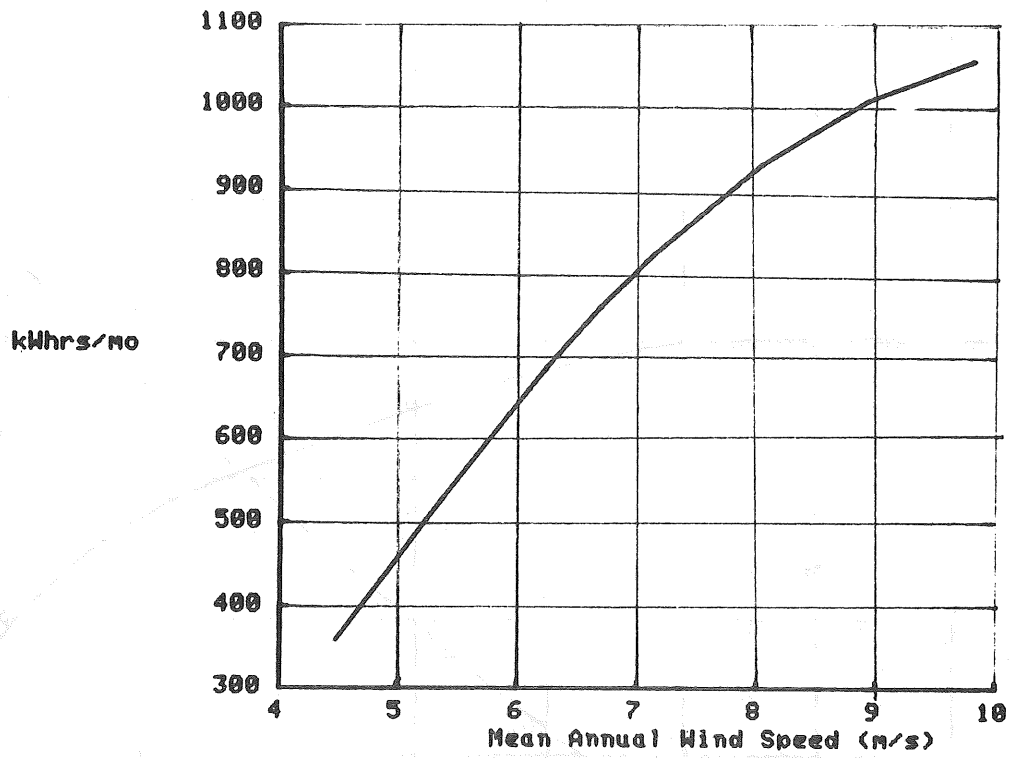


Figure 4.44
HR 2 Monthly Output

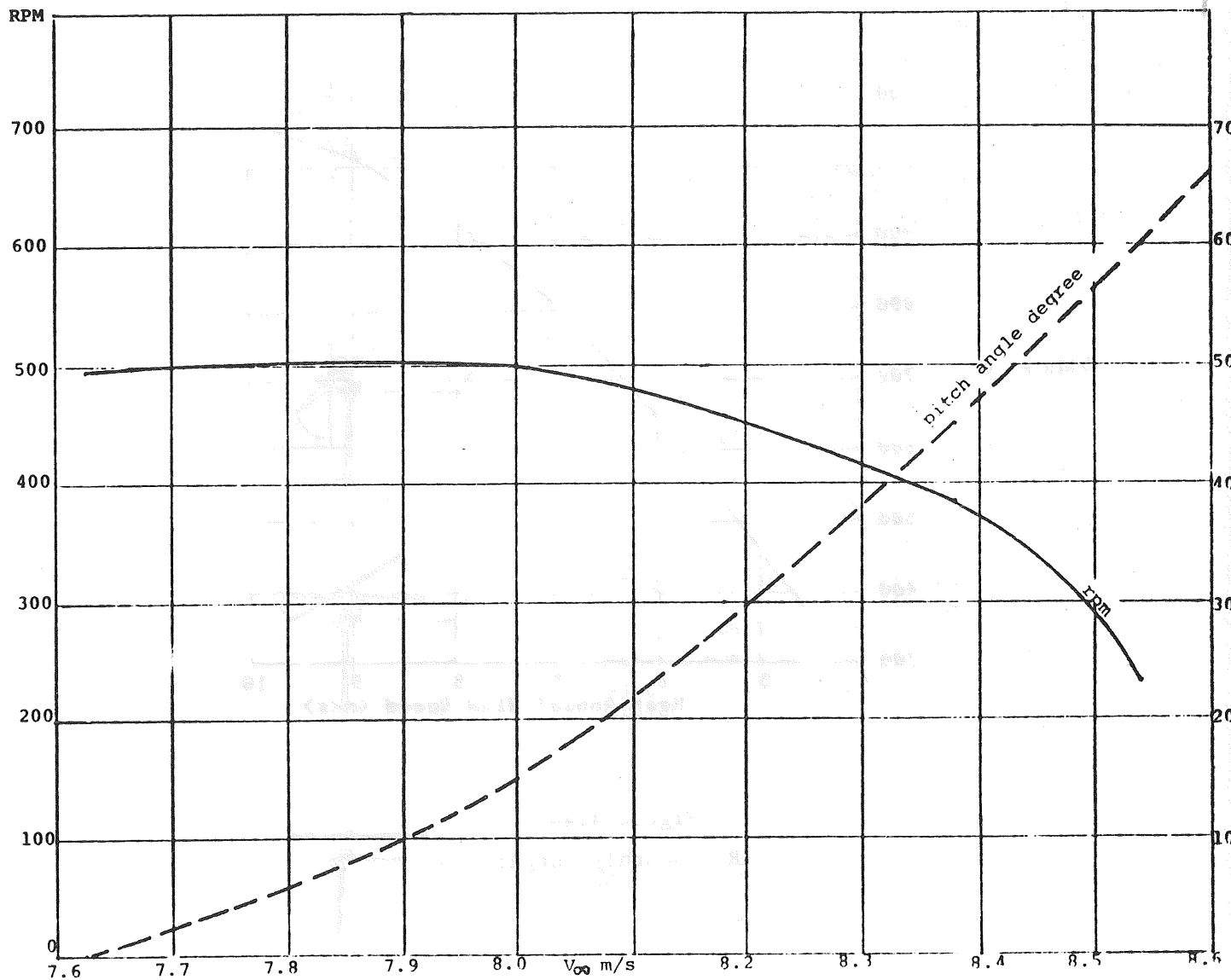


Figure 4.45
No-Load Characteristics of Rotor-VARCS Combination

4.4.3 Design Testing and Verification

The VARCS appears analytically to be an effective and safe overspeed control system for a wind turbine both loaded and unloaded. However, the analytical model developed for this program is unconfirmed by empirical testing. The VARCS is based upon the control system used in the Parris-Dunn, a machine whose rotor never exceeded 14 feet in diameter and which was used in rural and agricultural applications. The control system had been developed through trial and error exclusively. For the high reliability machine, NWPCo applied an analytical model, yet to be confirmed through prototype testing.

The test program developed at the dynamics review specified testing a prototype on a movable test bed to confirm rotor performance and load calculations for the full range of pitch angles. Testing an operating prototype VARCS to confirm its operating characteristics and make minor spring adjustments (if necessary) were also specified. Section 4.2.3 described the facility employed for this test program. Considerable effort and time were expended in order to get calibrated data from the load beam. Figure 4.17 from Section 4.2.3 is the record of a run at 10° at approximately 15 mph. The top track is the record of the load beam signal for this run. Note the noisiness of the signal. Coupled with a resolution of only 205 in-lb per division, load beam data were difficult to reduce. Data points were determined by visually averaging the signal for a given period. The overturning moment measured was reduced to axial thrust subtracting the calculated effect of simple aerodynamic drag for the given pitch angle and wind speed. Converted to co-efficients of thrust for the tip speed ratio at the data point, the data were overlaid on the graph of theoretical C_t versus tip speed for that pitch angle (see Figures 4.46 through 4.50.) Throughout these tests, the five meter rotor was flown on the #2 prototype alternator which was not yet capable of absorbing the available torque, thus allowing the rotor to overspeed. Most of these data points were taken at tip speed ratios above the optimum and beyond the limit of the Lissaman and Wilson theoretical model. A shadow line indicating the probable extension of the graph has been included to indicate the relative accuracy of this data. For all pitch angles tested, with the exception of 45° , data points fall within a broad band somewhat above the projected curve. At the pitch angle of 45° , the machine is very nearly balanced and it was extremely difficult to determine the effect of the weight of the machine. The data at 30° were taken without varying field excitation. As a consequence, all data points for 30° occur within a narrow range of tip speed ratios.

It is possible to draw from this data a few general qualitative conclusions about the analytical model. These data confirm the expectation that axial thrust increases with increasing tip speed ratio and therefore, the VARCS will be an effective control system for an unloaded rotor. The data also appear to support the analytical model's prediction of the relative thrust values for various pitch angles and tip speed ratios. The apparently higher thrust recorded for 10° and 31.5° may be due to the deformation of the flow field caused by the truck as described in Section 4.2.3.

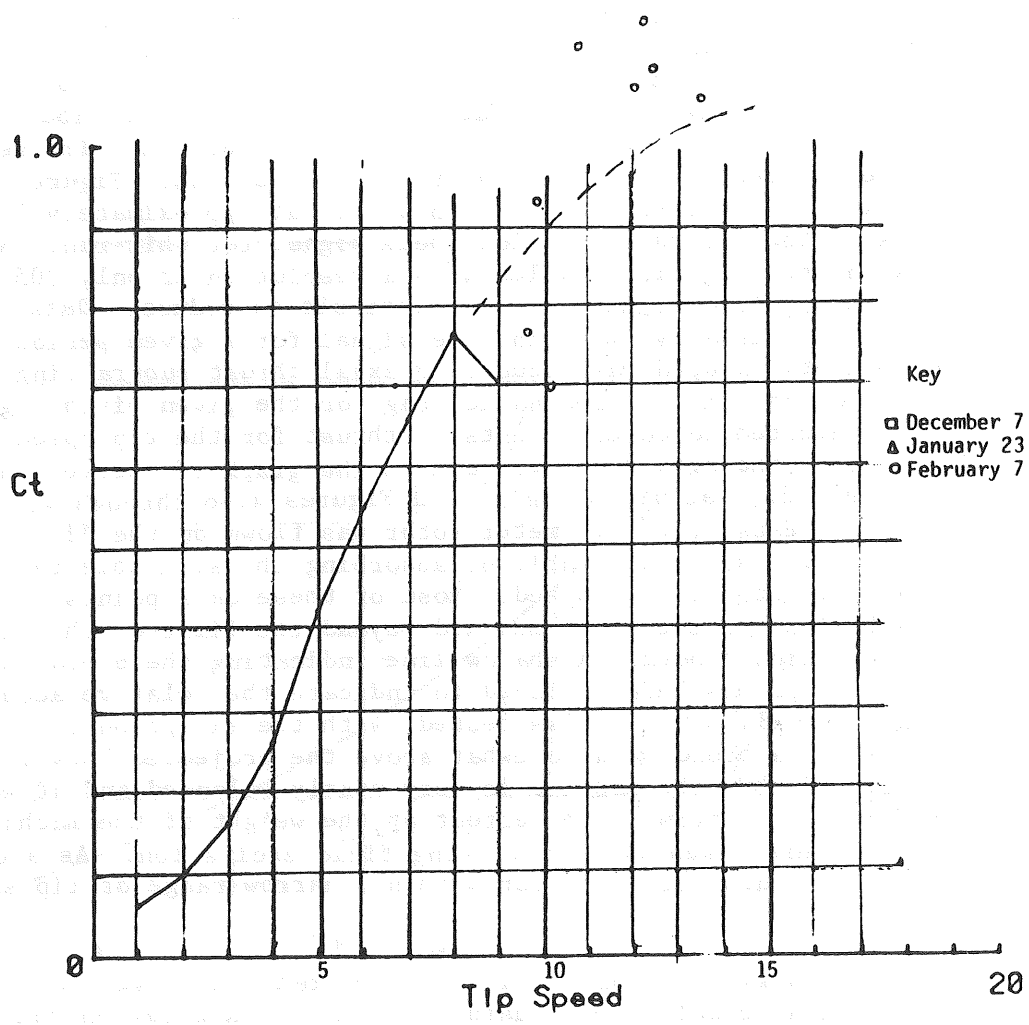


Figure 4.46
 C_t Vs Tip Speed at $10^\circ \beta$

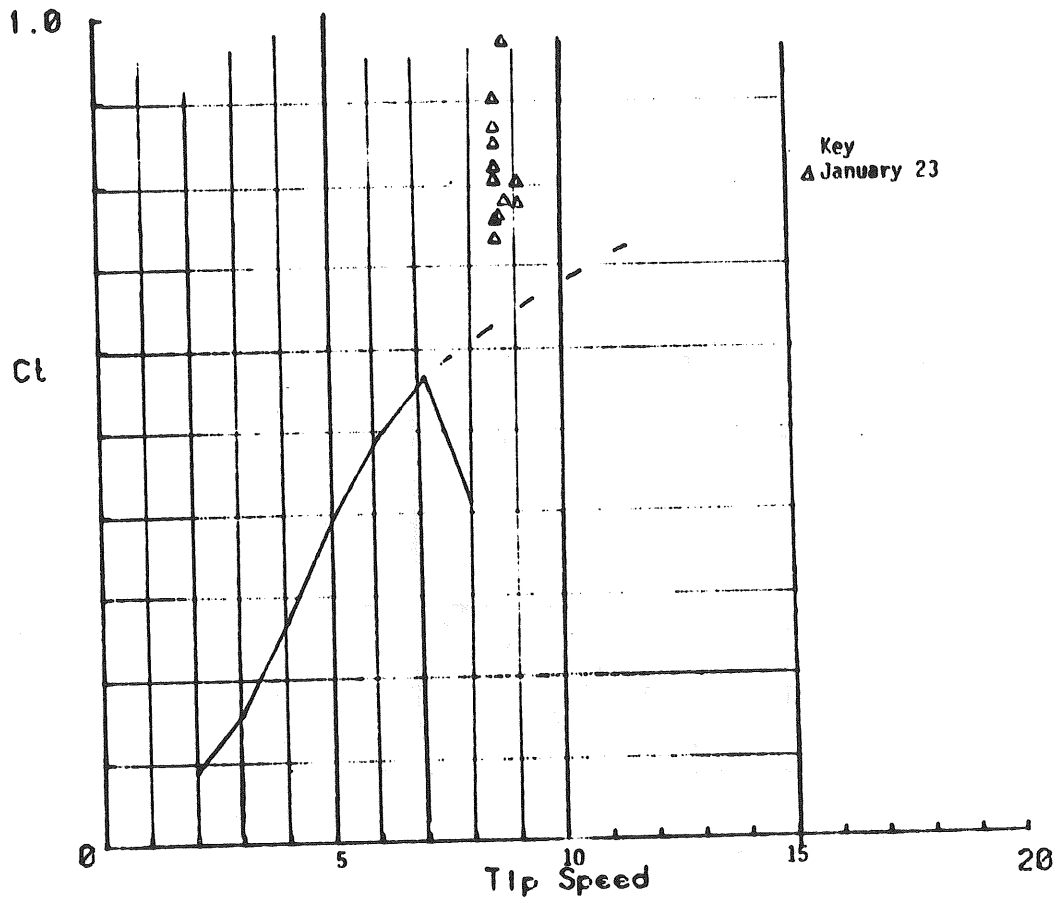


Figure 4.47
 C_t Vs Tip Speed at $31.5^\circ \beta$

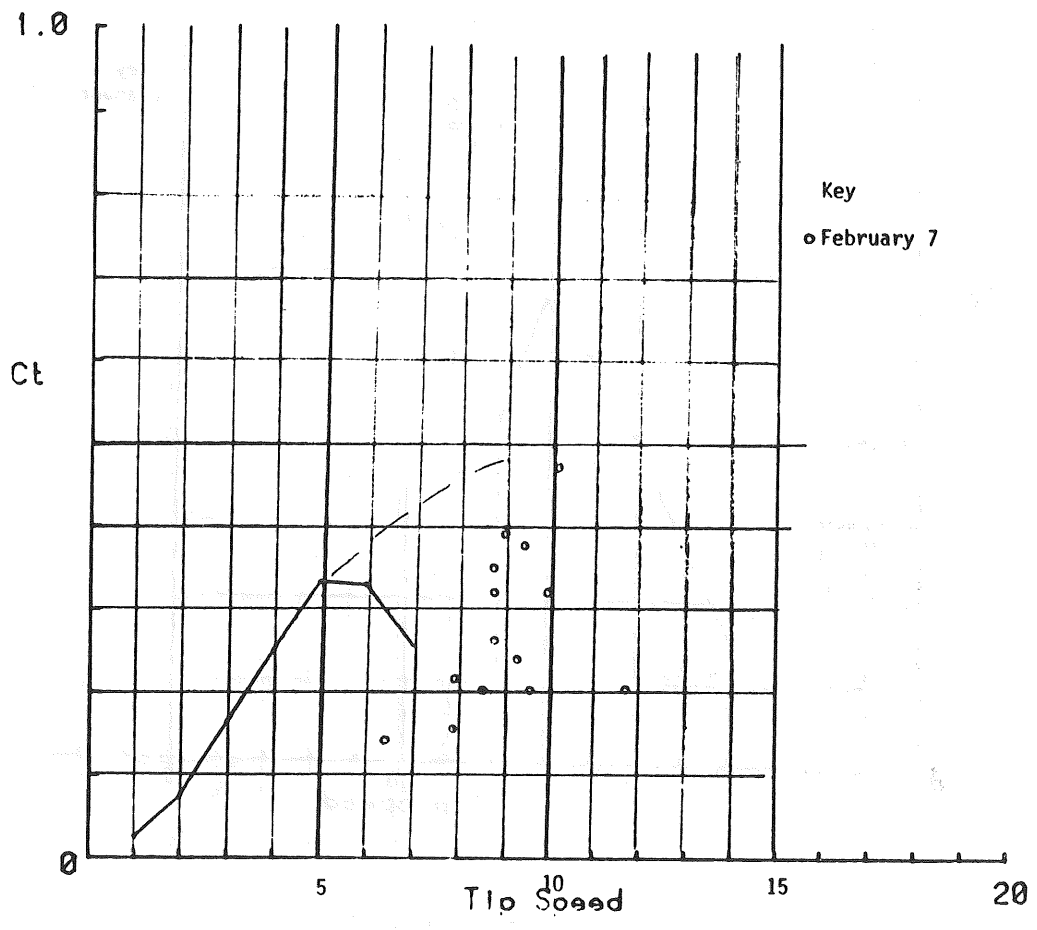


Figure 4.48
 C_t Vs Tip Speed at $45^\circ \beta$

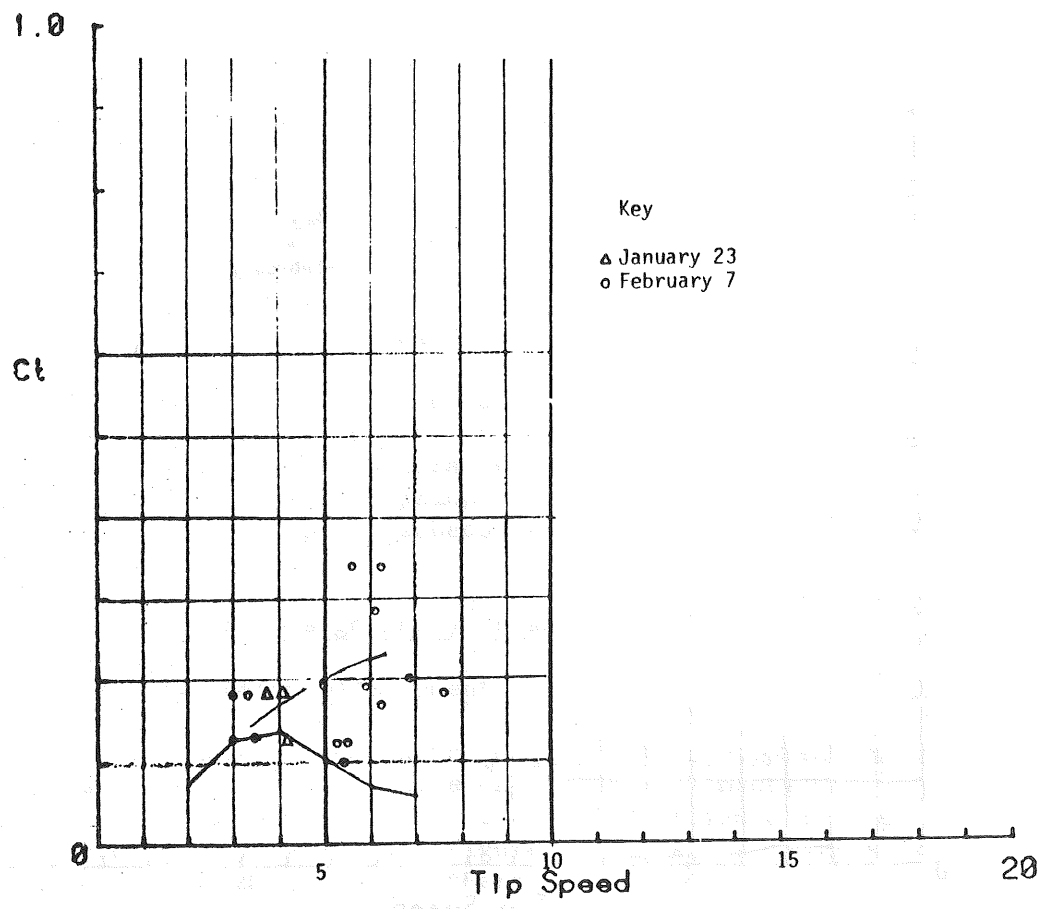


Figure 4.49
 C_t Vs Tip Speed at $60^\circ \beta$

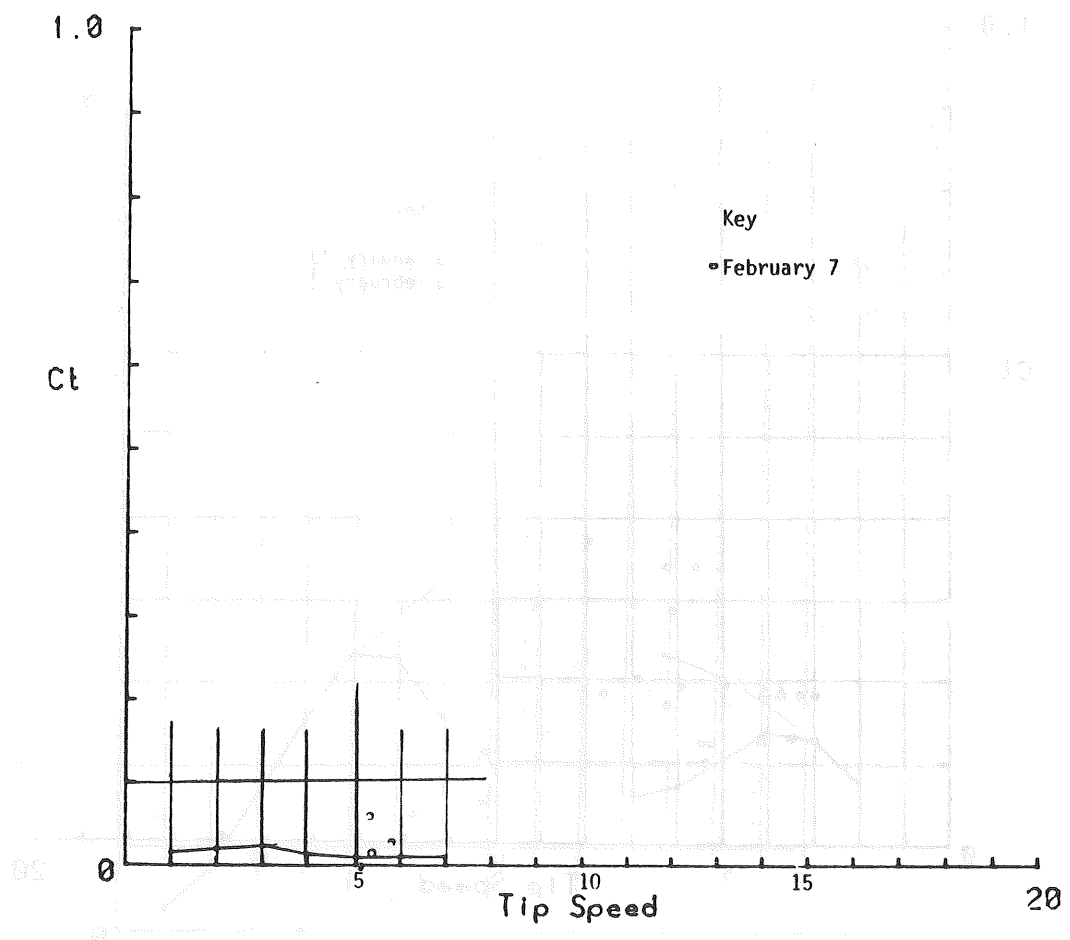


Figure 4.50
 C_t Vs Tip Speed at $75^\circ \beta$

The second series of tests were conducted with the 5 meter rotor mounted on the #2 prototype alternator using a first prototype of the VARCS spring. The rate for this spring was not linear throughout the pitch range, nor was it as stiff as had been expected. In order to test the accuracy of the theoretical model, a performance matrix was developed which matched the low torque requirements of the #2 alternator (see Figure 4.51) to rotor power according to a pitch schedule so that the slope of the graph of overturning moment versus pitch angle matched the approximate spring rate of the prototype spring.

With the field excitation at the highest setting of four amperes, numerous test runs were taken. Figure 4.52 shows data points from these tests overlaid on the power curve based on the performance matrix. This figure indicates excellent consistency of data and good correlation between analytical and empirical data for these parameters. However, although pitch angle data exhibits good consistency in Figure 4.53, the correlation between the empirical and the analytical is not close. A careful look again at the power data and the RPM data (Figure 4.54) shows a slight shift to lower wind speeds. Again this shift as well as the discrepancy between test and theoretical pitch data may be assigned in part to the flow disturbance around the truck, which caused the rotor to "see" more wind than the anemometer measured.

On the basis of test data recorded during the two series of truck tests, NWPCo was confident of the ability of the analytical model, given known airfoil and alternator torque characteristics, to predict, within manufacturing tolerances ($\pm 10\%$), the spring characteristics necessary to give the specific performance and pitch schedule desired.

4.5 Support Structure Design Analysis and Testing

4.5.1 Preliminary Design Development

Previous sections have discussed the design and development of the operating elements of this system. While many of the elements of the proposed design changed through the program, the basic configuration, except for the size, remained very similar. Figure 4.55 is the designer's sketch of the proposed design. Using the Parris-Dunn as a model, NWPCo hinged the VARCS behind and below the alternator. The tail was attached to the free-yawing saddle and a bumper was provided for the alternator at rest. Instead of a coil spring behind the generator connected to the tail, NWPCo proposed a spiral torsion spring fixed on the VARCS shaft. Figure 4.56 is a cut-away drawing of the final design. The VARCS hinge point is still behind and below the rotor/assembly, the tail is mounted as on the Parris-Dunn, on the saddle, and the VARCS spiral torsion spring is fixed on the VARCS shaft. All of these elements have been the subject of extensive trades and engineering analysis which will be reviewed in the following section.

Figure 4.51
Rotor #7/Alternator #2a Matches

<u>Pitch Angle</u>	<u>C_T</u>	<u>D_G</u>	<u>V_{m/s}</u>	<u>X</u>	<u>RPM</u>	<u>C_p</u>	<u>Q_{N-M}</u>	<u>Rotor (Watts)</u>
0	.773	.196	8.9	9.02	308	.369	95.0	3064
10	.77	.374	9.0	8.9	306	.351	94	3012
20	.75	.569	9.2	8.36	294	.316	94.3	2903
30	.62	.913	9.4	7.29	262	.258	92.2	2529
40	.43	1.278	9.8	6.01	225	.185	86.9	2047
50	.275	1.834	10.6	4.4	178	.103	77.3	1441
60	.07	2.442	11.4	1.5	65.3	.013	33.4	228
70	.05	4.051	12.7	1.1	53.4	.006	27.6	154
80	.02	6.645	14.4	0.5	27.5			
90	.001475	14.141	17.4	0	0	0	0	0

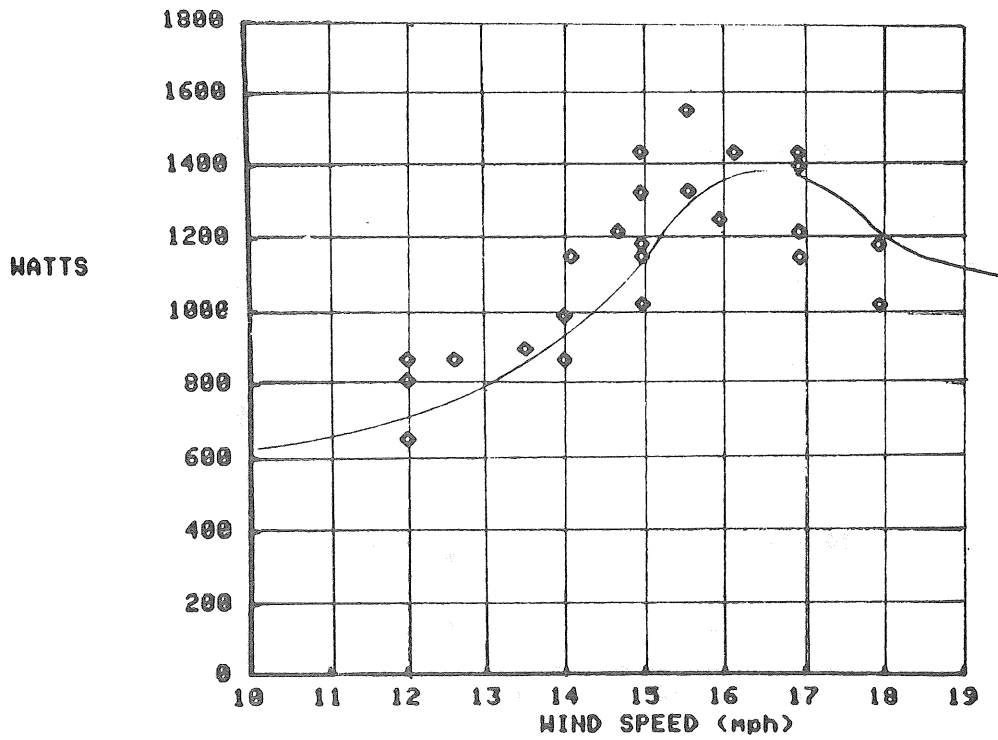


Figure 4.52

PPM #3 Power Output Vs Wind Speed (MPH)

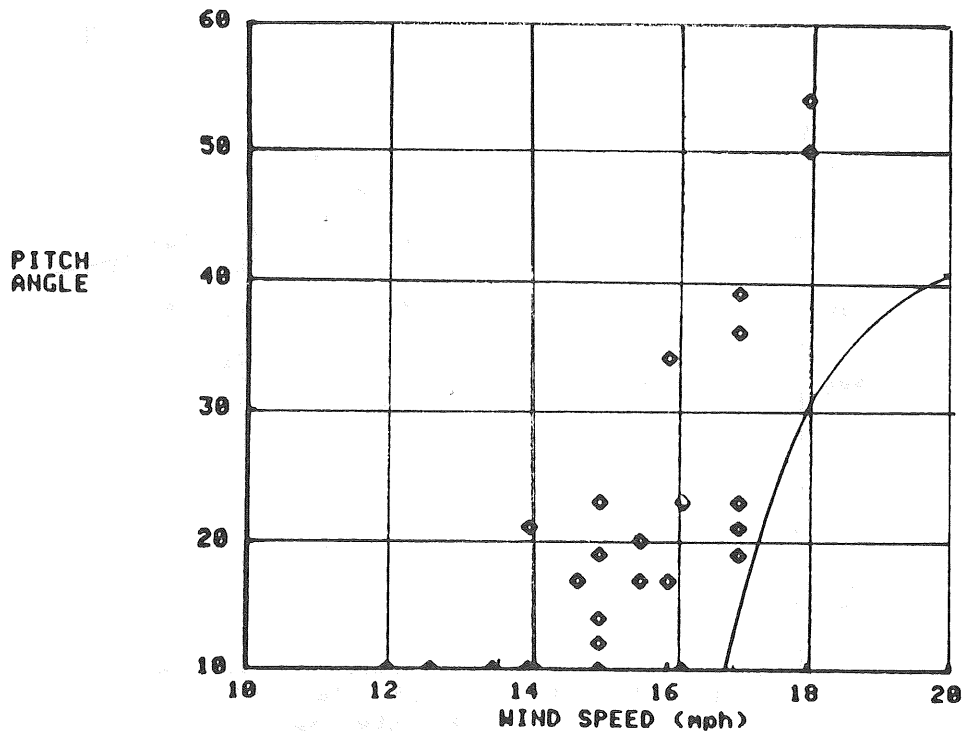


Figure 4.53
Pitch Angle Vs Wind Speed (MPH)

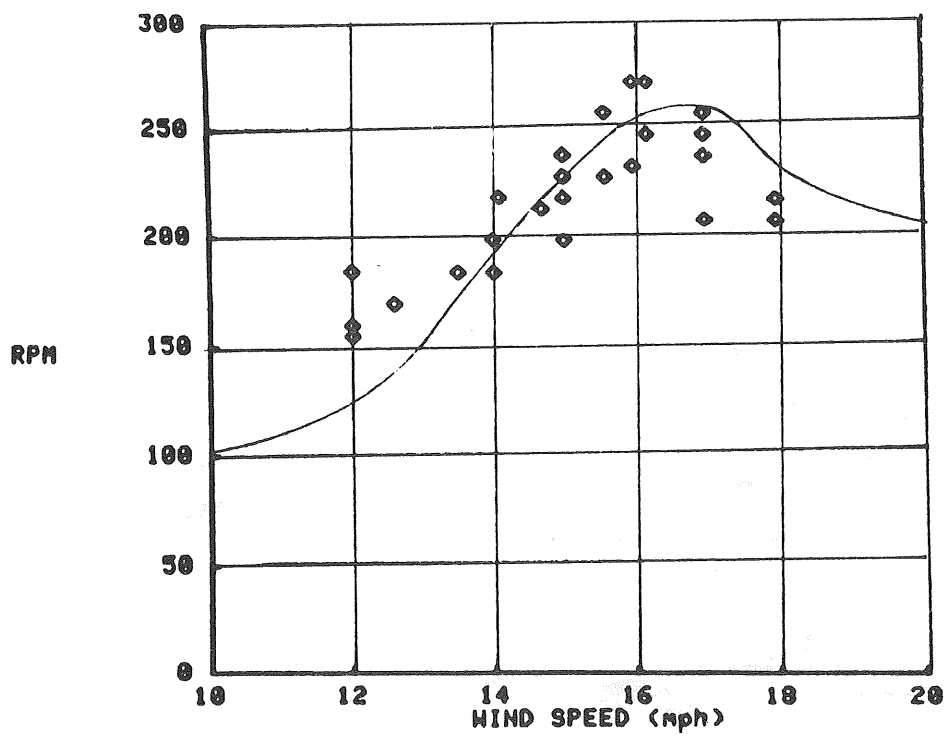


Figure 4.54
 PPM #3 RPM Vs Wind Speed (MPH)

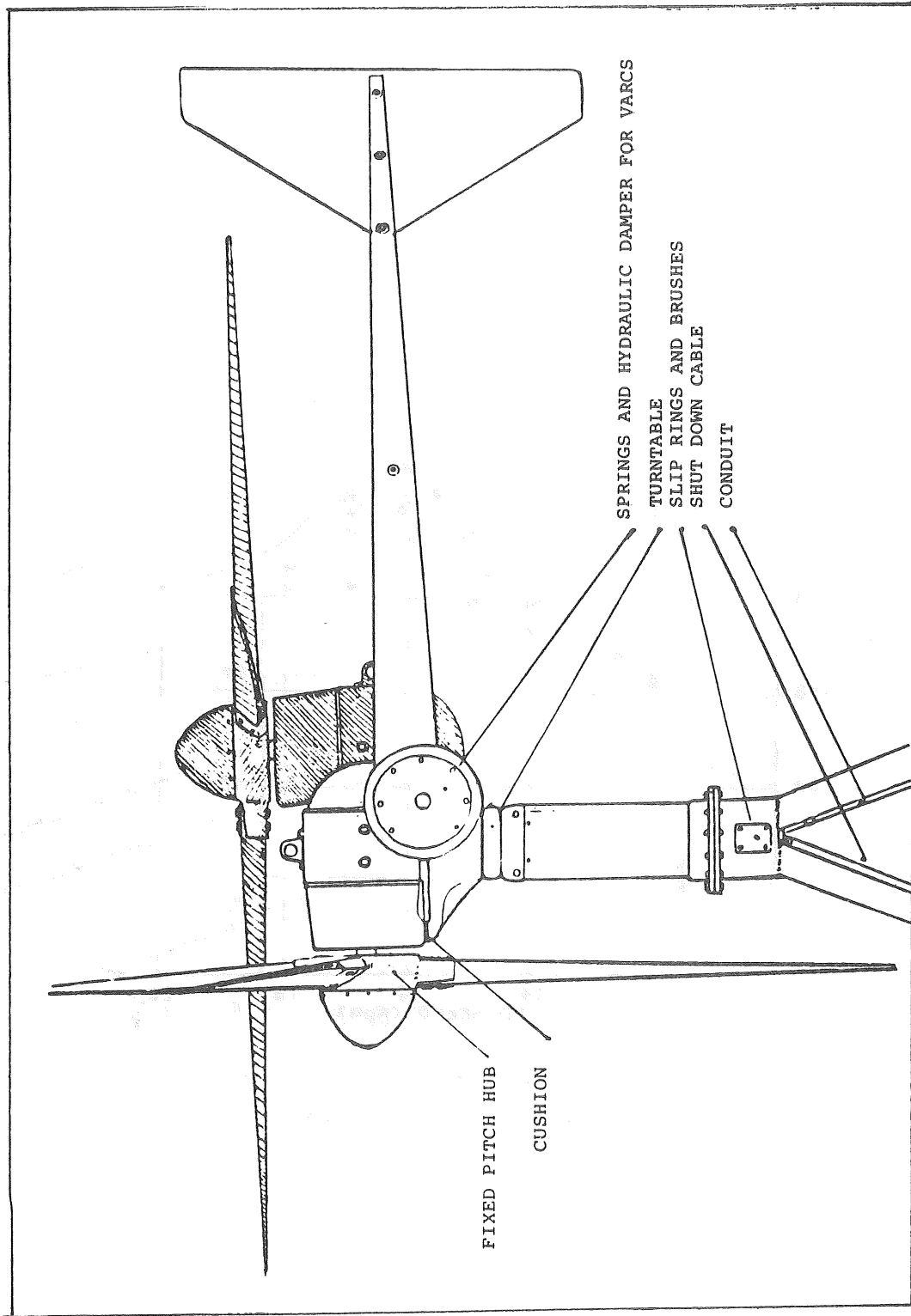


Figure 4.55
Designer's Sketch of HR2

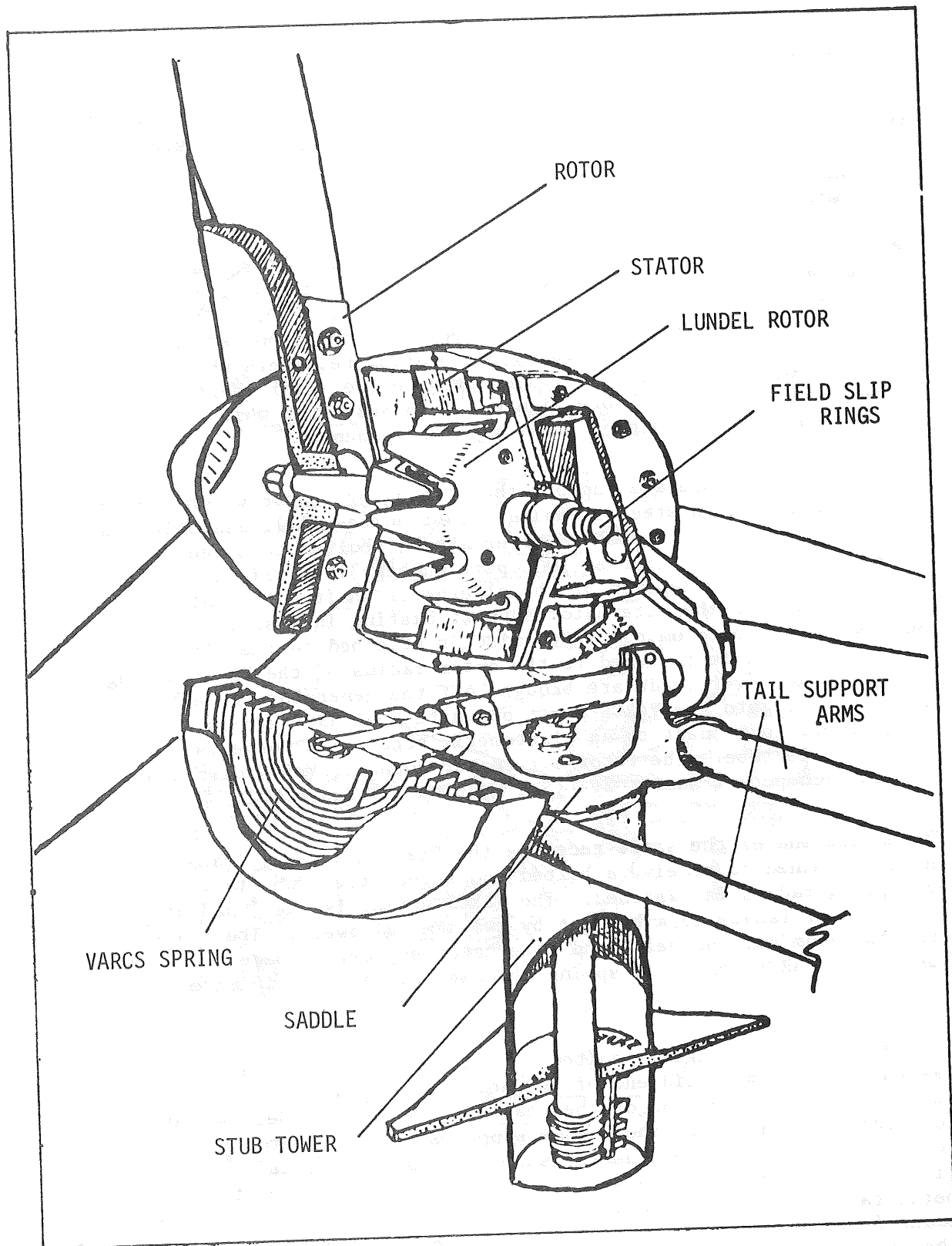


Figure 4.56
HR2 Cutaway View

4.5.2 Overall Final Design Analysis

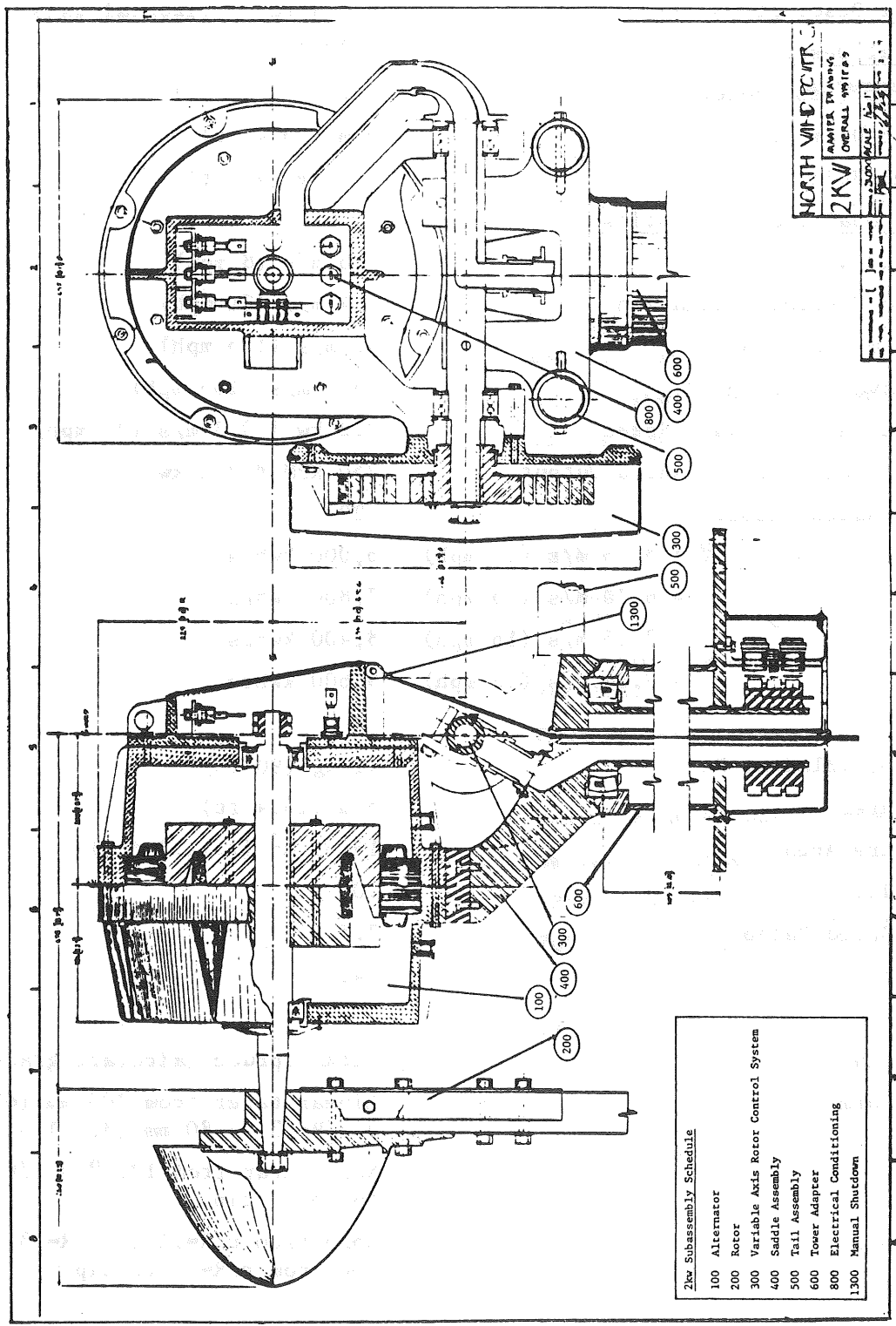
Figure 4.57 is the master drawing for the high reliability 2kw SWECS. This drawing shows in elevation and section the major sub-systems and components with overall dimensions. The parts sub-assembly numeration is shown and keyed in the lower left hand corner. Figure 4.58 is a complete specification chart for this system.

The assembled rotor is mounted rigidly to the alternator shaft using a tapered and keyed fit. The Lundel rotor of the alternator is also mounted on this shaft using a shrink and keyed fit (Series 200.) This assembly element consists of steel, wood and copper and is supported in the aluminum end bells by two stainless steel bearing retainers which reduce the potential for electrolytic corrosion between the steel shaft and aluminum end bells (Series 100.) Note Figure 2.1 in Section 2 which is a schematic of the relationship of these major components.

The end bells enclose and support the alternator stator which consists of laminated silicon steel stampings (part number 111), assembled and dipped in epoxy. The assembled alternator is bolted to a tenzallo alloy aluminum support casting (Series 300, part number 310). Field slip rings are mounted on an extension of the alternator shaft such that field brushes can be mounted on the alternator support casting in a sealed enclosure (Series 800). The aluminum VARCS disc is attached to the alternator support casting and is fastened to the outer radius of the VARCS spring. One field and two power leads are brought off the generator through an aluminum conduit into the VARCS shaft opposite the VARCS spring. The shaft is bored out to connect to an elastomeric boot which connects the shaft to the saddle tube. The rotor/alternator support, VARCS disc and wireway constitute component number 2. (See Section 2, Figure 2.1.)

The hollow end of the shaft receives the field and power leads. The solid end is machined to receive a bolted and keyed steel hub to which the inner spring radius is fastened. The VARCS spring is steel and attached at the outer radius to a bracket by two cam followers. The transition from the aluminum end bells and alternator support is made to the stainless steel VARCS shaft and spring through bearings to minimize corrosion potential.

The VARCS shaft is rigidly bolted to the cast steel saddle. One bolt passes through the solid end of the shaft. A second bolt passes over and clamps the hollow end of the shaft to the saddle (Series 400). Prior to pitchback, an arm of the saddle supports the alternator on a cast silicone bumper. The 2½-in diameter support arms for the tail assembly fit into seats cast in the steel saddle and support a sheet metal tail vane of triangular shape (Series 500.) The main yaw bearing is mounted over a machined seat in the casting and seated in the upper part of the stub tower. A steel tube is welded to the saddle and passes through the lower sleeve-type yaw bearing. Two power slip rings and the field slip



2kW Subassembly Schedule

100	Alternator
200	Rotor
300	Variable Axis Rotor Control System
400	Saddle Assembly
500	Tail Assembly
600	Tower Adapter
800	Electrical Conditioning
1300	Manual Shutdown

Figure 4.57
Master Drawing

Figure 4.58

Table of System Specifications

<u>General Description</u>	3 bladed, horizontal axis, upwind
<u>Physical Description</u>	
Weight (less tower)	356 kg (785 lb)
Rotor Diameter	5 m (16.4 ft)
Tower Height	12.2 m (40 ft)
<u>Operational Characteristics</u>	
Cut-in Wind Speed	3.6 m/s (8 mph)
Speed Control Initiation	9.4 m/s (21 mph)
System Shutdown	47 m/s (105 mph)
Survival Wind Speed	73.7 m/s (165 mph)
Rated Output @ Wind Speed	2.2 kw @ 9.3 m/s (21 mph)
Rotational Speed @ Rated Output	250 RPM @ 2.2 kw
C_s @ Rated Output	.29
Yearly Output in $\bar{v} = 5.36$ m/s (12 mph)	6,000 kWhrs
= 6.70 m/s (15 mph)	7,800 kWhrs
= 7.15 m/s (16 mph)	8,400 kWhrs
= 8.04 m/s (18 mph)	9,600 kWhrs
<u>Rotor</u>	
Weight (Blades, Hub)	41 kg (90 lb)
Diameter	5 m (16.4 ft)
Capture Area	19.63 m ² (2.11.2 ft ²)
Solidity	.04
Tip Speed Ratio	7.5
C_p at Rated Output	.41
<u>Blades</u>	
Material	Sitka spruce (aircraft grade)
Planform	Linear taper from 200 mm (8") @ $r/R=.3$ to 80 mm (3.1") @ tip
Twist	Non-linear from 12.5° @ $r/R=.3$ to .5° @ tip
Airfoil	G625 from $r/R=.1$ to $r/R=.3$, N60 from $r/R=.3$ to tip

Figure 4.58 (cont'd)
Table of System Specifications

<u>Hub</u>	
Material	Cast and wrought steel (ASTM 148-73 Class 80-50)
Type	Fixed Pitch
<u>Generator</u>	
Type	3-phase synchronous alternator (Lundel rotor)
Nominal Voltage	24 vDC
Size	458 mm (18") by 368 mm (14.5")
Number of Poles	12
Synchronous Speed @ 25 Hz	250 RPM
Rated Power @ Speed	2.2 kw @ 250 RPM (150' trans- mission line)
Efficiency	70% @ rated speed and output
Weight	133 kg (295 lb)
<u>Speed Control</u>	
Type	Variable Axis Rotor Control System (VARCS)
Spring	Spiral Torsion Spring K = 71 in-lb/degree
Pitch Range	5° to 90° (from horizontal to vertical)
<u>Yaw Control</u>	
Free yawing	
<u>Tower</u>	
Type	Unarco Rohn 45 GSR dbl. guyed
Material	Galvanized steel
Height	12.2 m (40 ft)
Weight	700 kg (1555 lb)
<u>System Cost</u>	
Unit	\$2867
Tower	\$ 700
Storage	\$2000 (24 volts)
Installation	<u>\$1200</u> (site dependent)
TOTAL	\$6767

Figure 4.58 (cont'd)
Table of System Specifications

Cost of Energy

Installed Cost	\$6767
Fixed Charge Rate	.085
Annual Operation & Maintenance Cost	\$135
Annual Kilowatt Hours Produced	7,800 (assume 6.7 m/s (15 mph) average)

$$\text{COE} = \frac{\text{IC (FCR)} + \text{AOM}}{\text{kwhrs}}$$

$$\text{COE} = \frac{6767 (.085) + 135}{7800}$$

$$\text{COE} = \$0.091 \text{ per kilowatt hour}$$

ring are mounted at the bottom of the tube below the bottom plate of the stub tower.

The entire tower adapter assembly (Series 600) is set on the tower (Series 700). This assembly consists of a machined steel disc, providing a seat for the upper main yaw bearing, welded to a 7½-in diameter by 12-in long steel pipe in turn welded on a triangular steel plate sized to adapt to a standard Rohn 45GSR tower section. The saddle tube passes through a sleeve bearing set in the tower plate. Power and field brushes are mounted on the underside of the stub tower and protected by a weathertight cover.

The manual shutdown assembly (Series 1300) consists of a shielded aircraft cable fastened to the alternator support, passing through a plastic sleeve in the saddle down through a channel inside the saddle tube and out the center of the power and field slip ring cover. The cable is connected to a ball bearing swivel which allows the system to yaw without twisting the cable. The unit can be cranked manually from the tower base to 90° pitch-back for shutdown and service.

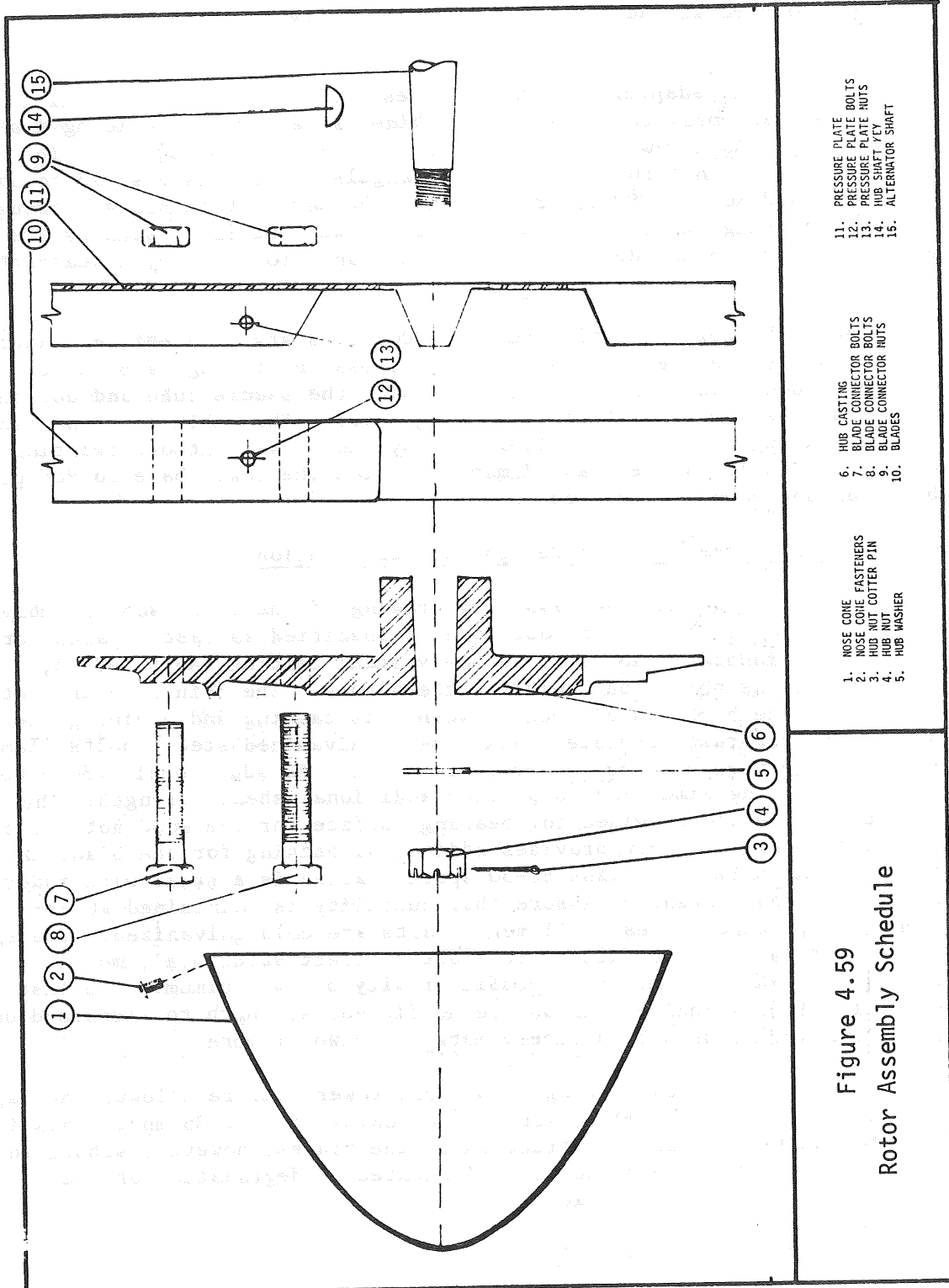
4.5.3 Rotor Assembly Final Design and Verification

Figure 4.59 is an exploded assembly drawing of the rotor sub-assembly with a complete parts list. The nose cone is specified as cast royalex for durability and manufacturability. A heavy steel casting (ASTM 148-65, Class 80-50) is bolted on upwind of the blades. The 2-in by 6-in root section of the blade is clamped between this casting and a nine-gauge stamped steel pressure plate. Six ¾-in galvanized steel bolts clamp the blade between casting and pressure plate. An additional 3/8-in bolt passes through the long dimension to provide additional shear strength. The ¾-in diameter bolts are provided for bearing surface for the wood not for clamping. The pressure plate provides additional backing for the blade in bending. The ASTM 148-65, Class 80-50 specification is a steel with moderate to high carbon content to assure that ductility is maintained at extremely low temperatures. All metal parts are cold galvanized. The spruce blade material is specified as to grade: select structural; moisture content of 19% maximum; and specific gravity of .4 minimum. The last specification is included to assure sufficient strength to withstand out-of-plane bending loads with a safety margin of two or more.

In the course of truck testing, a support tower failure allowed the rapidly rotating rotor (400 RPM+) to strike the runway at over 35 mph. This incident resulted in total destruction of the blades; however, subsequent examination of the hub connections indicated no degradation of the quality of the blade or hub connections.

4.5.4 Alternator Sub-Assembly

Figure 4.60 is the exploded sub-assembly drawing for the alternator with parts list. This assembly consists basically of the shaft, bearings, end bells, rotor and stator. Due to the magnetic characteristics of the Lun-

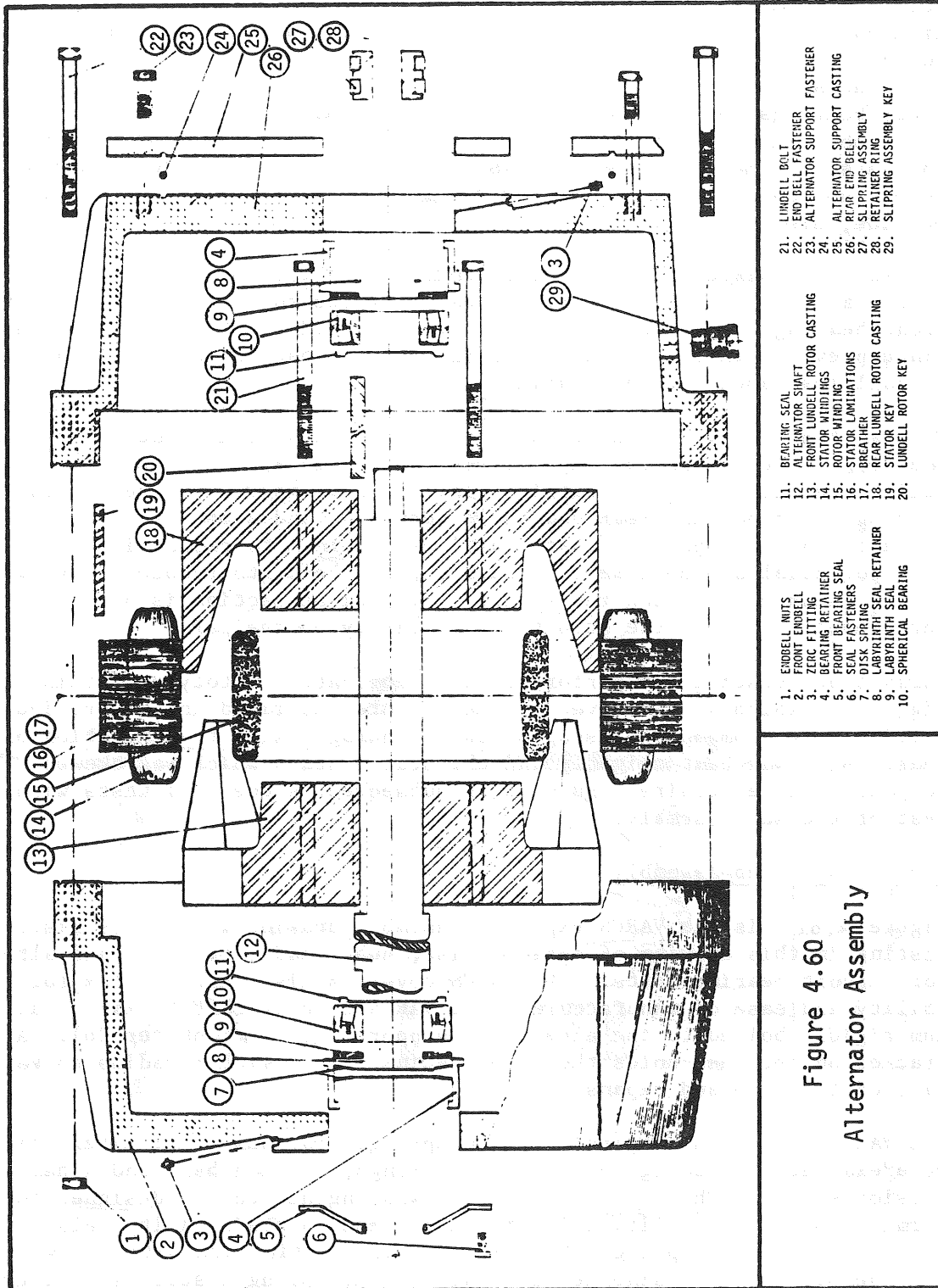


- 11. PRESSURE PLATE
- 12. PRESSURE PLATE BOLTS
- 13. PRESSURE PLATE NUTS
- 14. HUB CASTING
- 15. ALTERNATOR SHAFT

- 6. HUB CASTING
- 7. BLADE CONNECTOR BOLTS
- 8. BLADE CONNECTOR NUTS
- 9. BLADE CONNECTOR BOLTS
- 10. BLADES

- 1. NOSE CONE
- 2. NOSE CONE FASTENERS
- 3. HUB NUT COTTER PIN
- 4. HUB NUT
- 5. HUB WASHER

Figure 4.59
Rotor Assembly Schedule



- 21. LUNDELL BOLT
- 22. END BELL FASTENER
- 23. ALTERNATOR SUPPORT FASTENER
- 24. ALTERNATOR SUPPORT CASTING
- 25. ALTERNATOR SUPPORT CASTING
- 26. REAR END BELL
- 27. SLIPPING ASSEMBLY
- 28. RETAINER RING
- 29. SLIPRING ASSEMBLY KEY

- 11. BEARING SEAL
- 12. ALTERNATOR SHAFT
- 13. FRONT LUNDELL ROTOR CASTING
- 14. STATOR WINDINGS
- 15. ROTOR LAMINATIONS
- 16. BREATHER
- 17. REAR LUNDELL ROTOR CASTING
- 18. STATOR KEY
- 19. LUNDELL ROTOR KEY
- 20. LUNDELL ROTOR KEY

- 1. ENDBELL NUTS
- 2. FRONT ENDBELL
- 3. ZERO FITTING
- 4. BEARING RETAINER
- 5. FRONT BEARING SEAL
- 6. SEAL FASTENERS
- 7. DISK SPRING
- 8. LABYRINTH SEAL
- 9. LABYRINTH SEAL RETAINER
- 10. SPHERICAL BEARING

Figure 4.60
Alternator Assembly

del rotor, the end bells must be made of a non-magnetic material, such as aluminum. The front bearing is pre-loaded by a set of disc washers to take up differential thermal expansion and to limit machinery tolerances. Both bearings are grooved for lubrication, as are all other bearings in the system. Early investigations of bearings indicated that lubricant life expectancies limited sealed bearing life to less than 15 years. To meet the 25-year system life goal, NWPCo specified bearings to be lubricated every year or as necessary. Seals, both inside and outside, are steel.

The shaft is sized to support the Lundel rotor with minimal deformation of the air gap, and to support the cantilevered rotor loads ahead of the front bearing. Particular attention was devoted to this latter dimension since previous experience with the Parris-Dunn had indicated a tendency to fail just ahead of the bearing.

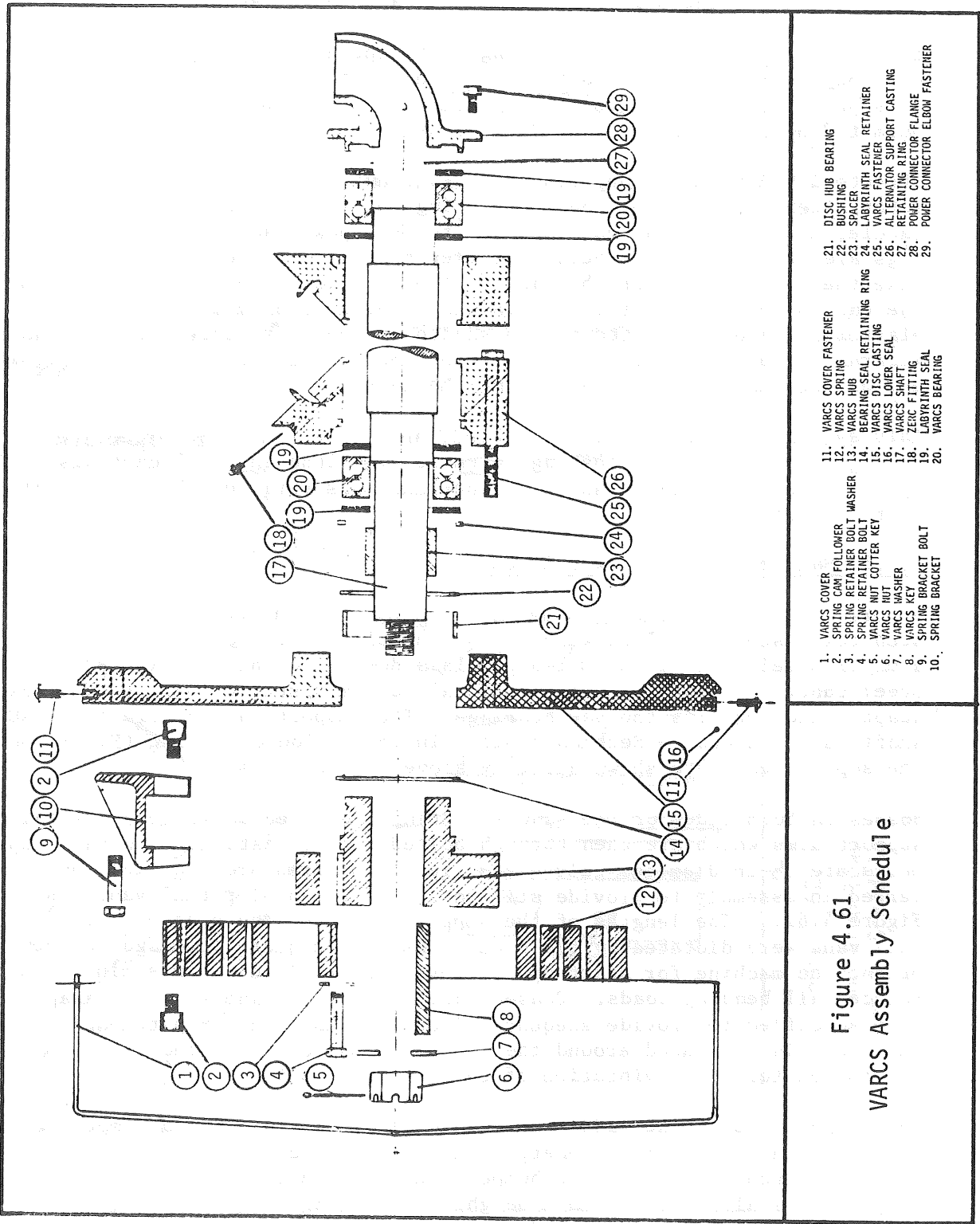
Figure 4.60 shows the alternator support at its attachment to the rear end bell. The alternator support was maintained as separate from the end bell to permit greater versatility in the early manufacturing process by keeping the front and rear end bells identical and simplifying part changes. The alternator support is cast tenzallo aluminum to reduce dielectric potential at the interface with the end bell, to reduce active weight, and to enhance corrosion resistance. Sufficient section is provided throughout to insure the structural integrity of the part.

Early truck testing was performed on a fabricated prototype of this configuration which was involved in the failure described in the previous section. All components escaped without damage, with the exception of the shaft which was bent slightly and the stator stack which was skewed. These components were repaired and used in subsequent successful tests with the rest of the sub-assembly.

4.5.5 VARCS Sub-Assembly

Figure 4.61 is the VARCS exploded assembly drawing with parts listed consisting in this drawing of spring, disc, hub, shaft, bearings and alternator support bearing seats. The VARCS cover is also cast royalex for durability and ease of manufacture. The VARCS disc is cast tenzallo aluminum rigidly bolted to the alternator support leg (part number 26). A bracket on the disc holds the outer radius of the spring radius to vary with contraction and expansion.

The VARCS spring is a spiral torsion spring. Various other alternatives were examined including coil torsion springs, torsion bars and a helical torsion spring. This last alternative was engineered and designed to determine cost, reliability and performance and maintainability relative to the spiral torsion spring. The spiral configuration was ultimately selected due to assembly and maintenance advantages. The spring itself is fabricated from $1\frac{1}{2}$ -in and $\frac{1}{2}$ -in AISI 4340 spring steel, coiled hot and treated after fabrication. Depending on the location of the cam followers, the spring rate can vary from 82 in-lb per degree to 65 in-lb per degree. The



- | | | |
|--------------------------------|---------------------------------|------------------------------------|
| 1. VARCS COVER | 11. VARCS COVER FASTENER | 21. DISC HUB BEARING |
| 2. SPRING CAM FOLLOWER | 12. VARCS SPRING | 22. BUSHING |
| 3. SPRING RETAINER BOLT | 13. VARCS HUB | 23. SPACER |
| 4. SPRING RETAINER BOLT WASHER | 14. BEARING SEAL RETAINING RING | 24. LABYRINTH SEAL RETAINER |
| 5. VARCS WIPER | 15. VARCS DISC CASTING | 25. VARCS FASTENER |
| 6. VARCS HUB | 16. VARCS LOWER SEAL | 26. ALTERNATOR SUPPORT CASTING |
| 7. VARCS WASHER | 17. VARCS FITTING | 27. RETAINING RING |
| 8. SPRING BRACKET BOLT | 18. ZINC FITTING | 28. POWER CONNECTOR FLANGE |
| 9. SPRING BRACKET | 19. LABYRINTH SEAL | 29. POWER CONNECTOR ELBOW FASTENER |

Figure 4.61
VARCS Assembly Schedule

inner radius of the spring is clamped in a machined steel hub keyed and bolted to the VARCS shaft. As the unit pitches back, the disc rotates through 90° , contracting the spring. The spring is set up so that it is open beyond the at-rest position through 30° to assist pitchback. Beyond this point it contracts to resist pitchback. The spring is coiled to permit $3/8$ -in clearance between coils when contracted.

The steel VARCS shaft supports spring and hub, transfers the load to the rotor/alternator assembly on two bearing legs to the support ears of the saddle, and provides an enclosed way for the power and field wires. Bearings are double-acting spherical roller bearings, sealed and greasable like the alternator shaft bearings. The wire way is bored through from one end to the center of the VARCS shaft where it passes through a cast elastomeric boot connected to the saddle. A bolt prevents torsional and lateral movement of the shaft. A second bolt over the top of the hollow end of the shaft assists in keeping the unit seated in the saddle.

This system was fabricated, assembled, and tested in a pre-prototype configuration for truck testing in Phase I. Although final castings will not be completed until Phase II, experience has verified the feasibility of this configuration.

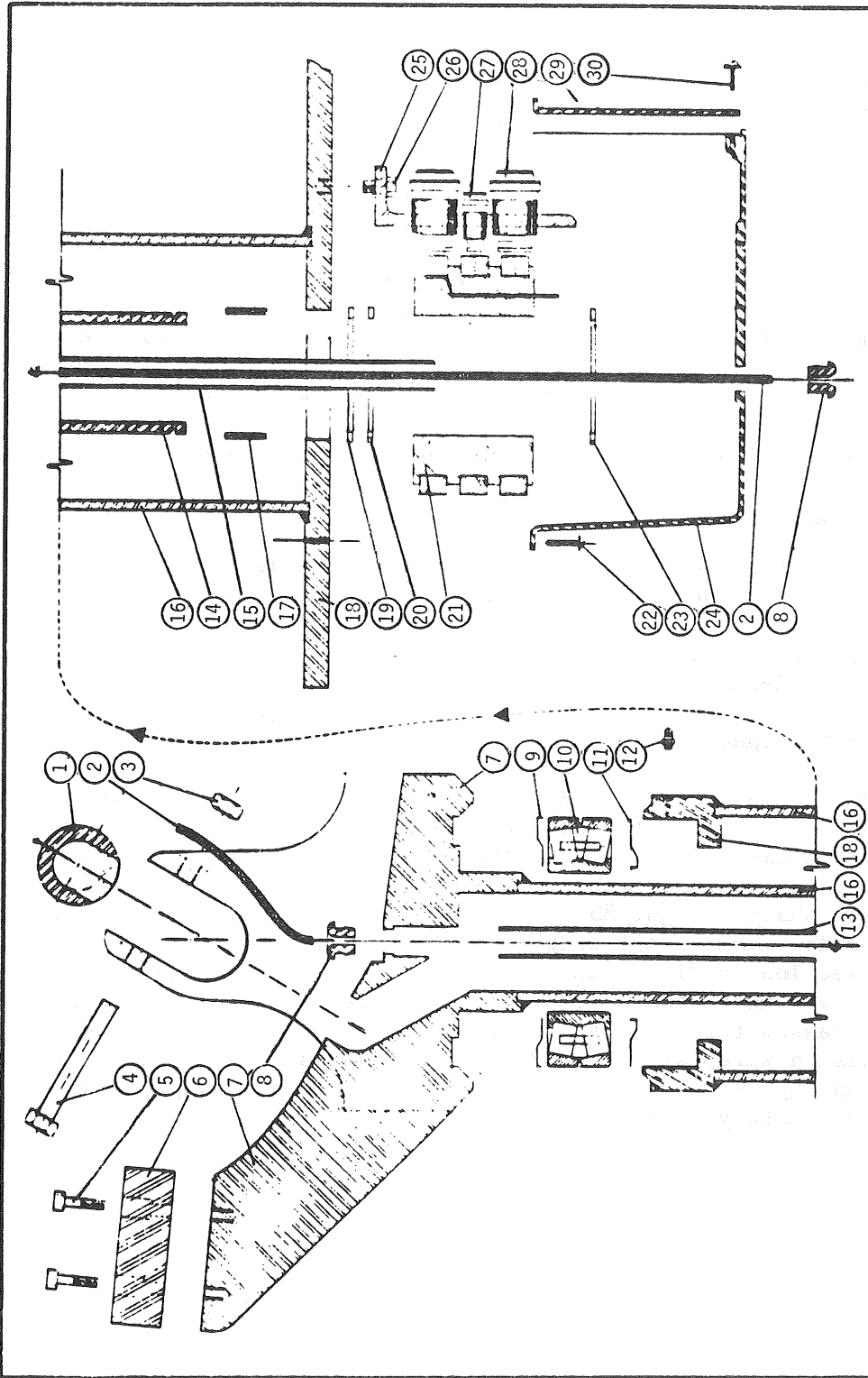
4.5.6 Saddle and Stub Tower Assembly

Figure 4.62 is an exploded assembly drawing of both the saddle and stub tower sub-assemblies with parts schedule. The saddle consists of a major steel casting (ASTM 148-65 Class 80-50) to which is welded a steel tube. This assembly transfers all dynamic/static loads to the tower adaptor and supports the yaw bearings. The support ears cradle the VARCS shaft as explained in Section 4.5.5. In the exploded drawing (Figure 4.62) the support ears are shown directly above the yaw axis.

Bosses on both sides of the saddle casting are cored to receive the tail support arms which are then through-bolted to the casting. The tail supports are $2\frac{1}{2}$ -in diameter galvanized pipe. The arms are identical but inverted in assembly to provide stiffening for triangular tail vanes (see Figure 4.62.) The lengths of the support arms and the area of the tail vane were dictated by the need to assure adequate leverage to properly orient the machine for start-up. However, overall length was minimized to reduce tail bending loads. Consequently, the tail vane size and shape were specified to provide adequate blade clearance at 90° pitchback. The vane was also balanced around the support arms to reduce the potential for forced torsional vibration of the tail assembly.

The support arm of the saddle is cushioned by a cast silicon bumper of sufficient size to absorb the energy and minimize the impact of a release from 90° pitchback. With the bumper, such a release is equivalent to dropping the alternator from a height of three inches. In Phase I truck testing, release occurred numerous times without effect on the alternator components.

In addition, the saddle and tube provide a way for field and power leads



- 21. SLIPRING ASSEMBLY COVER FASTENER
- 22. SLIPRING LOWER RETAINER
- 23. SLIPRING ASSEMBLY COVER
- 24. BRUSH HOLDER SUPPORT
- 25. BRUSH HOLDER FASTENER
- 26. BRUSH HOLDER
- 27. BRUSH ASSEMBLY ACCESS PLATE
- 28. BRUSH ASSEMBLY ACCESS PLATE FASTENERS
- 29. BRUSH ASSEMBLY ACCESS PLATE
- 30. BRUSH ASSEMBLY ACCESS PLATE FASTENERS

- 11. BEARING LOWER SEAL
- 12. ZINC FITTING
- 13. PULLOUT CABLE TUBE
- 14. SADDLE TUBE
- 15. TOP TOWER CASTING
- 16. LOWER SUPPORT TUBE
- 17. LOWER BEARING
- 18. LOWER BEARING RETAINER
- 19. LOWER BEARING RETAINER
- 20. SLIPRING TOP RETAINER

- 1. VARGES SHIRT
- 2. PULLOUT CABLE
- 3. VARGES SHIRT FASTENER NUT
- 4. VARGES SHIRT FASTENER
- 5. BUMPER FASTENER
- 6. BUMPER
- 7. SADDLE CASTING
- 8. PULLOUT CABLE BUSHING
- 9. BEARING UPPER SEAL
- 10. UPPER SADDLE BEARING

Figure 4.62
Saddle and Stub Tower
Assembly Schedule

and for the manual shutdown cable. This latter component passes through a cast elastomer, with a low coefficient of friction, into a conduit and out through the bottom of the slip-ring cover along the yaw axis. At the bottom of the saddle tube, enclosed in the power slip-ring cover, are the slip-rings.

The stub tower or tower adaptor is of the simplest and toughest construction. The top machining, welded to the support tube, supports a large, greasable double-acting spherical roller bearing. The bottom punched plate, welded to the support tube, supports a small plain bearing to stabilize the system, and is bolted directly to the top flanges of a standard Unarco-Rohn 45GSR tower section. Underneath this bottom plate and inside the tower section, a cast Royalex[®] cover protects the slip-rings and brushes mounted on the saddle tube and lower plate respectively. This configuration, as on the alternator support, permits easy access to slip-rings and brushes for inspection and replacement, if necessary.

4.5.7 Final Design Installation

The design of all support components provides adequate material and structural characteristics to sustain the loads imposed by contract power and wind regime specifications within the environmental extremes of snow, ice, salt water, heat and extreme cold. In addition, the overall design attempts to simplify field assembly procedures to minimize the potential for improper field assembly and/or injury. The unit arrives in four packages containing blades, alternator and VARCS assembly, saddle and stub tower assembly and tail. First, the saddle/stub tower assembly is bolted to the tower top (weight approximately 225 pounds.) Second, the tail assembly is hoisted and mounted on the saddle (weight 50 pounds.) Third, the alternator/VARCS assembly is bolted to the saddle (weight 415 pounds.) Finally, the rotor is assembled on the ground and then lifted and fixed to the alternator shaft (weight 85 pounds.) The total system weight on the tower is 775 pounds. (Note that weights used here are actual, while those in the costing section (6.3) are estimated.) At this point, manual shutdown connections are made at the alternator support and swivel. Power and field leads are passed through the saddle tube and connected to the slip rings. Transmission wires are then brought through the power slip ring cover and made up at the brush terminal. The entire erection procedure should take approximately 1½ hours.

5. RELIABILITY, MAINTAINABILITY AND SAFETY ANALYSIS

5.1 Introduction

Throughout this development program, reliability, maintainability and safety have been driving factors in the design process. NWPCo has discovered through its own experience that these factors are the primary purchase considerations for the intended market for this system. This section discusses the techniques and results of the analyses which were applied to quantify these factors and to assure that they were adequately satisfied by the design. In general, our analyses have confirmed the accuracy and effectiveness of the design philosophy applied from the beginning of the project. Where analysis revealed shortcomings and potential weak areas in the design, appropriate design modifications were made.

5.2 Reliability Analysis

This section discusses the techniques and results of the analysis and calculation of system reliability. For purposes of this analysis, a lambda, or rate of failures per million hours, was estimated for every part of the system. All serial lambdas for components within a subsystem, such as the alternator, were summed to develop a single failure rate for that subsystem. Subsystem lambdas were in turn summed to develop the overall failure rate in failures per million hours for the entire system, which was converted to failures per year by the following formula:

$$\frac{\text{failures}}{\text{year}} = \frac{\text{failures}}{10^6 \text{ hrs}} \times \frac{10^6}{114}$$

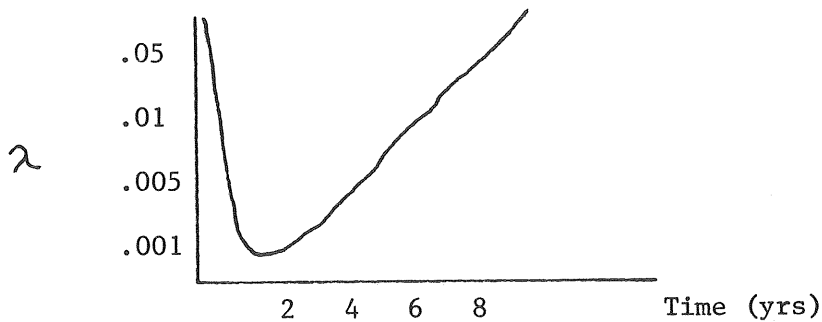
Mean time between failure and lambda (in years) are derived one from the other by inversion. Reliability (R_t) is derived from lambda by the following equation:

$$R_t = E^{-\lambda t}$$

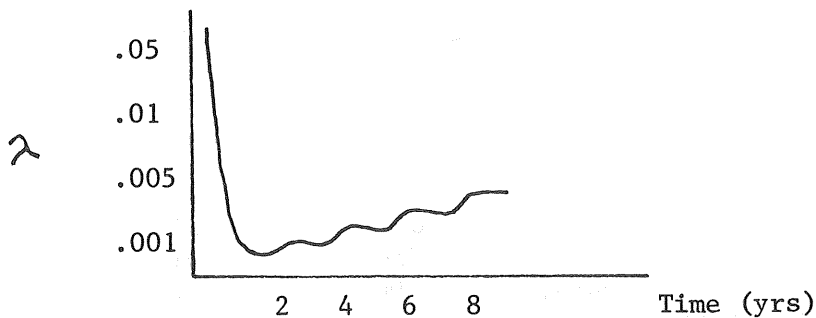
On the data sheets and flow charts in this section, t equals one year in all cases. For parts exhibiting redundancy, such as brushes and bolts, a single lambda was calculated for the aggregate, using the following formula:

$$R(t) = 1 - (1 - R_1) \dots (1 - R_n)$$

All parts are assumed to survive in the system for a mean time between failure (MTBF) of ten years, except as noted. For components specified to be replaced in less than ten years, the lambdas for the components were based on an assumed reliability -- R_t for one year if the part were no older than the maintenance schedule specifies. This technique is applied to pieces with high wear rates such as blades. These parts have a low initial failure rate, but a short MTBF. Graphically:



By refinishing the blades every two years, we change the graph for this component to look like this:



This replacement schedule can adversely affect the reliability rate of fasteners and other parts associated with replaced part. Failure rates and replacement schedules have been adjusted accordingly for those components.

All lambdas account for the actual operating time of the part so that no further adjustment for actual service hours is required.

The greatest difficulty of this analysis was in estimating failure rates for these components. For most pieces, no generic failure data was available. Therefore, it became necessary to estimate failure rates based on metal corrosion rates, material fatigue life characteristics and previous field experience. In spite of the resulting roughness of this calculation, the analysis has produced substantial benefits in design changes to improve maintainability, reduce parts count, and introduce redundancy where necessary and effective.

5.3 Safety Analysis

This analysis identifies major hazards associated with construction, maintenance and normal operation of the 2kw SWECS.

5.3.1 Environmental Hazards

Due to the nature of the projected application of these machines, they will be installed in remote areas, subject to extreme environmental conditions. These conditions subject personnel to illness or injury due to exposure, snow blindness, and freezing of flesh to metal, as well as sunburn and sunstroke. Such locations have notoriously unpredictable weather, and it is recommended that protective clothing, shelter and supplies be provided for all personnel at all times when working at or travelling to and from the site. It should be noted also that judgment

and effectiveness are compromised above 10,000 feet. This condition will aggravate the hazards of working above the ground. All personnel should be cautioned about the above hazards, and special attention must be paid to safe procedures. Under no circumstances should a site be visited alone.

5.3.2 Site Preparation

In the course of site preparation, normal precautions must be taken to protect personnel from injury due to forced particles (i.e. dust, rock, wood chips) and from injury due to excessive noise associated with heavy machinery and air drills and hammers in particular. It must be noted that mountaintop sites offer limited working space and pose special hazards, such as falling or rolling machinery, in addition to those mentioned above.

Precautions for such work are detailed in the Federal OSHA regulations and include eye protection, ear protection, roll bar equipped machinery, lifelines, and procedural recommendations. An Oak Ridge Laboratory report on WECS safety (see Reference 6), also refers to the OSHA requirement for protection from toxic and irritating plants. In general, a site considered for application of this machine should be carefully surveyed for potential hazards and the on-site clearing and excavating process should be carefully planned ahead of time.

5.3.3 Erection and Installation

This operation is generally recognized to be the most hazardous aspect of WECS operation. Tower erection hazards and procedures are well documented and understood (protective measures are detailed in the OSHA register). NWPCo has had experience in all types of tower erection for SWECS. On the basis of this experience, we have specified the Unarco-Rohn 45 GSR tower, as not only strong and stable, but also easy and safe to erect, both with and without the assistance of a crane. The use of helicopters for mountaintop erection and installation must be approached with great caution, as the wind conditions which make a good SWECS site also create hazardous flying conditions.

The installation of the SWECS itself is less understood and poses certain special hazards. There is, of course, the danger of dropped and falling tools and parts, and the major hazard of falling. The 2kw high reliability SWECS is designed to be pre-assembled in the factory (alternator/VARCS and saddle/support tower). The rotor and tail are assembled on site on the ground and the sub-components are then lifted to the tower top and assembled. Power transmission and manual shutdown connections are made. This procedure limits overall time spent on the tower as well as the number of discrete parts and tools required up top. It also augments overall system reliability by reducing to a minimum critical assembly operations under uncontrolled and adverse conditions. Our experience indicates that the tension and discomfort of working up on the tower compromises the quality of workmanship. Therefore, we have concluded that

only simple and gross operations should be performed on the tower in as short a time as possible.

In line with OSHA regulations and sensible practice, hard hats should be worn at all times on the site. Steel-toed and steel-shanked boots are also recommended. The former are recommended for work around heavy objects; the latter reduce fatigue and discomfort from the ladder rungs. When climbing the tower, safety belts should always be used.

Excessive muscle strain is a potential hazard when working with heavy machinery and is aggravated in different circumstances. Development and refinement of installation procedures will reduce the potential for this type of injury.

5.3.4 Inspection, Testing and Maintenance

In addition to the ongoing environmental hazards and those posed by working above the ground (falling, etc.), these operations present the following dangers: impact from the rotor, impact from the unit if released from manual shutdown, and electric shock.

The North Wind machine is designed so that it should not be necessary for the rotor to be turning while personnel are on the tower. Impact from a rotating windmill blade has been known to kill an individual climbing the tower. At the very least, a blade can knock a person to the ground. For this reason, we have included the first ten feet of manual shutdown cable (the section below the rotor-swept area) in the critical components list. We also recommend painting a broad red stripe around the tower three feet below the limit of rotor sweep.

The manual shutdown system provides pitches the unit to 90° where no rotation will occur. Inspection and maintenance can then take place with no danger from blade rotation, regardless of what sudden wind direction changes occur. A yaw locking device such as a lanyard to the tower will prevent sudden unit movement and resultant injury from being pinched or knocked from the tower.

The danger of electrical shock is always present when working on electric generating machinery. However, the low voltage DC power produced by this system presents a very small threat of severe injury. In any case, all electric connections meet or exceed national electric codes. This precaution only makes good sense from the reliability perspective as well.

5.3.5 Operation

Under operating conditions, the hazards of a SWECS system are generally reduced. (See Oak Ridge Lab Report.)⁷ Danger to authorized personnel can be significantly reduced by safety training and system familiarity. Public access to the installation must be restricted, either by fencing or simply by the remote location. In any case, clear warning signs should be provided. The rotor sweep band on the tower is one example.

Figure 5.1
Reliability Flow Chart

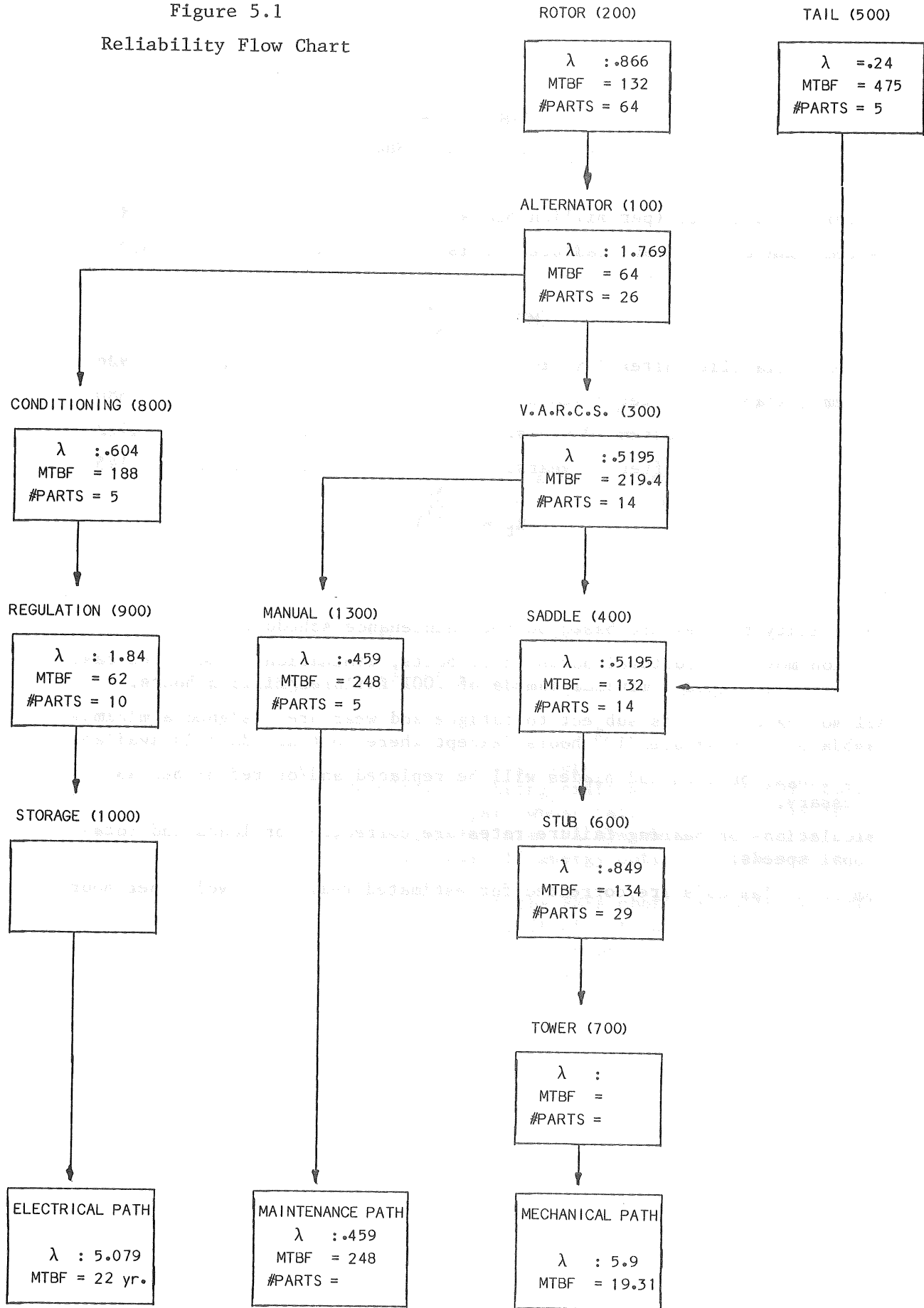


Figure 5.2
Reliability Data Sheet

System failure rate (per million hours).....	8.8
System mean time between failures (years).....	13.0

$$(MTBF = \frac{114}{\lambda})$$

System reliability after 1 year.....	.926
System reliability after 5 years.....	.680
" " after 10 years.....	.462
" " after 25 years.....	.145

$$(R_t = e^{\frac{-\lambda t}{114}})$$

Note:

Reliability figures are based on the maintenance schedule.

All non-moving structural parts (i.e. bolts, laminations, and fixed castings) are assigned a minimum lambda of .001 failures/million hours.

All moving components subject to fatigue and wear are assigned a minimum lambda of .07 failures/10⁶ hours (except where contrary data is available).

Slip rings, brushes and blades will be replaced and/or refinished as necessary.

Calculations of bearing failure rates are corrected for loads and rotational speeds.

Component lambda's are corrected for estimated real life cycles per hour.

As the Oak Ridge report pointed out,⁸ rotor failure resulting in blade sheddings poses a threat to operating personnel and the public. This hazard is reduced by good engineering and workmanship, aspects identified and addressed with care throughout the unit design and testing process.

5.3.6 Conclusions

With few exceptions, most major hazards associated with the installation and operation of this SWECS are well documented and addressed under other headings in the OSHA regulations. The exceptions are injury from the blades in rotation, the alternator/rotor in pitch, and the system in yaw. Our design responds to these hazards with failsafe pitch and yaw locks, warning signs and procedural recommendations.

The greatest and most prevalent hazards (falling equipment and falls from towers) are common to many industries. Tested and approved safety devices are available, and safe procedures are documented. NWPCo's previous experience has encouraged the design of an installation procedure that reduces to an absolute minimum the amount of time spent on the tower and the number of tools and parts carried up the tower.

Environmental hazards are the most unusual and perhaps least generally understood. We cannot emphasize enough the need for respect and preparation when taking personnel and equipment onto sites such as those for which the 2kw high reliability SWECS is intended.

5.4 Failure Mode and Effects Analysis

5.4.1 Introduction

Failure mode and effect analyses (FMEA's) were performed on each component in the system which was identified as being critical. A critical component, for purposes of this analysis, is a part whose failure, due to its function in the system, will cause a system failure. A system failure is defined as a significant reduction of the overall energy output of the system.

The comments in the last two columns of the FMEA chart indicate the conclusions of the analysis of each part as it affects manufacturing and quality control procedures and the maintenance program. The following charts detail the FMEA's conducted on the 2kw high reliability SWECS:

FAILURE MODE AND EFFECT ANALYSIS					
ITEM #	PART NAME, #, FUNCTION	FAILURE			CORRECTIVE ACTION AND REMARKS
		MODE	CAUSE	EFFECT	
1	Stator #110 - The output power is produced in the stator windings - all coil connections are soldered.	<p>1. Winding coil connections broken (soldered).</p> <p>2. Winding shortened to stator laminations.</p>	<p>a. Excessive vibration breaks connection.</p> <p>b. A poor factory connection fails.</p> <p>a. Insulation is cut in the process of fabrication.</p> <p>b. Insulation is worn through due to rough handling or excess vibration in operation.</p>	<p>Partial loss of electric output will be the effect of all these failure modes.</p>	<p>Good packaging for shipment and good rotor balance, careful assembly and inspection procedures, including the use of paper in slots will reduce potential for these failures.</p> <p>Careful assembly will prevent this unlikely failure. Inspection procedure should include measurement of phase winding conductance. This should be done in field if reduced output is suspected. If discovered, a complete rewind of stator may be necessary.</p>

FAILURE MODE AND EFFECT ANALYSIS					
ITEM #	PART NAME, #, FUNCTION	FAILURE			CORRECTIVE ACTION AND REMARKS
		MODE	CAUSE	EFFECT	
2	Rotor (Alt) #120 - Magnetic flux for generation of stator output is produced in rotor. Current is very low and the winding is a single coil. Includes castings, one shrunk on shaft and one keyed, windings, shaft and key.	1. Lundel casting rotates on shaft freely.	a. Loose fit due to poor machining of Lundel and shaft causes key to shear. b. Abrupt extraordinary overload stopping rotation shears the key.	Complete loss of electrical output.	This failure mode is unlikely. Corrective action if necessary would involve disassembly of alternator and failure probability. Must be done in shop. Disconnection of slipring wires may indicate this failure.

FAILURE MODE AND EFFECT ANALYSIS						
ITEM #	PART NAME, #, FUNCTION	FAILURE			PREVENTIVE ACTION	CORRECTIVE ACTION AND REMARKS
		MODE	CAUSE	EFFECT		
3	Field Slipring Assembly #140 - Located in a box on the alternator support casting (#310), sliprings transfer current for field excitation and can be easily changed in field.	<p>1. Field wires are disconnected from sliprings.</p> <p>2. Good contact with brushes is lost.</p> <p>3. Field shorts at slipring.</p>	<p>a. Excess vibration breaks the connections at sliprings.</p> <p>a. Moisture from outside causes degradation of ring surface.</p> <p>b. Brush wear over time.</p> <p>a. Moisture from outside causes ring corrosion.</p>	<p>Loss of field and output power and/or</p> <p>Degradation of field power and hence, output power.</p>	<p>Good slipring connections and regular maintenance checks, including brush replacement as necessary.</p> <p>Regular inspection of sliprings and replacement when necessary.</p>	<p>Sliprings should be replaced when surface degradation is observed and gasket examined and replaced to assure weather seal.</p>

FAILURE MODE AND EFFECT ANALYSIS				CORRECTIVE ACTION AND REMARKS	
ITEM #	PART NAME, #, FUNCTION	FAILURE MODE	FAILURE CAUSE		
4	<p>Alternator Shaft Bearing Assembly (front & rear) #151-158 - Including bearings, inner and outer seals.</p> <p>Bearings must be lubricated and are sealed inside as well as outside.</p>	<p>1. Alternator shaft unable to rotate or difficult to rotate.</p>	<p>a. Bearing failure due to corrosion from failure of seals.</p> <p>b. Lack of lubrication due to improper maintenance.</p> <p>c. Random failure of bearing.</p>	<p>Wind turbine unable to rotate freely causing loss of system output.</p>	<p>Careful installation, regular maintenance check on condition of outer seals and strict adherence to maintenance program (lubrication) as well as proper assembly and bearing spec will reduce failure probability.</p> <p>Mechanical rotation of shaft and re-lubrication may correct condition, however, bearings should be replaced as soon as possible and seals immediately.</p>

FAILURE MODE AND EFFECT ANALYSIS				CORRECTIVE ACTION AND REMARKS	
ITEM #	PART NAME, #, FUNCTION	FAILURE			PREVENTIVE ACTION
		MODE	CAUSE	EFFECT	
5	Blades (3) #210 - Blades are aircraft quality Sitka spruce, coated with 3 coats of polyurethane paint; the leading edge is protected by self-adhering polyurethane tape.	1. Blade surface degradation. 2. Blade(s) broken.	a. Impact from rain, hail, dust and UFO's. a. Material defect. b. Blade overload due to control failure. c. Overload due to winds above design limits.	Rotor output decreases reducing overall system output. Loss of power and aero imbalance causes extreme vibration thru engine system and possible failure of other components.	NWPCo experience has indicated that wind turbine blade surface degrades over time. However regular re-finishing will give blades an indefinite life. Blade design has been engineered for probable wind conditions in the proposed regime assuming proper system operation and allowing healthy margins of safety

FAILURE MODE AND EFFECT ANALYSIS					
ITEM #	PART NAME, #, FUNCTION	FAILURE			CORRECTIVE ACTION AND REMARKS
		MODE	CAUSE	EFFECT	
6	Rotor Hub #220 - Including nut and cotter pin, shaft key and pressure plate. Blade/hub connection is rigid with wooden blade clamped between steel cast hub and a wrought steel plate thru bolt.	1. Rotor turns freely on shaft 2. Rotor falls off of shaft.	a. Poor machine fit causes key to shear under normal loading. b. Excessive & abrupt electric loading of shaft shears key. a. See above. b. Cotter pin fails and nut unthreads.	Complete loss of power and eventual loss of rotor. Complete loss of system output and possible damage to other components.	With proper assembly this type of failure is extremely unlikely. After replacing blades and checking conditions of hub taper and key seat, verify regulator operation. NOTE: If rotor is observed to rotate and little or no power is being generated, failure mode #1 is always a possibility and #2 may follow shortly.

FAILURE MODE AND EFFECT ANALYSIS						
ITEM #	PART NAME, #, FUNCTION	FAILURE			PREVENTIVE ACTION	CORRECTIVE ACTION AND REMARKS
		MODE	CAUSE	EFFECT		
7	Alternator Support Assembly (including castings, bearings, seals and shafts) This casting supports the rotor/alternator VARCS assembly as it pitches back.	<p>1. Unit fails to pitch back.</p> <p>2. Unit fails to reset.</p> <p>3. Unit falls from tower.</p>	<p>a. VARCS bearing seizure.</p> <p>b. VARCS bearing seizure due to lack of lubrication.</p> <p>c. Bearing seizure due to corrosion.</p> <p>a. Same as above.</p> <p>a. Casting failure at bearing seats.</p>	<p>Rotor overspeed and eventual rotor destruction.</p> <p>Rotor is fixed in pitch out of the wind such that system produces no power.</p> <p>Failure mode #3 is the catastrophic failure.</p>	<p>Strict adherence to maintenance schedule - grease parts and inspection quality of seals.</p> <p>1. Quality control of castings by inspection.</p>	<p>Bearing failure is random and unlikely.</p> <p>Re-lubrication and mechanical movement may connect bearing seizure, but seals and bearings should be replaced as soon as possible.</p>

FAILURE MODE AND EFFECT ANALYSIS				CORRECTIVE ACTION AND REMARKS		
ITEM #	PART NAME, #, FUNCTION	FAILURE			PREVENTIVE ACTION	
		MODE	CAUSE	EFFECT		
8	VARCS Assembly #330-350 - Including hub, key, spring disc, bracket, cam followers, etc. This assembly provides the rotor speed control function.	<p>1. Spring does not resist pitchback.</p> <p>2. Pitch rate and schedule erratic.</p>	<p>a. Hub/Shaft key sheared.</p> <p>b. Spring broken (corroded, faults).</p> <p>c. Cam studs sheared (corroded, faults).</p> <p>d. Spring bracket bolts sheared (corrosion).</p> <p>a. Spring seizes in bracket due to corrosion.</p>	<p>Rotor does not stay in wind to contract maximum power, and if pitched back, will not reset. (see 7.1.1.1)</p> <p>System output erratic - rotor overspeeds occasionally.</p>	<p>Good assembly and machinery with Q/C on hub/shaft fit and key seats as well as maintenance check of weather seal.</p> <p>Maintenance check assures weather-tight cover.</p>	<p>In general, failures of these kinds are unlikely and can be prevented easily through Q/C and maintenance. Should one occur, the VARCS covers can be removed and any component easily replaced.</p> <p>Remove cover & oil and work can free grease surface and check weather seals.</p>

FAILURE MODE AND EFFECT ANALYSIS						
ITEM #	PART NAME, #, FUNCTION	FAILURE		EFFECT	PREVENTIVE ACTION	CORRECTIVE ACTION AND REMARKS
		MODE	CAUSE			
9	Power & Field Transmission Way #360 - Including connections at diode bridge, conductors, wire, connections at sliprings on shaft. Power produced in the stator is rectified and must be conducted back to the field and down the tower.	1. Loss of continuity between diodes and tower sliprings.	a. Power lead disconnected at tower bridge due to poor assembly or rough handling. b. Disconnected at slipring. c. Wire insulation worn thru and shortened to the conduit. d. Random diode failure.	Intermittant or total loss of output can result from any of these failure modes.	Assure proper factory connections and inspect regularly. Connection must be made properly in the field and inspected regularly. Care must be taken in feeding leads and deburring parts.	Remove alternator support casting cover and examine connections - repair if necessary. Remove tower slip cover and examine and repair if necessary. If none of these are the causes, disconnect wire at sliprings and uncouple conduit, feed out and examine wire. If defective, disconnect at diodes and replace.

FAILURE MODE AND EFFECT ANALYSIS					
ITEM #	PART NAME, #, FUNCTION	FAILURE			CORRECTIVE ACTION AND REMARKS
		MODE	CAUSE	EFFECT	
10	Power Transmission (con't.)	2. Loss of continuity between diodes and field sliprings.	a. Field wire disconnected at diodes. b. Field wire disconnected at brushholder.	Intermittent of total loss of field current and hence alternator output. See Above	Remove cover plate on alternator support casting. Inspection will reveal any faults which can be corrected in the field. Re-make the connection and check weather seal. NOTE: Loose connections may indicate excessive vibration due to aero imbalance.

FAILURE MODE AND EFFECT ANALYSIS					
ITEM #	PART NAME, #, FUNCTION	FAILURE			CORRECTIVE ACTION AND REMARKS
		MODE	CAUSE	EFFECT	
11	Field Brushholder Assembly #370 - Including brushes, holders, clips, brackets, etc. See 9.2 for connections. There is one slip ring for each half of the circuit and two brushes for each ring.	1. Brush does not track slip ring (see 3.2).	a. Misalignment of brush holders. b. Break in brush spring due to corrosion or faulty comp. c. Brush hangs up in box due to corrosion. d. Wear of brush box.	Intermittent or total loss of field power and hence output.	Remove cover plate on alternator support casting and re-adjust field brushholders. Remove cover plate and brush cap. Replace brush and check weather seal. Check brushholder for surface irregularity.
				Machine setting of brush holders and careful and regular inspection. Assurance of weatherseal, check regularly and replace brush as necessary.	

FAILURE MODE AND EFFECT ANALYSIS						
ITEM #	PART NAME, #, FUNCTION	FAILURE			PREVENTIVE ACTION	CORRECTIVE ACTION AND REMARKS
		MODE	CAUSE	EFFECT		
12	Saddle #410, 420 & 440 Including bumper casting, tube. Alternator support casting is hinged and supported on the saddle casting.	<p>1. Unit pitches too far forward.</p> <p>2. Unit falls off tower.</p>	<p>a. Bumper collapses or falls off.</p> <p>b. Saddle casting Support arm breaks due to corrosion or faulty casting.</p> <p>a. VARCS support ears break (faulty casting).</p> <p>b. Saddle tube weld fails (faulty weld).</p>	<p>Blades may strike the tower if bumper fails. If the arm breaks, the blades will certainly strike the tower.</p> <p>Extensive damage to entire system.</p>	<p>Assure elastomer quality, inspect regularly and replace as necessary.</p> <p>Q/C and load testing of support arm on casting.</p> <p>Assure casting and weld quality.</p> <p>Inspect regularly for corrosion.</p>	<p>Replace bumper and blades if necessary.</p> <p>Saddle assembly must be replaced, involving removal of unit from tower.</p> <p>In general, all of these failures can be prevented through Q/C and maintenance inspection.</p>

FAILURE MODE AND EFFECT ANALYSIS					
ITEM #	PART NAME, #, FUNCTION	FAILURE			CORRECTIVE ACTION AND REMARKS
		MODE	CAUSE	EFFECT	
13	Yaw Bearing Assembly #430 - Including upper bearing at saddle casting and lower sleeve bearing at lower tower plate. Bearings permit free yaw response to wind direction shifts and relief of pitch induced gyro loads.	1. Unit will not yaw freely.	a. Upper bearing seizure due to random failure, lack of lubrication or corrosion. b. Lower sleeve bearing seizes.	Failure to orient to wind direction shift and loss of overall system output.	Assure good bearing seal, check regularly for corrosion and lubricate according to schedule. Assure good machine practices. Q/C of assembly. Horizontal play should be checked regularly and lower bearing examined.
		2. Unit has excessive horizontal play.	a. Degredation of upper bearing seal. b. Lower bearing has creeped out of tower plate. Loss of retainer rings. c. Lower bearing wears thin.	Excessive play can increase stress, levels beyond endurance causing saddle failure and loss of unit.	

FAILURE MODE AND EFFECT ANALYSIS						
ITEM #	PART NAME, #, FUNCTION	FAILURE			PREVENTIVE ACTION	CORRECTIVE ACTION AND REMARKS
		MODE	CAUSE	EFFECT		
14	Power Slipring Assembly #460 - Assembly at bottom of saddle tube below lower tower bearing. There are 3 sliprings, one for each half of power circuit and one for the field (one power lead is common).	1. Loss of brush contact & circuit continuity.	a. Corrosion or glazing of ring surface prevents brush contact. b. Power lead/slipring connection fails.	Partial, intermittent, or complete loss of electric output.	Assure good weather seal on cover and check the sliprings regularly. Replace when necessary. Assure good connections and protect from vibration and corrosion.	Examination will indicate condition of rings and brushes which can be disconnected and replaced on tower.

FAILURE MODE AND EFFECT ANALYSIS					
ITEM #	PART NAME, #, FUNCTION	FAILURE			CORRECTIVE ACTION AND REMARKS
		MODE	CAUSE	EFFECT	
15	Tail #510 - Including vane, tubes, bolts, etc. The tail serves to orient the machine to wind direction at start-up and maintain upwind orientation in severe direction shifts under operation.	<p>1. Loss of tail assembly.</p> <p>2. Loss of vane</p> <p>3. Loss of one or more members.</p>	<p>a. Failure of connecting bolts due to vibration.</p> <p>b. Failure of support arms due to corrosion or loads above design limit.</p>	<p>Excessive play in tail can propagate destructive vibrations thru system.</p> <p>Loss of tail results in loss of orientation support arm to wind direction changes - when question loss of overall output.</p>	<p>The major threat to the tail assembly is vibration - fasteners must be tight. If they loosen up between maintenance visits excessive system vibration may be indicated.</p>

FAILURE MODE AND EFFECT ANALYSIS						
ITEM #	PART NAME, #, FUNCTION	FAILURE			PREVENTIVE ACTION	CORRECTIVE ACTION AND REMARKS
		MODE	CAUSE	EFFECT		
16	Stub Tower Assembly #600 - Including upper and lower tower plates with pipe - a welded unit and connection bolts. The stub tower is the interface between the SWECS and the standard tower, supports the yaw bearings, and encloses the sliprings.	1. Upper or lower plate breaks away from pipe.	a. Weld failure due to faulty weld. b. Failure due to corrosion. c. Weld failure due to high levels of vibration.	System falls off of tower. The rotor at least will be destroyed.	O/C must assure sound welds and coating. Maintenance must check condition of welds and tighten bolts.	This is a catastrophic failure resulting from faulty manufacturing or poor maintenance examination.

FAILURE MODE AND EFFECT ANALYSIS						
ITEM #	PART NAME, #, FUNCTION	MODE	FAILURE		CORRECTIVE ACTION AND REMARKS	
			CAUSE	EFFECT		
17	Collector Brushes #680 - Including bracket, brush-holders, brushes, springs and caps. There are two brushes for each slipring, mounted on the underside of the lower tower plate, enclosed in a weathertight box.	1. Brushes do not track on slipring. (See 13.1)	<p>a. Brushholder misaligned in bracket.</p> <p>b. Brush spring broken due to corrosion, wear or faulty comp.</p> <p>c. Brush hangs up in holder due corrosion or surface irregularity.</p>	Intermittent, partial and/or total loss of electric output.	<p>Assure proper alignment in manufacturing and check yearly.</p> <p>Assure Q/C of component and weather seal -check yearly</p>	Collector brushes are scheduled for regular check and there is redundancy in the system. It is expected that this component will not be subject to random failure and that regular maintenance will keep it in service.

FAILURE MODE AND EFFECT ANALYSIS						
ITEM #	PART NAME, #, FUNCTION	FAILURE			PREVENTIVE ACTION	CORRECTIVE ACTION AND REMARKS
		MODE	CAUSE	EFFECT		
24	Manual Pullout Assembly	1. Cable breaks.	a. Cable kinked from poor handling.	Inability to shut machine for maintenance.	Careful handling in shipping and installation.	If the cable fails, it can be repaired in the field with care to avoid rotor blades.
			b. Corrosion weakens cable.		Regular maintenance check of condition of cable.	Cable material is stainless & should last, but it can be replaced.
		2. Clevis fails.	a. Shackle pin unscrews.		Assure lock tight screw.	Note that this failure may indicate excessive system vibration.

6.0 PRODUCTION AND COST ANALYSIS

6.1 Introduction

Cost and production analysis for this effort is based upon NWPCo's experience in the short run production of reconditioned Jacobs Wind Electric systems. Since NWPCo intends to commercialize this wind turbine system, every effort has been made to have this analysis correspond to realistic production planning. All costing figures are in 1977 dollars.

6.2 Production Facility

It is estimated that 39 man-hours per unit will be required in production quantities of 1000 per year. Using a production rate of 20 units per week (for 50 weeks), we project a factory employment of approximately 24 individuals, not including a production manager and a quality assurance engineer.

The factory will be organized by sub-assembly as follows:

Series 100 -- Alternator Assembly	2 semi-skilled workers 1 machine operator 1 semi-skilled assembler
Series 200 -- Rotor Assembly	1 skilled blade carving machine operator 1 finisher 2 assemblers
Series 300 -- VARCS Assembly	4 semi-skilled assemblers
Series 400 -- Saddle Assembly	1 skilled worker
Series 500 -- Tail Assembly	
Series 600 -- Stub Tower Assembly	
Series 1300 -- Manual Shutdown/Final Assembly	2 semi-skilled assemblers
Inspection & Crating	1 quality assurance engineer 1 assistant 1 carpenter
Shipping & Receiving	1 inventory controller 1 assistant/fork lift operator
Maintenance	1 maintenance engineer 1 assistant
TOTAL	<hr/> 24 persons

Factory machinery required for this level of production include the following:

- 6 - 15" drill presses (3 with indexing tables)
- 2 - 14" grinders
- 1 - 8" tool grinder
- 1 - 10 ton arbor press
- 1 - 8" dip tank
- 1 - paint spray booth with 18" exhaust
- 1 - coil winding machine
- 1 - 2'x2' dip tank
- 1 - baking oven
- 1 - MIG welder
- 1 - radial arm saw
- 1 - pneumatic hammer-tacker
- 9 - pneumatic 3/8" impact wrenches
- 1 - fork lift (1 ton)
- 1 - floor crane (1 ton)
- 1 - 36"x12" lathe with tools

Approximately 10,000 square feet of production space will be required with an additional 2,000 square feet required for warehousing.

The finished product will be shipped in three crates as follows:

1. Alternator, VARCS, saddle and stub tower assembled together.
2. Rotor hub and matched blades disassembled.
3. Tail assembled.

6.3 Estimated System Costs

Cost of 1st unit (1979 dollars).....	\$4,736.00*
Cost of 100th unit (1979 dollars).....	\$3,551.00*
Cost of 1000th unit (1979 dollars).....	\$2,508.00*
Cost of 1000th unit (1977 dollars) including overhead and profit.....	\$2,867.00
Dollars per pound for 1000th unit (1977 dollars)..	\$ 4.59/pound

*Cost does not include overhead and profit

6.3.1 Estimated Turnkey Costs

(1977 dollars)

Wind machine (1000th machine).....	\$2,867.00
Tower (40 ft. Rohn 45GSR).....	\$ 700.00
Installation costs.....	\$1,200.00
(assumes local labor & relatively accessible site; include concrete, site preparation & labor)	

Storage.....\$2,000.00
TOTAL TURNKEY COST.....\$6,767.00*

*Turnkey costs can be as much as 100% higher depending upon site accessibility, storage requirements and required auxiliary generated facilities.

6.4 Cost of Energy Calculation*

Base data:

IC = initial installed cost (turnkey) = \$6,767.00
FCR = fixed charge rate (commercial) = \$ 0.085
AOM = annual operation & maintenance cost= \$ 135.00
AKWH = annual kilowatt hours produced
(assumes 15 mph mean wind) = 7,800 kilowatt hours

The cost of energy (COE) can be calculated using the following formula:

$$\text{COE} = \frac{(\text{IC}) (\text{FCR}) + (\text{AOM})}{(\text{AKWH})}$$
$$\text{COE} = \frac{6767 (0.085) + 135}{7800}$$
$$\text{COE} = \$0.091 = 9\text{¢/kilowatt hour}$$

* The fixed charge rate cost of energy calculation method used in this report was specified by Rockwell International to allow comparison of the North Wind High Reliability wind system with other machines developed under DOE sponsorship. The reader should be aware that life cycle costing provides a more accurate cost of energy determination. A good introduction to this method--as it is applied to wind systems--can be found in SWECS Cost of Energy Based on Life Cycle Costing, W.R. Briggs, Rocky Flats Wind Systems Program, RFP-3261, May 1980 (available from NTIS.)

Figure 6.1
Manufacturing Cost Estimates by Sub-Assembly

2kw HR

FINAL DESIGN REVIEW

Code	Sub-Assembly	Cost 1st Unit	Cost 100th Unit	Cost 1000th Unit	Sub-Assembly Cost as % of System Cost (1000th Unit)
100	Alternator	\$ 1201	823	638	25.4
200	Rotor	\$ 764	650	350	14.0
300	VARCS	\$ 1207	778	548	21.9
400	Saddle	\$ 339	292	207	8.3
500	Tail	\$ 53	46	37	1.5
600	Stub Tower	\$ 356	336	194	7.7
800	Electrical Conditioning	\$ 177	104	104	4.1
900	Electrical Regulation	\$ 300	220	200	8.0
1300	Manual Shutdown	\$ 164	137	107	4.3
TOTALS		\$ 4561	3386	2385	
<u>Additional Costs</u>					
	100' Transmission Cable	\$ 75	70	43	1.7
	Final Assembly & Crating	\$ 55	50	44	1.8
	Quality Assurance	\$ 20	20	20	.8
	Material Handling & Scrappage	\$ 25	25	16	.6
TOTALS		\$ 4736	\$ 3551	\$ 2508	100.0

Figure 6.2
Manufacturing Costs by Sub-Assembly - 1000 Units

2kw HR		FINAL DESIGN REVIEW							Projected Tooling Costs
Code	Sub-Assembly	Weight lb(kg)	Material Costs	Direct Labor Hours/Cost	Sub-Contract Hours/Cost	\$/lb.			
100	Alternator	235(106)	\$ 448	12.5/\$50	7/\$140	\$ 2.71		\$15,714	
200	Rotor	75(34)	\$ 250	5.0/\$20	4/\$80	\$ 7.83		\$ 7,950	
300	VARCS	90(41)	\$ 428	5.0/\$20	5/\$100	\$ 6.09		\$ 1,500	
400	Saddle	64(29)	\$ 119	2.0/\$8	4/\$80	\$ 3.23		\$ 1,500	
500	Tail	49(22)	\$ 35	.5/\$2	-----	\$.76		-----	
600	Stub Tower	65(29)	\$ 162	.5/\$2	1.5/\$30	\$ 2.98		\$ 1,000	
800	Electrical								
	Conditioning	2(1)	\$ 100	1.0/\$4	-----	\$52.00		-----	
900	Elec. Regula.	10(4)	\$ 200	-----	-----	\$70.00		-----	
1300	Manual Shutdown	35(16)	\$ 106	.25/\$1	-----	\$ 3.06		\$ 1,990	
TOTALS		625(282)	\$1848	26.75/\$107	21.5/\$430	\$ 3.82		\$29,654	
<u>Additional Costs</u>									
	Final Assembly & Crating	---	\$ 20	6.0/\$24	-----	-----		-----	
	100' Transmission Cable	---	\$ 43	-----	-----	-----		-----	
	Quality Assurance	---	---	2.0/\$20	-----	-----		-----	
	Material Handling	---	---	4.0/\$16	-----	-----		\$ 7,000	
TOTALS		625(282)	\$1911	38.75/\$167	21.5/\$430	\$ 4.01		\$36,654	
<u>1000th Unit Manufacturing Cost</u>									
	Labor Overhead @ 83% of Direct Labor Cost		\$2508						
	G & A @ 15% of Total Cost		\$ 139						
	Profit @ 15% of Total Cost		\$ 397						
TOTAL			\$ 457						
	Adjust for 1977 Dollars (10% & 9%)		\$3501						
			\$2867						

7. PROGRAM STATUS AND SCHEDULE

7.1 Phase I Schedule

Figure 7.1 charts the initiation and completion of the major milestones in Phase I of the high reliability 2kw design and development program. Projected completion dates for Phase I design reviews are also shown as open bullets. As can be seen, we were unable to meet the initial nine month timetable to FDR. This was due in part to the difficulties of adapting a young company to the requirements and methods of this type of contract. However, a large element in the extension was the expansion of the scope of the project to encompass ambitious and extensive pre-prototype fabrication and testing. As a result of this Phase I work, the overall program schedule does not reflect the extra four months in Phase I.

The following parameters will be measured during the testing of Prototype I at Rocky Flats:

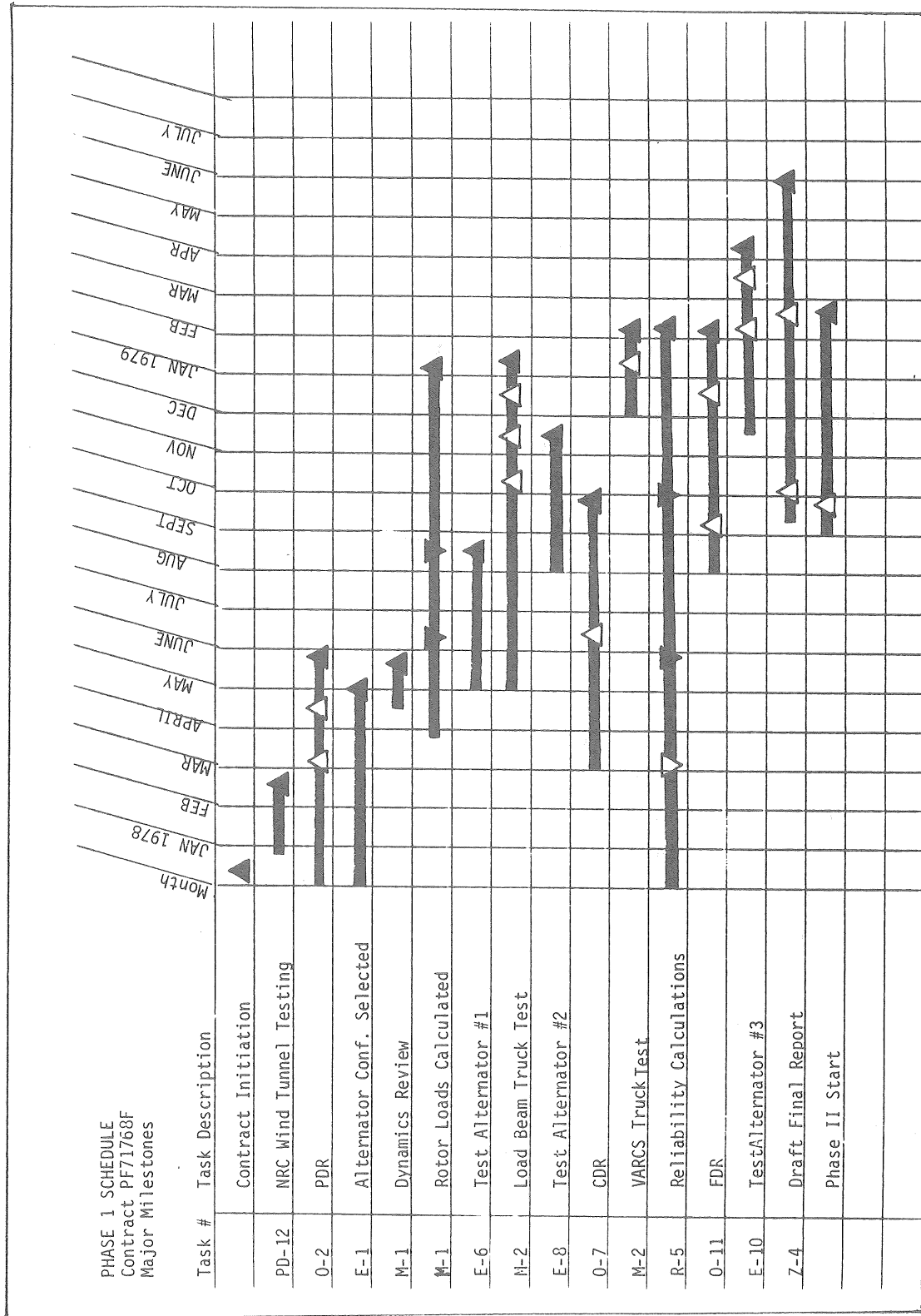
- Wind speed, V (mph, m/s)
- Wind direction, WD (degrees)
- Air density, ρ (slugs/ft³, gm/cm³)
- Out of plane blade bending, M_3 (in-lb, n-m)
- Alternator input torque, Q (n-m)
- Rotor RPM (RPM, rad/sec)
- Rotor azimuth, ψ (degrees)
- Field current, I_{field} (amperes)
- Line current, I_{line} (amperes)
- Alternator temperature, T_A (°C)
- Alternator vibration (Hz)
- Rotor pitch, β (degrees)
- Machine yaw, Y (degrees)
- Tower vibration (Hz)
- Line voltage, E_{line} (volts, DC)
- Field voltage, E_{field} (volts, DC)

Rocky Flats testing will itself have two components: intensive testing data collection (ITDC) and long term data collection (LTDC).

ITDC will require measurement of the following variables for which provision will be made on prototype I where necessary:

V	M_3	ψ	I_{line}	β
WD	Q	I	T_A	Y
	RPM	I_{field}	Vibration	

Figure 7.1
Major Milestones - Phase I



LTDC will require measurement of the following variables for which provision where necessary will be made on both Prototypes I and II:

V	l_{field}	Y
WD	l_{line}	Fline
RPM	β	

Data collected during LTDC should be reduced and presented graphically in the following format:

Pitch Output vs. Wind Speed
Pitch vs Wind Speed
RPM vs Wind Speed
RPM vs Pitch
Pitch Rate vs Wind Speed Rate
Pitch Rate vs Yaw Rate
Pitch Rate vs RPM

The first four required plots are self-explanatory, however, the last three relate to specific questions which are critical to machine operation. High change rates (either positive or negative) directly affect pitch rate. This is the only area that we are currently aware where data sampling rates must be faster than one per second. Our experience with the 800 watt Par-ri-Dunn machine indicated yaw rates of $20^\circ/\text{second}$ and pitch rates exceeding $65^\circ/\text{second}$. This last condition was caused by a 2.6 gust in a 6.0 m/s wind.

Another area that we would like to look at would require a circuit that would indicate the difference between relative wind direction and machine orientation. There has been some speculation, with some possible confirmation from the NRC Wind Tunnel Data, that SWECS do not tend to orient themselves directly into the wind.

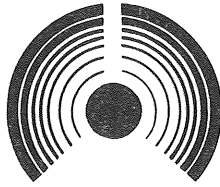
Other pertinent machine data should be collected over a long term but with no advantage over short-term, e.g. C_p vs Tip Speed Ratio, Tip Speed Ratio vs Wind Speed, Input Power vs Output. Once the alternator and rotor efficiencies had been mapped there would be no need for longer data collection.

This test program is designed to produce complete and useful data on the overall performance and suitability of the prototype. In addition, the test program will answer some more academic questions about the dynamics, loading and operating characteristics of a tilted rotor.

REFERENCES

1. Walter Frost, B.H. Long, R.E. Turner, Engineering Handbook on the Atmospheric Environmental Guidelines for Use in Wind Turbine Generator Development, NASA-Lewis Research Center: Cleveland, Ohio, December 1978. (NASA Technical Paper 1359)
2. F.W. Schmidt, Aerodynamics of the Model Airplane, Translation Branch, Redstone Scientific Information Center, Research and Development Directorate: U.S. Missile Command, Redstone Arsenal, Alabama, 1941. (N70-39001)
3. R.E. Wilson, P.B.S. Lissaman, S.N. Walker, Aerodynamic Performance of Wind Turbines, National Science Foundation: Washington, D.C., 1976. (ERDA/NSF/04014-76/1)
4. Forrest S. Stoddard, Momentum Theory and Flow States of Windmills, University of Massachusetts: Amherst, Massachusetts, n.d.
5. Carl Rohrbach, Rose Worobel, Performance Characteristics of Aerodynamically Optimum Turbines for Wind Energy Generators, Hamilton Standard, Division of United Technologies Corporation: Windsor Locks, Connecticut, May 1975.
6. A.H. James Jr., Safety Aspects of Wind Energy Conversion Systems, A Review and Bibliography, Oak Ridge National Laboratory: Oak Ridge, Tennessee, 1978. (ORNL/ICES-4)
7. Ibid
8. Ibid
9. William C. Cliff, Wind Velocity Change (Gust Rate) Criteria for Wind Turbine Design, Battelle-Pacific Northwest Laboratories: Richland, Washington, 1978. (PNL-2526)

APPENDIX A
LOW REYNOLDS NUMBER WIND SECTION
TESTS IN THE MIT 12" X 12" WIND TUNNEL



NORTH WIND POWER CO

BOX 315
WARREN
VERMONT 05674
802 496 2955

1 KW
AERODYNAMIC SECTOR
16 March 1978

LOW REYNOLDS NUMBER WING SECTION TESTS IN THE MIT 12" x 12"
WIND TUNNEL

Very little airfoil section data at low Reynolds Numbers have been published. Indeed, had it not been for the model aircraft enthusiasts, the world would be completely without low Reynolds Number data. NACA's single effort in this area, Ref 1, has long been discredited due to the high turbulence levels in the VDT Wind Tunnel.

Small WECS rotors operate at Reynolds Numbers ranging from 100,000 to 300,000 and as low as 20,000 during start-up conditions. Local angles of attack on untwisted blades can exceed 30° and angles of attack during start-up can be as high as 85° . Existing published data was obtained to serve as a tool to the aircraft designer and does not cover the angles of attack or Reynolds Number range of interest to the WTG rotor designer.

MIT's 12" x 12" wind tunnel is a low-turbulence, open-circuit wind tunnel equipped with a three-component strain gage balance. Wind sections are cantilever mounted from the bottom wall of the test section. Velocity is monitored by the difference in static pressure between the test section and settling chamber as based on a pitot static calibration of the test section.

Our wing section models had a 3" chord and were trimmed in length to allow a 1/32" clearance from the top wall of the test section.

The strain gage balance was calibrated with the following results:

Initial Settings on Strain Indicator
Gage Factor = 2 , add 25/1000

No Load Settings for Channel 1, 2, and 3 was 2500

If: $L_1 = (\text{Strain Reading})_{\text{Channel 1}} - 2500$

$D_2 = (\text{Strain Reading})_{\text{Channel 2}} - 2500$

$M_3 = (\text{Strain Reading})_{\text{Channel 3}} - 2500$

$$\begin{aligned}\text{Then: } L \text{ gm} &= -0.23286L_1 - .01302D_2 \\ D \text{ gm} &= 0.20335D_2 - .01314L_1 \\ M \text{ gm in} &= .6328M_3\end{aligned}$$

A balance tare drag was determined for each of the four test speeds with the following results:

<u>Re</u>	<u>V</u>	<u>Manometer Setting</u>	<u>D₂ Correction (Counts)</u>
50,000	21.32 mph	0.32"	19
100,000	42.64	1.18"	66
150,000	63.97	2.68"	145
200,000	85.29	4.66"	260

The air density was determined by monitoring the temperature and barometric pressure.

The two sections tested were the FX 76MP120 modified to a thicker section by flattening the bottom of the section as shown in Fig. 1 and the 20% GU 25-5(11)8 section which had been previously tested at Reynolds Numbers ranging from 390,000 to 630,000, Ref. 2. The Wortman section had never been tested before.

The data obtained are presented Figures 2 - 9. In Fig. 2, note the lack of a distinctive stall at a Reynolds Number of 50,000. This is characteristic of thick unsymmetrical sections at very low Reynolds Numbers as is shown in data from Ref. 3, which is reproduced in Fig. 10.

The GU section was designed to be an optimum at a Reynolds Number of about 600,000 where like a Liebeck section, the downward slope on the leeward side is on the verge of laminar separation in order to minimize drag and maximize lift. Hence, at a Reynolds Number as low as 50,000, a laminar separation occurs at very small angles of attack and the stall characteristics usually associated with angles of attack from 10° to 20° are not evident in that the stall has occurred at much lower angles of attack.

Despite low L/D's at low Reynolds Numbers, the GU 25-5(11)8 section with its 20% thickness is a good section for a small WTG rotor because of the ruggedness of the blade required to provide the necessary torque. This section is a natural for large WTG rotors because of its outstanding L/D's at higher Reynolds Numbers.

Fig. 3 shows CL vs. Reynolds Number, and the curves exhibit a distinctive bell-like shape. Similar data from Ref. 3 (Fig. 12) also exhibits this bell shape.

The Wortmann section was designed to be optimum at about 200,000. The lift channel of the strain indicator ran out of range at very low angles of attack, precluding obtaining data near 200,000, but the section looks very promising in an aerodynamic sense. It is by far the best performing section that I have flown on my radio controlled sailplane, $Re \approx 100,000$.

References

- Ref. 1: Kelling, Experimental Investigation of a High Lift, Low Drag Aerofoil, University of Glasgow Report No. 6802.
- Ref. 2: Jacobs, Airfoil Section Characteristics, NACA 586.
- Ref. 3: Schmidt, Aerodynamics of the Model Airplane, Part 1, Airfoil Measurement, N70-39001.
- Ref. 4: Hoerner and Borst, Fluid Dynamic Lift, Liselotte A. Hoerner, Publisher 1975.

Arnold R. Johnson

ARJ/ng

MIT Models

- o Two Required
- o Material: Maple
- o Thickness: .6" for GU Model
.45" for FX Model

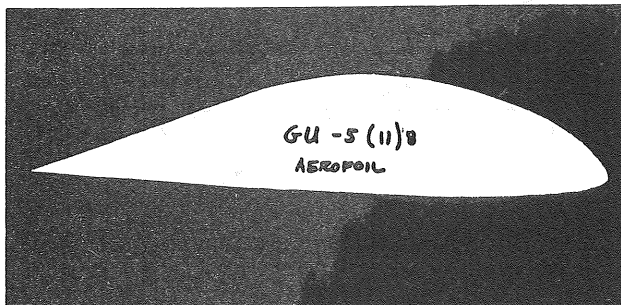
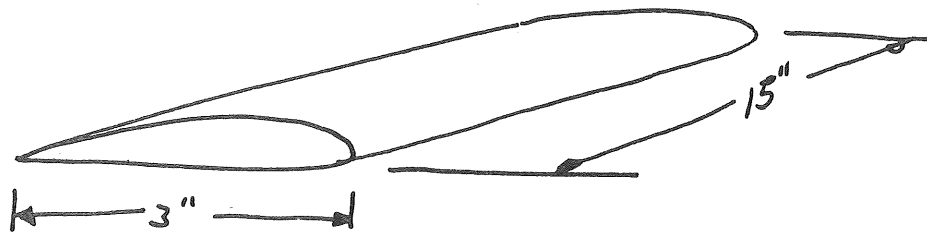


Figure 1
Sketch of Sections Tested

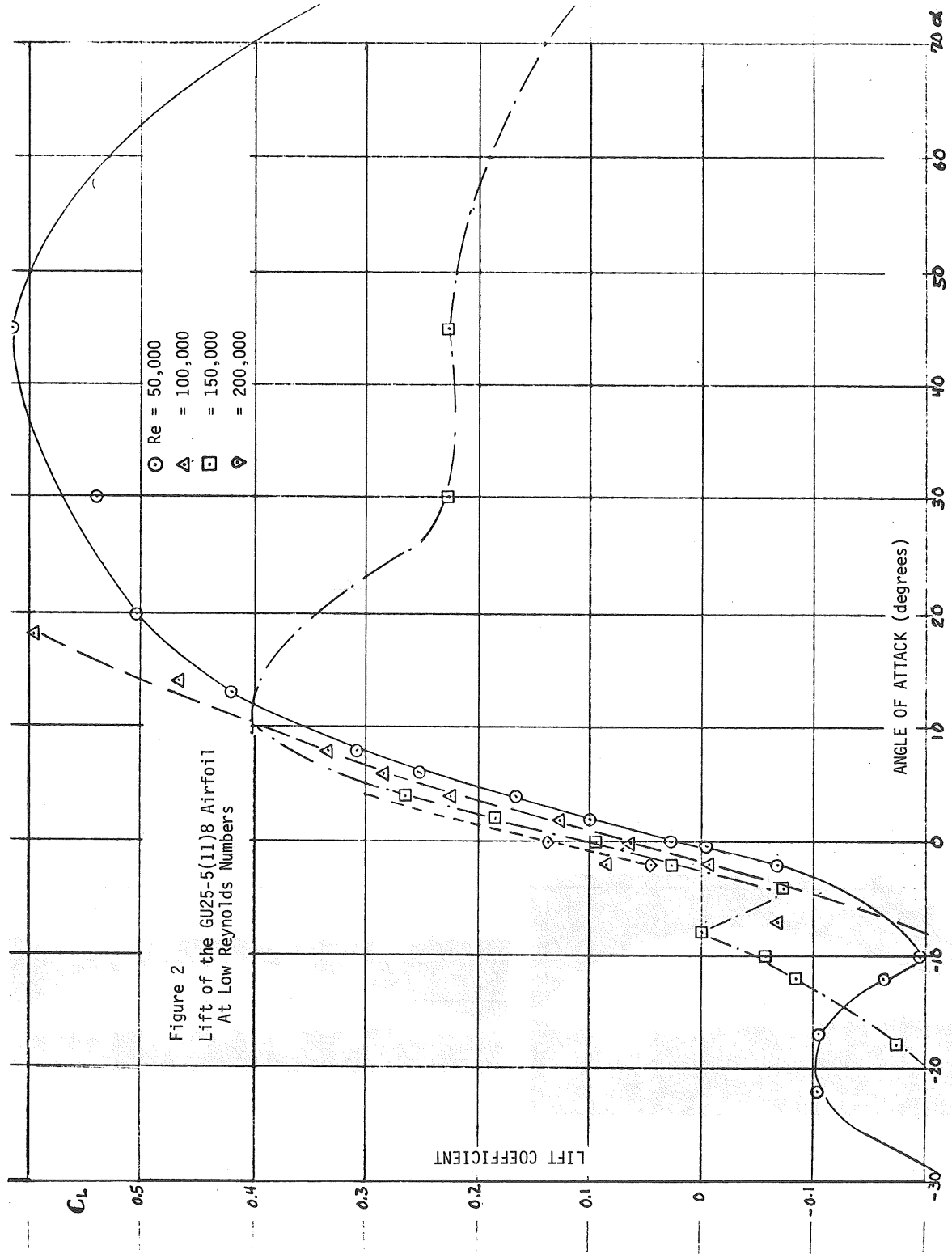
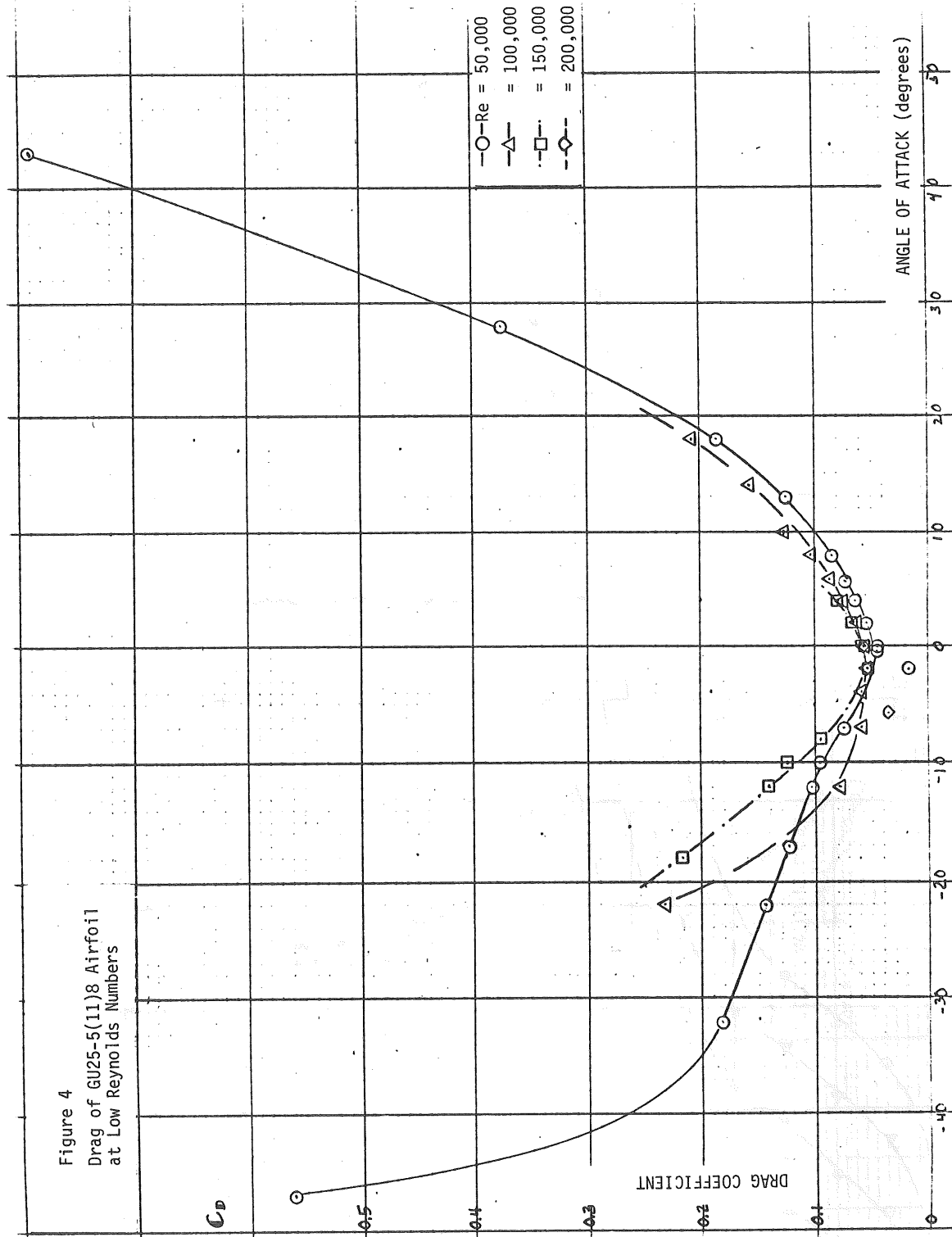


Figure 4
 Drag of G025-5(11)8 Airfoil
 at Low Reynolds Numbers



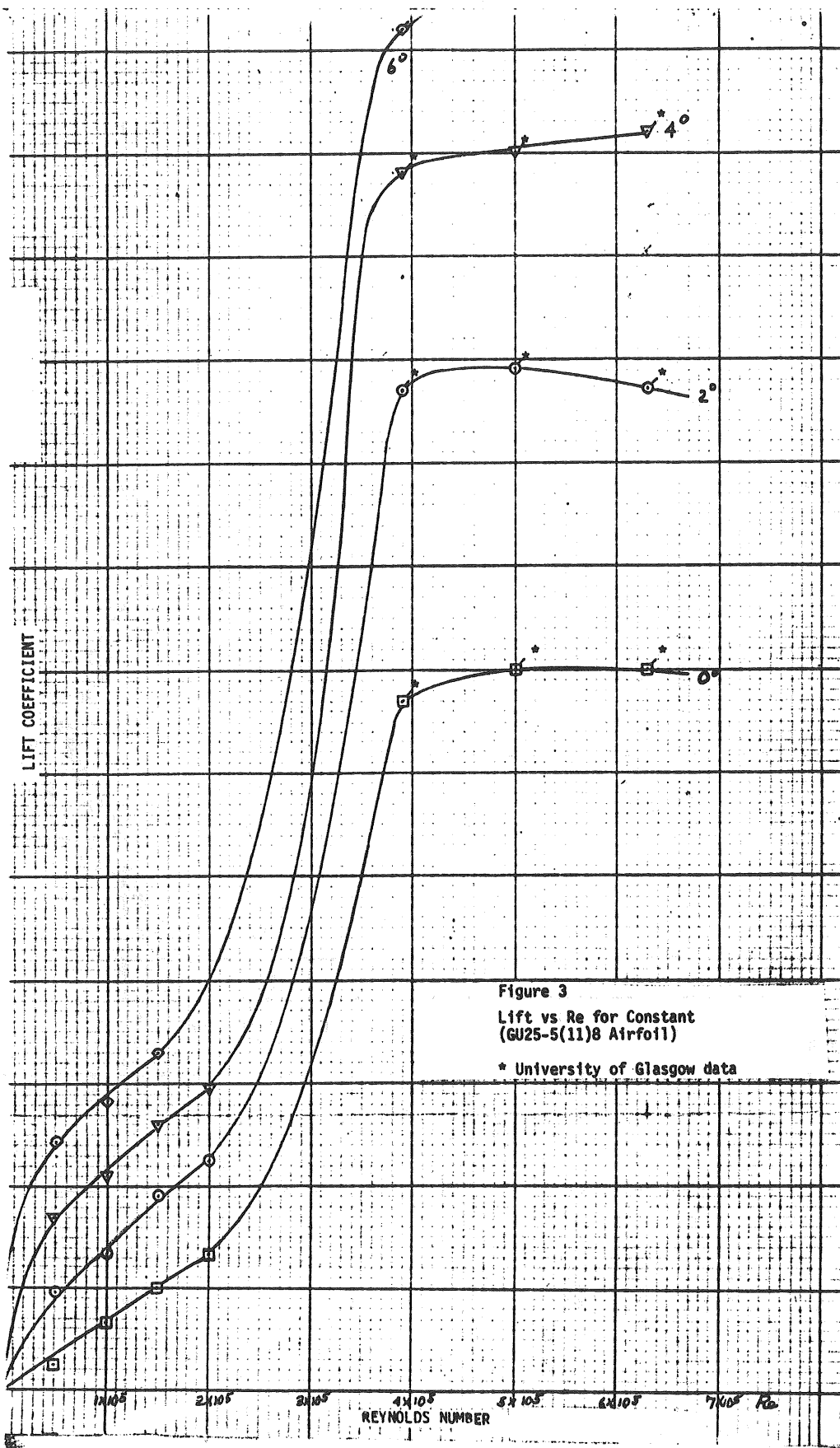
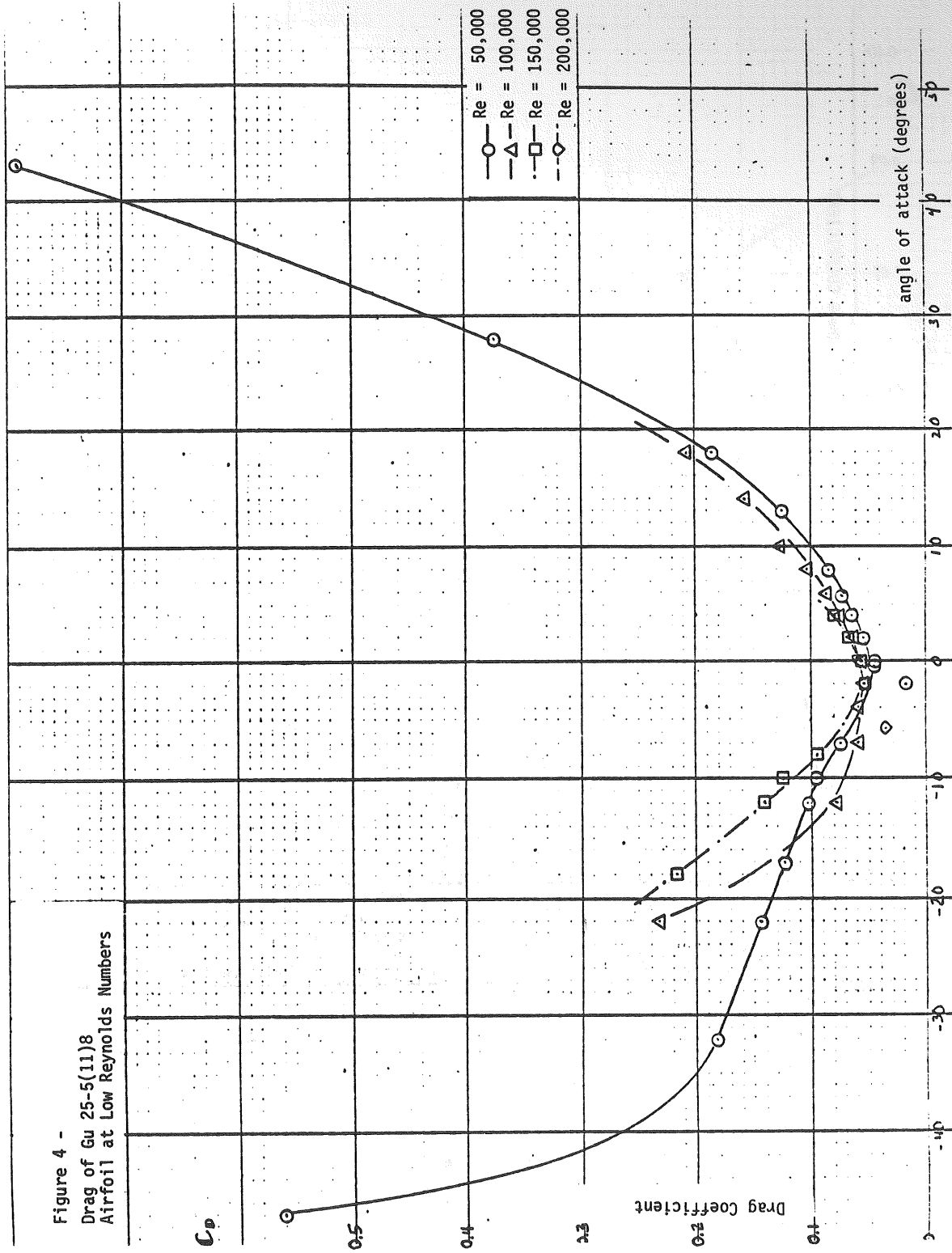
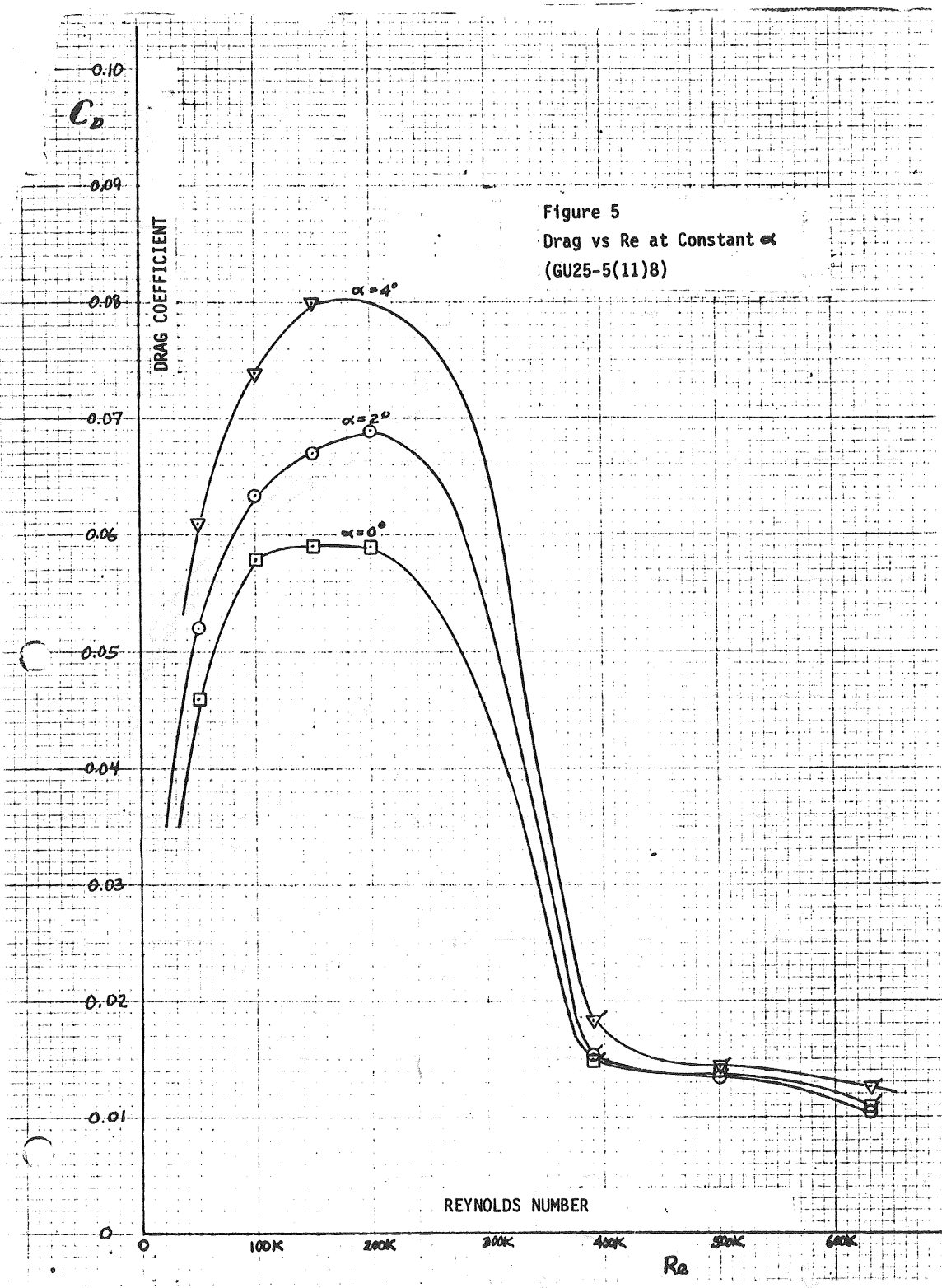
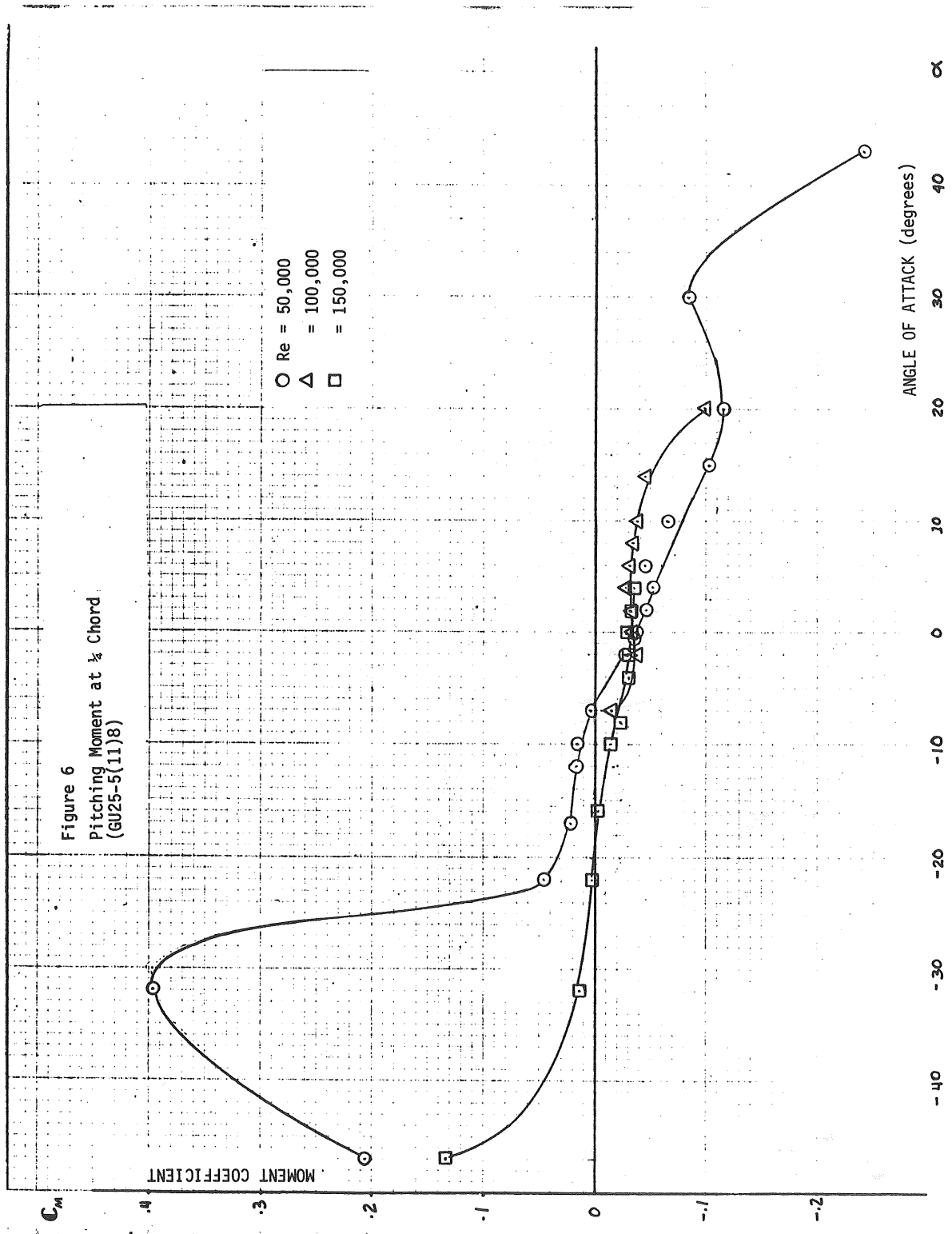


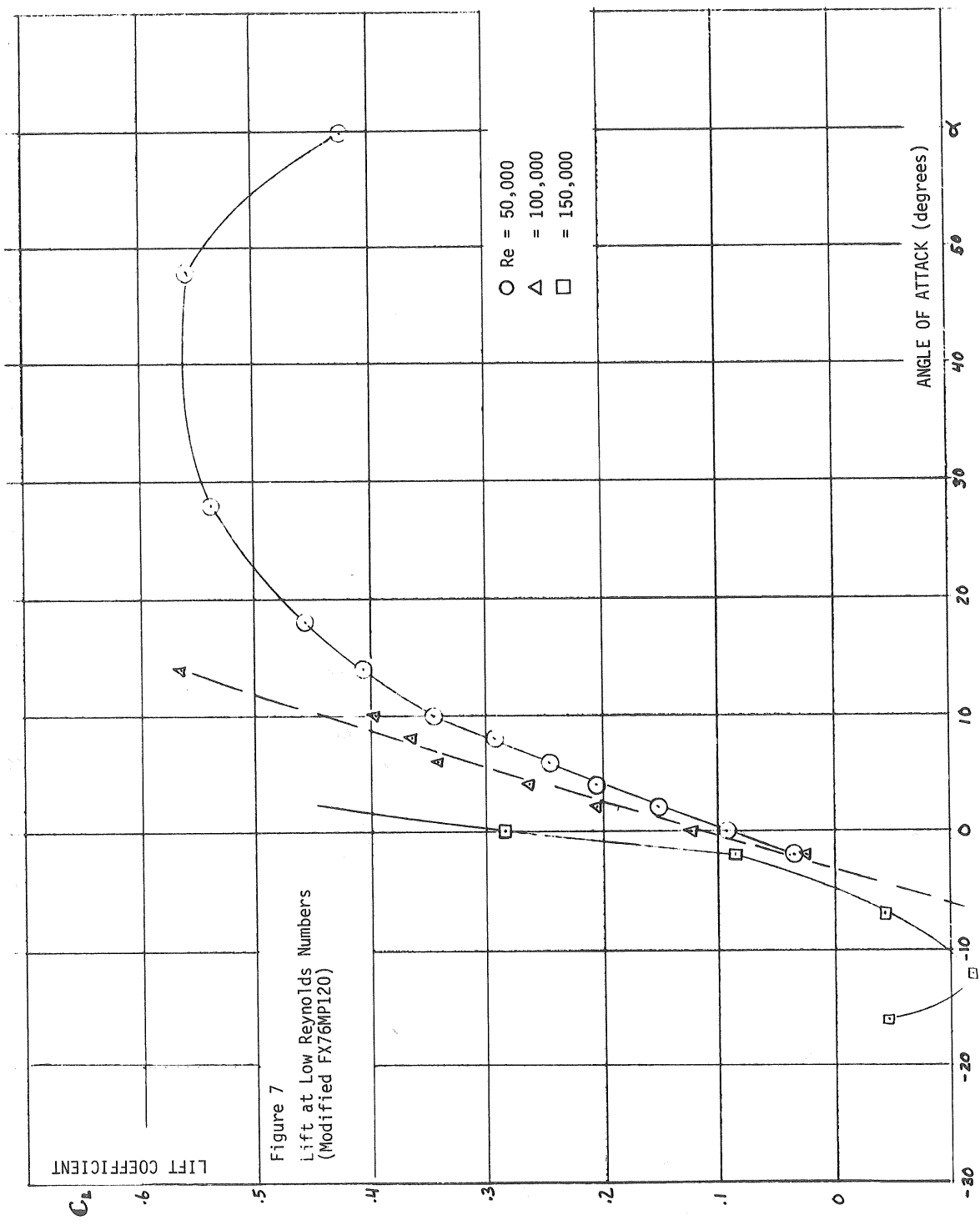
Figure 3
 Lift vs Re for Constant
 (GU25-5(11)8 Airfoil)
 * University of Glasgow data

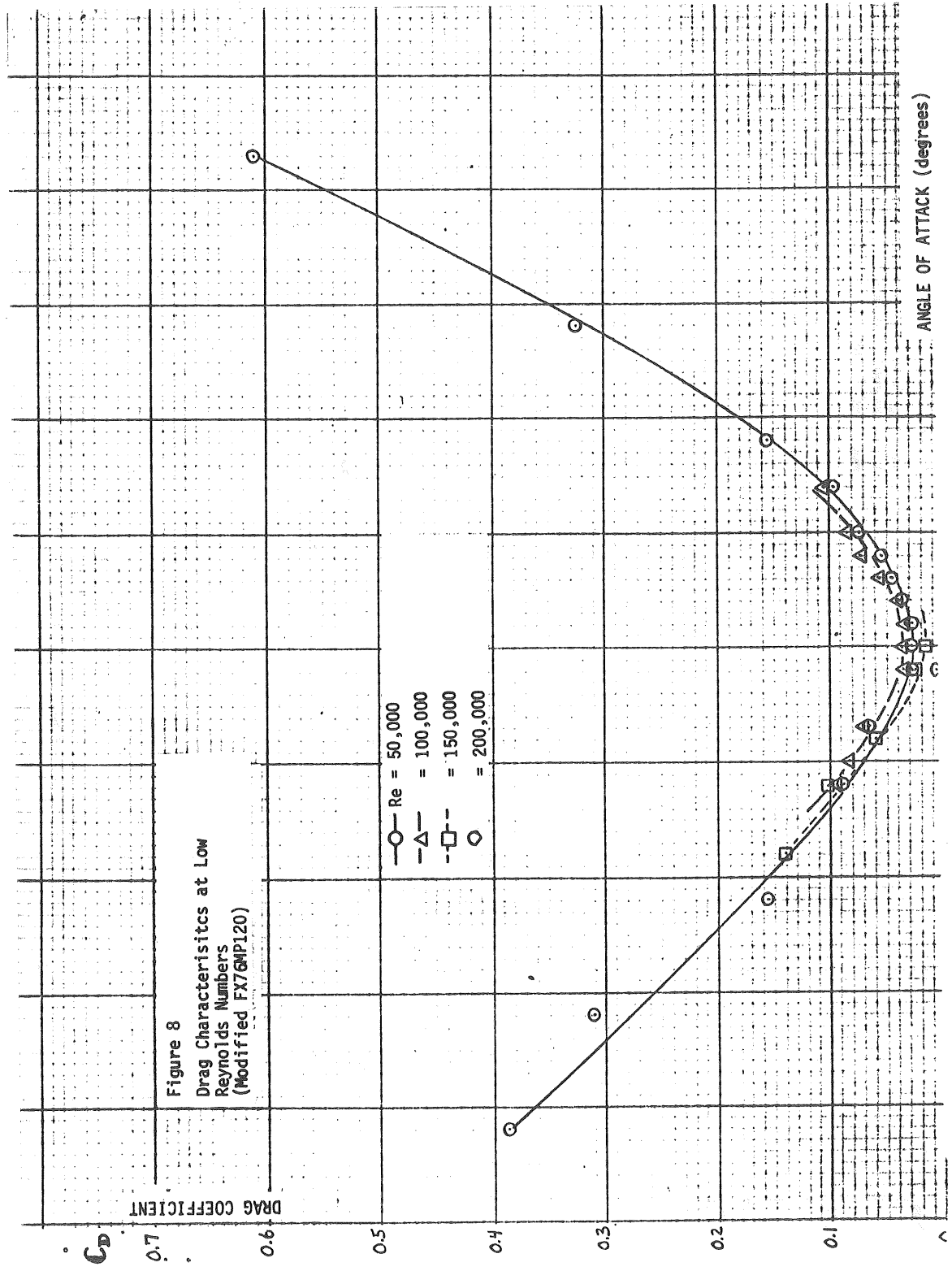
Figure 4 -
 Drag of Gu 25-5(11)8
 Airfoil at Low Reynolds Numbers

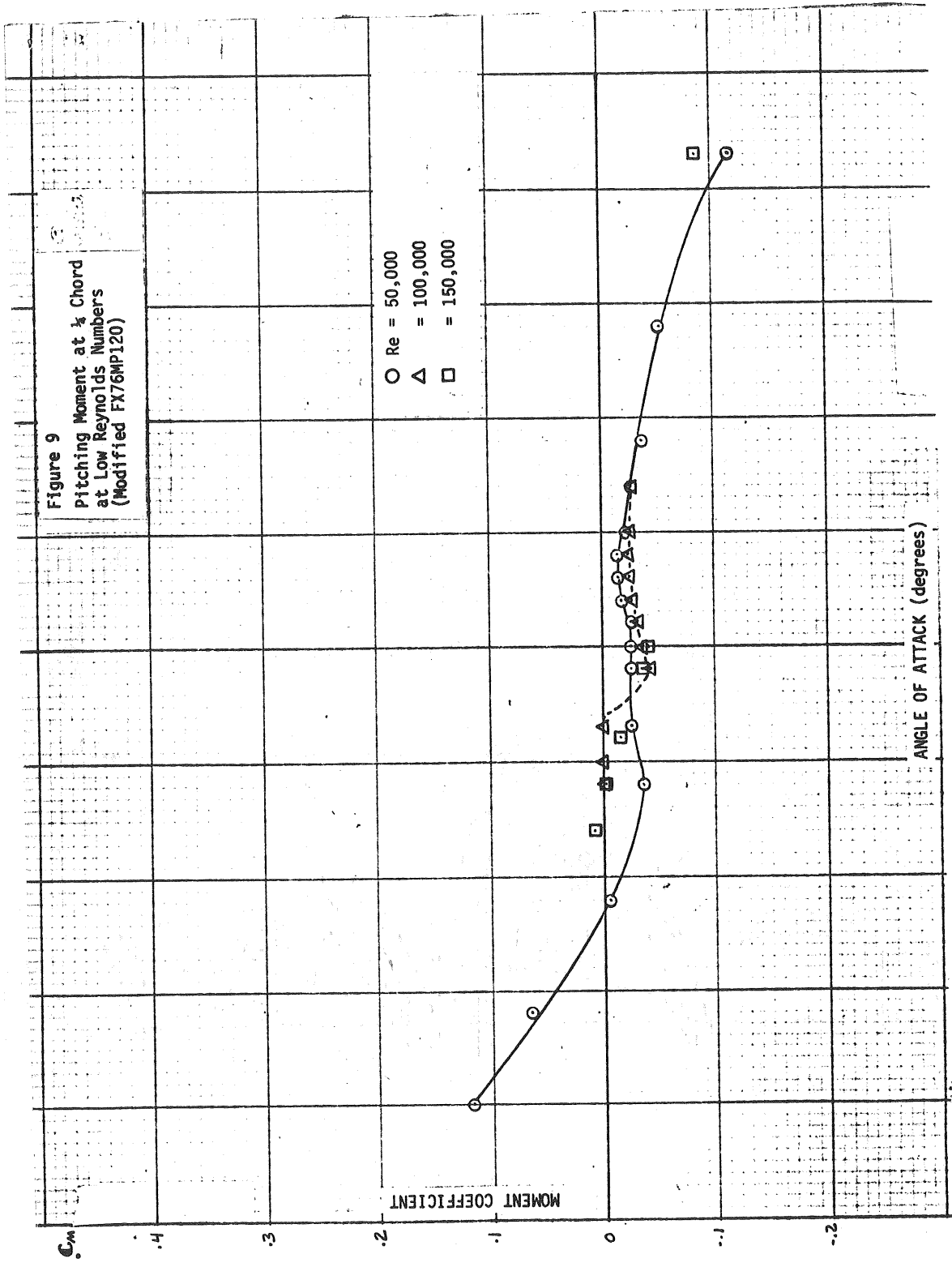












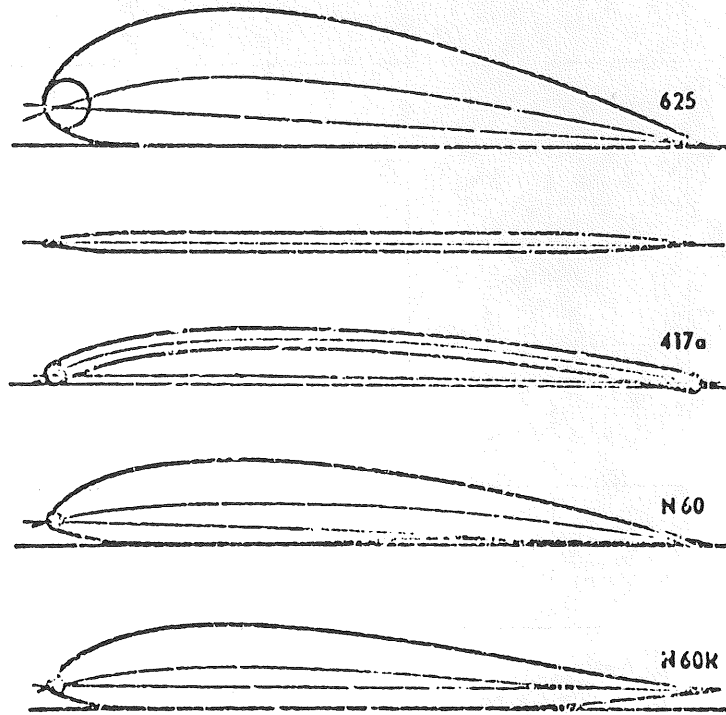


Figure 92. Summary of the five airfoil profiles measured.

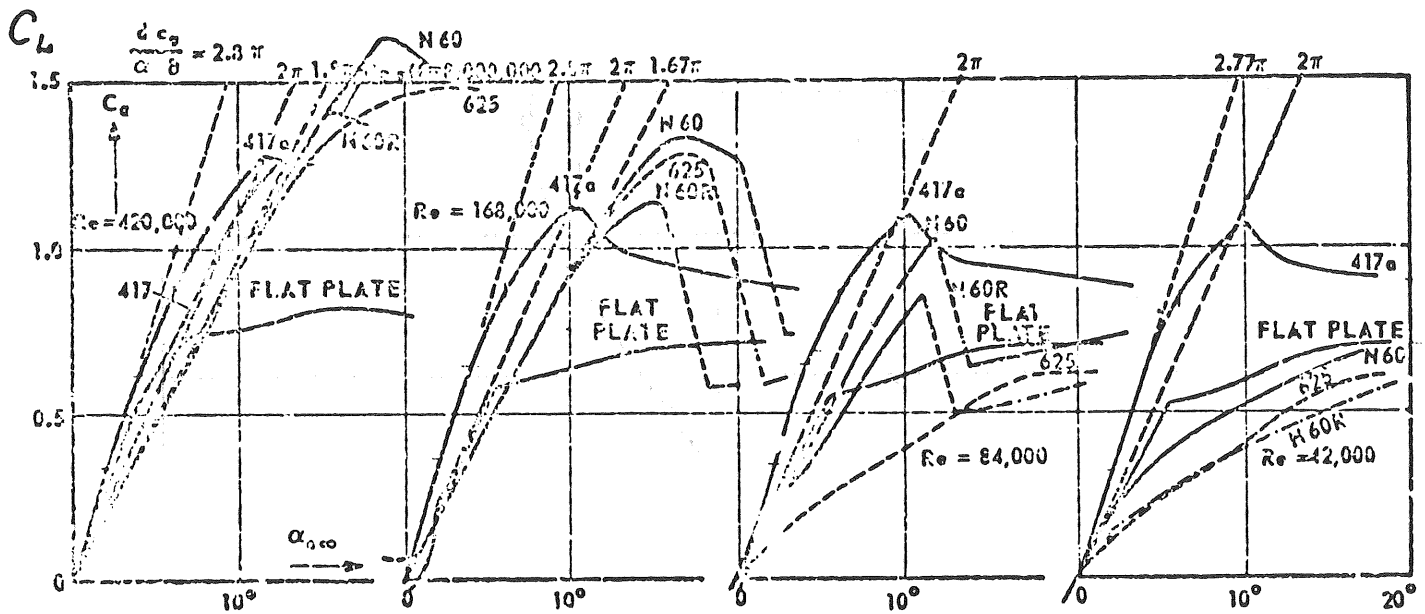


Figure 63. Comparison of lift slope for five different profiles in four different series of Reynolds numbers, in terms of the effective angle of air approach $\alpha_{0\infty}$ ($\alpha_{0\infty} = 0$ at $c_a = 0$).

Figure 10